THESIS

presented to obtain the Degree

DOCTOR OF PHILOSOPHY OF ECOLE POLYTECHNIQUE

Speciality:

Mechanics and Materials

by

Duy-Hao LUU

Subject of the thesis:

Gradient Theory:

Constitutive Models and Fatigue Criteria; Application in Micromechanics

Defense on 11 June 2013 before the jury constituted with:

M.	**Nicolas SAINTIER**	**Reviewer**
M.	**Eric CHARKALUK**	**Reviewer**
M.	**Michel FREMOND**	**Examiner**
M.	**Ahmed BENALLAL**	**Examiner**
M.	**Habibou MAITOURNAM**	**Supervisor**
M	**Quoc-Son NGUYEN**	**Co-supervisor**

Acknowledgements

Mes remerciements vont, en premier lieu, à mes directeurs de thèse, Monsieur Habibou MAITOURNAM et Monsieur Quoc Son NGUYEN. Leurs qualités tant scientifiques qu'humaines ont été pour moi un soutien inestimable. Quand je suis arrivé au LMS (Laboratoire de Mécanique des Solides) pour commencer ma thèse, j'étais un master en génie civil plutôt qu'en mécanique. Grâce à leurs aides précieuses et patience, j'ai presque "refait ma base" en mécanique à partir de celle en génie civil, et enfin fini la thèse à temps.

Je souhaite ensuite remercier Monsieur Ahmed BENALLAL qui m'a fait l'honneur de s'intresser ce travail et d'en prsider le jury. Qu'il trouve ici l'expression de ma profonde reconnaissance.

Je voudrais exprimer ma gratitude à Messieurs Nicolas SAINTIER et Eric CHARKALUK qui ont accepté la lourde tâche d'être rapporteurs de cette thèse. Leurs critiques et suggestions sont très pertientes et précieuses et m'ont été d'une grande valeur pour sa présentation finale.

Je remercie également Monsier Michel FREMOND pour ses remarques et suggestions qu'il m'a apportées bien qu'il n'ait pas pu être présent à ma soutenance.

Je souhaite remercier aussi les personnes avec lesquelles j'ai pu discuter, pour leur aide précieuse: LE Minh Bao, NGUYEN Truong Giang, NGUYEN Dinh Liem, DANG Thi Bach Tuyet, Antoine LAUNAY, Roberto ALESSI, Eva HERIPRE et les autres ...En particulier, LE Minh Bao m'a aidé beaucoup comme s'il avait été mon "encadrant" pour cette thèse; et NGUYEN Truong Giang m'a guidé et discuté avec moi beaucoup de la partie numérique dans CAST3M.

En dernier lieu, j'aimerais adresser mes remerciements les plus profonds à ma mère et mon père défunt, à ma soeur et mon petit frère, surtout à ma femme et mes filles chéries, et à tous mes collègues ainsi que mes amis qui m'ont accordé leur soutien tout au long de ce travail de thèse.

Contents

Summary

In this thesis, two new classes of phenomenological models in the framework of the *continuum thermodynamics and gradient theory* are proposed. The first is **Standard Gradient Constitutive Model** dealing with problems **at micro-scale**, the other **Gradient Fatigue Criteria at small scale**. Using them, common effects not captured yet in classical mechanics but become significant at small scales, are taken into account. Two distinct effects usually confused in the literature, "size" and gradient effects, leading to both well-known phenomena "Smaller is Stronger" and "Higher Gradient is Stronger" are modeled.

The thesis contains two main parts, corresponding to the two new model classes as follows:

Part A- Standard Gradient Constitutive Models: Application in Micro-Mechanics

A formulation of Strain Standard Gradient Plasticity Models is proposed and numerically implemented. The models are based on a global approach in the framework of continuum thermodynamics and generalized standard materials where the gradients of internal parameters are introduced. The governing equations are derived from an extended version of the virtual work equation (Frémond 1985, or Gurtin 1996). These equations are also derived from the formalism of energy and dissipation potentials and appear as generalized Biot equations. The gradient formulation established in such way is considered a higher-order extension of the local plasticity theory, with the introduction of the material characteristic length scale ℓ and the insulation boundary condition proposed by Polizzotto 2003. The presence of strain gradient leads to a **Laplacian equation** and to **non-standard boundary value problem**. A computational method based on diffusion-like problem is used. Illustrations are given and then applied to typical problems in micro-mechanics to capture the "size" and gradient effects, thus to represent both phenomena **"Smaller is Stronger"** and **"Higher Gradient is Stronger"**. A good agreement between numerical and reference results is found. A mesh-independence of numerical results is observed.

Part B- Gradient Fatigue Criteria: Application in Fatigue at Small Scale

A formulation of gradient fatigue criteria is proposed in the context of multiaxial high-cycle fatigue (HCF) of metallic materials. The notable dependence of fatigue limit on some common factors not taken into account in classical fatigue criteria, is analyzed and modeled. Three factors are intimately interconnected, the "size", stress gradient and loading effects, are here investigated. A new class of fatigue criteria extended from classical ones with stress gradient terms introduced not only in the normal stress but also in the shear stress components, are formulated. Such a formulation allows to capture both "size" and gradient effects, as well as to cover a wide range of loading mode, then can represent both phenomena "Smaller is Stronger" and "Higher Gradient is Stronger". Gradient versions of some classical fatigue criteria such as Crossland and Dang Van are provided as illustrations. Furthermore, for the multiaxial low-cycle fatigue limit (LCF), some initial suggestions are also proposed.

A brief plan of the thesis:

Chapter 1 is General Introduction. *Chapters 2-3* correspond to part A and *Chapters 4-5* to part B. *Chapter 6* is General Conclusions and Perspectives. Finally, *Appendix* is detail of numerical implementation.

CHAPTER 1

General introduction

1.1 Problematics

Part A- Standard Gradient Constitutive Models: Application in Micro-Mechanics

In recent years there has been an increased interest in modeling plastic deformations at small scales. Examples are found in microelectronic components, micro-electro-mechanical systems (MEMS) and thin film applications. A large number of experiments have demonstrated that the length scale effect, also called the **"size effect"**[1], is of importance at length scales within the range from a fraction of a micron to tens of microns (Venkatraman and Bravman 1992 [169]; Fleck *et al.* 1993, 1994, 1997, 2001 [52; 55; 53; 54]; Nix and Gao 1998 [124]; Stolken and Evans 1998 [159]). The common point in many experiments appearing the "size effect" is that, the spatial strain distribution in the solid is usually not uniform, i.e. a strain gradient is present. That implies the phenomenon associated with the "size effect" is usually **gradient effect**[2]. Both phenomena are related to the material resistance in a visible general correlation that, **"the smaller the size, the higher the gradient, then the higher material resistance"**. There are also cases where the gradient exists but independent from the size, although both influence on material strength (e.g. residual surface stress cases). Examples about the "size effect" - also well known under a term **"Smaller is Stronger"**, are as follows. For the same material, geometry, loading mode and condition boundary: tension-compression test shows an increased material strength with decreasing radius of a specimen; decreasing thickness of the thin films gives a strengthening in bending test; thin wire torsion exhibits an increased strength for smaller diameters of the wires; decreasing indentation size in micro-indentation tests leads to an increased hardness, etc. For the sake of further analyses, it requires to clarify what are sources of the size effect by isolating it from the gradient effect, for instant. Size effect is commonly assumed related to two sources: Dislocation Starvation (DS) effect (Deshpande *et al.* 2005 [46], Greer *et al.* 2005 [72], etc), and pure size effect (Fleck *et al.* 1994, 1997 [55; 53]). The first concerning the dislocation mechanism is usually unimportant at micro scale (see Fig.2.1), and particularly is not our object of study; the second relevant to the metallurgical defects and heterogeneity of material, is proved also insignificant at scale considered and thus negligible (see Fig.2.2.a, or more detail in [55; 53]). Then a preliminary qualitative remark is that, such size effect is not very significant and thereby just is a part, but not enough to explain the experimental fact "Smaller is Stronger" discussed above.

[1] significance of the notation " " will be explained later.

[2] It is a brief writing. In Part A, this must be understood as strain gradient effect.

Consider now the gradient effect as another factor which may help to interpret that fact. Examples about gradient effect - termed here **"Higher Gradient is Stronger"**, are the following. For the same material, geometry, loading mode: a thin film shearing with passivated layers that constrain dislocations, gives a higher resistance than that with unpassivated layers; a thin wire torsion with exterior surface covered by a very thin elastic coating that blocks dislocations, has a higher strength than that with free surface, etc. For the same material, geometry, boundary condition: the strength in bending test is larger than in tension-compression test. Once again, sources of gradient effect must be clarified. Such gradient effect that we can just estimate but not observe, is related to three sources: boundary condition, loading mode, and size. The first is associated with constraints on dislocation glide (grain boundaries, interfaces, boundary layers such as thin films, thin wires, etc. as synthesized in Kostas 2010 *et al.* [93]); the second concerns loading type which decides the spatial stress distribution state in the solid (null gradient in tension-compression, non-zero gradient in bending, etc.); the last is associated with the size (e.g. geometry and grain sizes) and can be visibly seen via an example (see Fig.2.2.b, or [55; 53]): for the same loading mode (torsion), condition boundary (free surface), and nominal twist imposed on exterior surface of a thin wire, the smaller the wire radius the higher the strain gradient (and the higher the material strength). The figure shows that, although the variation here in material strength at various radii results from both size and gradient effects, such very clear difference is enough to conclude the dominance of the latter as the former is shown insignificant before in the case of tension test (Fig.2.2.a). Then the sources of the gradient effect prove two things: first, the phenomenon "Smaller is Stronger" experimentally observed is mainly attributed to the gradient effect in our cases (via its last source) - rather than totally to the size effect (DS and pure size effects) as usually believed; second, the gradient effect, i.e. "Higher Gradient is Stronger", is really a phenomenon different from the size effect.

All previous analyses for both the size and gradient effects imply that although the size and gradient effects are intimately interconnected and usually confused in the literature, they are actually two distinct phenomena. The former only contributing partially to "Smaller is Stronger" and requiring to be modeled by other approach, is negligible compared to the latter and thus left out in the current study; whereas the latter is not only "Higher Gradient is Stronger" but also a main factor contributing to "Smaller is Stronger" that we observe, and is the object of study here. In brief, from phenomenological aspect, "Higher Gradient is Stronger" is obviously related to the gradient effect only, while "Smaller is Stronger" is related to both size effect (DS and pure size effects) and gradient effect where the latter is dominant. Then in mechanical aspect, "Smaller is Stronger" here is just an "visible image" of gradient effect rather than the size effect. However in phenomenological aspect, "Smaller is Stronger" is an experimentally observed fact that evokes an "intuitive relation" to the size rather than the gradient. For this reason and also because of habit, henceforth in this research, the terminology **"size effect"** (placed within quotes) is still used for "Smaller is Stronger", but after a new conception, as an apparent size effect; and the terminology **gradient effect** is used for "Higher Gradient is Stronger". In such a sense, an important conclusion drawn is that, **taking into account only gradient effect (related to all its sources) is enough to capture both "size effect" and gradient effect on plastic behavior**.

Many other experimental evidences also show that, apart from the size and boundary condition of the test specimen as mentioned above, the microstructure of material also significantly impacts on deformation and failure. For example, the strengthening of metal-matrix composites by a given volume fraction of hard particles is greater for small particles than for large - for the same volume fraction of reinforcement; fine-grained metals are stronger than those with coarse grains, etc. Again, a non-zero strain gradient is present even in this case, as the GNDs induce strong plastic strain gradient at grain level (Section 2.4). The phenomenon associated with the microstructure "size effect" is therefore still the gradient effect. The idea about taking into account only the gradient effect to capture both "size" and gradient effects may be still available as before in the case of the influence of the geometry size and boundary condition. A brief classification about the "size" and gradient effects is the following. If one considers the all three factors (size, boundary condition, microstructure), three groups of "size" and gradient effects commonly discussed in the literature respectively are: the first related to the geometry size and the second to boundary condition of **microsystems** (thin wire, micro-foil, micro-/nano-indentation or similarly micro-void, sharp crack tip, thin film, etc.); the third to the **microstructure** of material (rigid particle in a metal-matrix composite, grain structure of a polycrystal material, etc.). Among these three groups, the group 1 and 2 with problems related to microsystems will be our main objective in this study. At such a length scale, the "size" and gradient effects obviously must be taken into account.

However, classical theories of plasticity possess no material length scale, therefore predict no "size" neither gradient effects. It leads to the need of new models to capture observed effects in micro-mechanics. To our knowledge, all these models belong to either *gradient or nonlocal class*, proposed since recent decades to overcome the lack of a *material characteristic length scale* in the classical plasticity. The existing models used in micro-mechanics, after the synthesis of Voyiadjis *et al.* 2010 [176], comprise: Discrete Dislocation Dynamics Simulations, Molecular Dynamics Simulations, Crystal Plasticity Theories, and **Gradient Plasticity Theories**. Thanks to its simplicity in both formulation and numerical implementation, the gradient plasticity theory, pioneered by Aifantis 1984, 1987 [4; 5], and then developed by other authors (Fleck & Hutchinson, Muhlhaus, Voyiadjis, Gurtin, Polizzotto, de Borst, Gudmundson, Willis, Andrieux, Benallal, etc., and that by Q.S. Nguyen which will be used in this work), has been largely applied. This is in turn divided in two classes: strain gradient plasticity (SGP) and stress gradient plasticity models. In the current work, **Strain Standard Gradient Plasticity (SSGP) Constitutive Model**[3] proposed by many authors including Q.S. Nguyen [118; 116] will be presented and used. In time-independent processes, two models are discussed: Gradient-Independent Dissipation Potential (Model I), and Gradient-Dependent Dissipation Potential (Model II). The latter is the trickiest due to the indetermination of dissipation forces for null associated fluxes and overcome with the *Energy Regularization Method* proposed by Q.S. Nguyen [118].

A question posed is "Are Gradient Models effective for micromechanical plasticity behavior"? Note that the "size effect" always exists (at least the pure size effect), while the gradient effect may be present or not, independently. Here in this study, **only cases where the gradient effect is present apart from**

[3] henceforth briefly called "Gradient Model" in the current study, except when it must be more concretized.

the inherent pure size effect, are considered. In this condition, the theory about "Geometrically Necessary Dislocations (GNDs)" ([12; 13; 52; 55; 53; 89; 137]) can explain the mechanism of the strain gradient effect on material strength as well as the role of material length scale in a consistent framework. Following the theory of GNDs, Gradient Models with "gradient terms" introduced in their energy and dissipation potentials, can capture the gradient effect. Together with such an important conclusion above, these models are finally considered possible to capture both "size" and gradient effects to represent both phenomena "Smaller is Stronger" and "Higher Gradient is Stronger" as seen in illustrations in this work. Using an extended version of virtual work principle (Frémond 1985 [65], Gurtin 1996 [76]) and the classical laws of continuum thermodynamics in the framework of the SSGP theory and the generalized standard materials (Halphen and Q.S. Nguyen 1975 [84], Q.S. Nguyen 2000, 2005, 2011, 2012 [117; 119; 118; 116]), thermodynamically consistent equations of the **"SSGP Constitutive Model"** are derived for the standard gradient plasticity yield criterion and associated flow rule. The gradient formulation can be considered a higher-order extension of the classical plasticity theory. This SSGP theory still lies within the general framework of the *classical continuum thermodynamics (macro model)*. However, in addition to the inherent boundary conditions of classical plasticity, secondary boundary condition (insulation boundary condition, *cf.* Polizzotto 2003 [141]), is introduced. The introduction of strain gradients into the local theory formulations leads to a Laplacian equation needing to be solved at *global level*, and to *boundary value problem* governed by partial differential equations of higher order with *non-standard boundary conditions*, therefore more difficult to solve. Nevertheless, these difficulties are overcome with a computational method based on diffusion-like problem. Indeed, the **Laplacian equation at global level** is here easily numerically solved with user subroutine (UMAT) built in usual available Finite Element codes (e.g. CAST3M).

The SSGP Constitutive Model with linear or nonlinear isotropic and kinematic hardening, where the gradient of accumulated plasticity is introduced, is here investigated as illustration. The model is used to treat typical problems (thin wire torsion, thin film shearing, micro-void growth, etc.). The issue of numerical convergence is also considered. Algorithms with implicit schemas after *deformation theory* are used. A good agreement between numerical results and reference counterparts is found. Conditions for avoiding the pathological mesh dependence are obtained. By means of numerical calculations for those problems, upper and lower saturation bounds with respect to the specimen size out of which no change in numerical results are found, are observed. They also present the validity limit of the model. Thus, in the light of reference data, problems concerning the *microsystems' geometry size* are successfully treated. Those concerning the *material microstructure size* expected to be also done via the *material characteristic length* related to the grain size, are temporarily left out. Then it is shown that, our final objective in this thesis - capturing both "size" and gradient effects to represent both phenomena "Smaller is Stronger" and "Higher Gradient is Stronger", is confirmed.

Part B- Gradient Fatigue Criteria at Small Scale

Similarly to modeling mechanical behaviors at micro-scale, in recent years, there has also been an increased interest in establishing fatigue criteria for metals capable of dealing with particular issues related

to small scales (problems with the size effect, the high stress gradient effect as around notches, voids, contacts..., and loading effect, etc.). At sufficiently small sizes, some factors whose effects on fatigue limits are inherently not captured by classical fatigue criteria, become important and must be taken into account through new criteria.

Among such factors, experimental evidences from the literature show three interconnected factors: "size effect", gradient effect[4] and loading effect (*cf.* [135; 131; 132; 179]). At this stage we just give some qualitative analyses as follows (more details will be given in Chapter 5). *(1)* For the same nominal stress, material and smooth geometry, spatial stress distribution in tension-compression fatigue test, the smaller the sample size, the higher the fatigue limit. This variation in fatigue strength is attributed to the pure size effect as the gradient is null; *(2)* For the same nominal stress, material and smooth geometry, the specimen in tension-compression test sustains lower fatigue stress than in bending test. The presence of the stress gradient in bending, but not in tension-compression, is considered beneficial effect of the stress gradient; *(3)* For the same nominal stress, material and smooth geometry, and stress gradient, fatigue limit in plane bending test is always higher than that in rotative bending test. This difference is regarded as the loading mode effect; A visible general correlation between the previous factors is that, **"the smaller the size, the higher the gradient, then the higher fatigue resistance"**.

Similarly to Part A, it also requires to analyze again the effects just mentioned above, but now in the point of view of fatigue resistance. Size effect in fatigue tests is actually the pure size effect which will be also proved negligible compared to the others at scale considered (see Chapter 5); while the gradient effect is again related to three sources: boundary condition, loading mode, and size. From the same rationale as in Part A about the distinction between the size and gradient effects, the dominance of the gradient effect as well as the negligibility of the pure size effect at scale considered, the new conception for "size effect" to mention the real nature of the phenomenon "Smaller is Stronger", and noting that the loading effect is naturally attached to the gradient effect, an important conclusion drawn is also that, **taking into account only the gradient effect (related to all its sources) is enough to capture the "size", gradient and loading effects on fatigue limits**.

Classical fatigue criteria without material length scale however predict no "size", gradient neither loading effects. The objective is to establish a new class of fatigue criteria for considering the previous factors. These criteria are applied to not only small devices (electronic components, electro-mechanical devices), but also to devices in the transfer of fatigue data from laboratory specimens to components in industrial design. Because in both cases, at sufficiently small sizes, the previous effects become important and must be captured. In this context there have been a few existing approaches such as (*cf.* [131; 17; 132; 112; 179]): *(i)* critical layer approaches; *(ii)* distance approaches (e.g. effective distance approach, theory of critical distances); *(iii)* nonlocal approaches (e.g. maximum stressed-strained volume, volumetric energy based criterion; gradient method); *(iv)* local approaches (e.g. gradient dependent criteria, etc).

In the present investigation, a new simple gradient version of local type fatigue criteria, i.e. Gradient Fatigue Criteria, is developed in the spirit of Papadopoulos and Panoskaltsis 1996 [135]. The main idea

[4] It is a brief writing. In Part B, this must be understood as stress gradient effect.

is to maintain the general framework of the classical fatigue criteria, but to embed into it gradient terms which enable to describe the effects concerning the stress heterogeneous distribution and loading mode. Three steps are used: first, phenomenological analyses on dependence of fatigue limit on the previous factors under uniaxial stress cyclic loadings; second, formulation of stress gradient fatigue criteria which can capture the previous observed effects; and finally, a generalization to multiaxial loadings.
To confirm the effectiveness of Gradient Fatigue Criteria at small scale, similarly in Part A, note that the "size effect" always exists, while the gradient effect may be present or not, independently. Once again, here in this study, **only cases where the gradient effect is present apart from the inherent pure size effect, are considered**. However, the notch effect,[5] regarded as a particular case of the gradient effect, will be deliberately left out in the study confined in macroscopically elastic behavior. In such a context and along with such a notable conclusion above, Gradient Fatigue Criteria with stress gradient terms introduced are capable to capture the "size", gradient and loading effects, and thus to reproduce both phenomena "Smaller is Stronger" and "Higher Gradient is Stronger", as found in the applications here.
Basing on this approach, the current study re-uses the review of Papadopoulos and Panoskaltsis 1996 [135] and develop to make more clear the connection as well as the distinction between the effects by analyzing the role of each dimension of sample in fatigue resistance (the role related to pure size effect or gradient effect, or both?). The interpretation of [135] concluding the independence of torsion fatigue limits from the shear stress gradient effect is re-considered. Two issues that remain, are: first, the non-effect of the shear stress gradient on fatigue limits is only found for some metals - but not all!; second, the influence of the stress gradient amplitude must be clarified. Gradient fatigue criteria extended from classical ones with stress gradient terms introduced not only in the normal stress but also in the shear stress components, are thereby proposed and validated to clarify the issues. For example, the new criteria are shown effective when used to well reproduce the torsion tests by Massonnet [104], what are impossible with [135]'s model.
Such a formulation allows new criteria to capture the "size" and gradient effect, as well as to cover a wide range of loading effect. These are then naturally generalized to multiaxial. Gradient versions of some classical fatigue criteria such as Crossland and Dang Van are provided as illustrations. A good correlation between experiment results from the literature and simulation results is found. Then our final objective here - modeling the "size", loading and gradient effects to represent both phenomena "Smaller is Stronger" and "Higher Gradient is Stronger", is confirmed.

This work mainly deals with the multiaxial high-cycle fatigue limit (HCF). However some initial propositions will also be given for the multiaxial low-cycle fatigue limit (LCF).

1.2 Synthesis

In the framework of micro-mechanics, two new classes of simple phenomenological model extended from classical models, **Strain Standard Gradient Constitutive Model** and **Gradient Fatigue Criteria**,

[5] A very high stress concentration around notches can cause high local plastic strain here.

are proposed in this thesis. Both model classes are based on the Continuum Thermodynamics and Gradient Theory, and here generally called **Gradient Models**. Using them, common effects not included yet in classical mechanics but becoming significant at sufficiently small scales, are now captured. The final objective here is to model "size" and gradient effects, then to reproduce both well-known phenomena **"Smaller is Stronger"** and **"Higher Gradient is Stronger"**. Outstanding computational advantages of the model classes adopted make them convenient for applications in micro-mechanics.

1.3 Thesis organization

- *Summary* is an abstract of the whole study dealing with the two new model classes, Standard Gradient Constitutive Models, and Fatigue Gradient Criteria, corresponding to parts A and B.
- *Chapter 1* gives a General Introduction with an overview for each part.
- *Chapters 2-3* present the content of the Part A where a Literature Review is given in Chapter 2, and Standard Gradient Constitutive Models in Chapter 3.
- *Chapters 4-5* are dedicated to the content of the Part B with a Literature Review in Chapter 4, and the Gradient Fatigue Criteria in Chapter 5.
- *Chapter 6* are devoted to General Conclusions and Perspectives.
- *Appendix* is detail of numerical implementation by deformation plasticity methods.

PART A: Standard Gradient Constitutive Models: Application in Micro-Mechanics

CHAPTER 2

Literature review

2.1 Overview of micro-mechanics: plasticity at the micron scale

Material engineering has recently advanced at an ever increasing pace, and nowadays one has reached to engineer materials at scales approaching the micro, nano, and even atomic scale. Applications of metals and polymers at the micron scale are multiplying rapidly. Plasticity as well as the elasticity of the materials are important, and much efforts have been underway to model behavior at the micron scale. In solid mechanics, one has found that constitutive models conceived for the macro scale, become increasingly insufficient when approaching the micro scale. The problem lies at the fact that, over a scale which extends from about a fraction of a micron to tens of microns, metals display a strong size-dependence when deformed non uniformly into the plastic range. Although not always, the associated effect with the "size effect" is usually the gradient effect. The smaller the size is, the larger the gradient is, the larger the material strength is. A general phenomena are hence **"Smaller is Stronger"** and **"Higher Gradient is Stronger"** associated with the "size" and gradient effects. This effect has important implications for an increasing number of applications in electronics, structural materials and MEMS. Nevertheless plastic behavior at this scale cannot be characterized by classical plasticity theories because they possess no **material length scale** and thus predict no "size effect" neither gradient effect. The need has thereby become evident about new models to capture the relevant effects in the material behavior. The complexity of such models on the one hand is appropriate in describing the behavior, on the other hand must also be limited, since increased complexity leads to increased computational cost. One approach, prioritized in the present research, is to maintain the general framework of the macro-scale model (continuum thermomechanics), but to embed into it micro-mechanical characteristics which enable the "composite" model to describe the experimentally observed micro-scale effects. Moreover, while micron sized solids are too small to be characterized by classical theory, they are usually too large to conform to approach based on discrete dislocation mechanics. The relatively large numbers of dislocations governing plastic deformation at the micron scale motivate the development of a continuum theory of plasticity incorporating size-dependence. SGP theories have been developed for this purpose. The motivation and potential for such theories will be discussed. Issues around the foundations of the SGP theories will also be discussed and a few typical results are given (*cf.* [89; 137]).

2.2 Bibliography on experimental results in micro-mechanics: important effects

In addition to common effects in classical mechanics such as plasticity, viscosity, cyclicity,... effects, at sufficiently small scale, some other relevant effects such as the size, gradient and anisotropy effects, become important and must be taken into account.

2.2.1 Size and gradient effects

The synthesis and analysis of [52; 55; 53; 137; 89] are reported here to continue to be discussed. The specific citations will be detailed later.

a) Distinction: difference and correlation

As partially discussed in Chapter 1, the size and gradient effects are on the one hand two distinct phenomena, but on the other hand very closely correlative. The gradient effect concerns to three sources: boundary condition, loading mode and size; while the size effect is commonly assumed related to two sources: Dislocation Starvation (DS) and pure size effects; Here some experimental evidences about the effects are given. The Dislocation Starvation (Deshpande *et al.* 2005 [46]) concerning dislocation mechanism, always exists in plasticity problems. This mechanism accounts for the size effect experimentally observed in the cases without both pure size (i.e. material without defects) and strain gradient effects. Another example of the DS size effect in the absence of the pure size and gradient effects, carried out on the gold in a tension test, is also given in Fig.2.1. In view of the figure one can observe that, with gold pillar diameters more than about a micron, DS size effect becomes insignificant, thus negligible at micron scale. Not similarly to the size effect by Dislocation Starvation, the pure size effect is interpreted with the theory of metallurgical defects and heterogeneity of material at small scale. The pure size effect always exists whatever the other effects are. For example, in the uniaxial tension test (Fig.2.2.a), if not including some experimental errors, a slight size effect (DS presumedly and pure size effects) after the thin wire diameter is shown in the absence of the strain gradient here. In the torsion case (Fig.2.2.b), both size and gradient effects exist where the size effect is still insignificant at scale considered (as the size effect is loading-independent). Thereby it permits to deduce that the gradient effect is exactly dominant factor to contribute to the phenomenon "Smaller is Stronger" experimentally observed here. A remark drawn is that, although "Smaller is Stronger" directly related to the specimen size, this actually is the gradient effect related to the sample size, but not totally to the size effect as commonly expected. Despite that real nature, a terminology "size effect" (placed within quotes) is still used for this phenomenon because of the "intuitive" sense and habit.

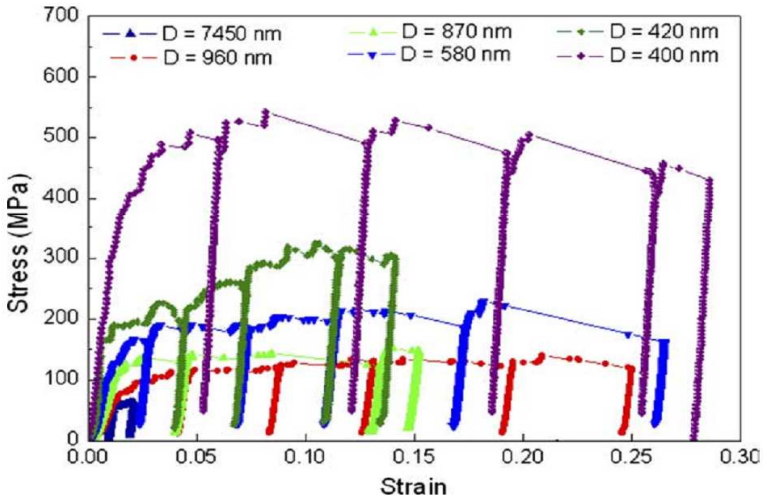

Figure 2.1 : *Dislocation Starvation (DS) size effect in the absence of pure size and gradient effects:* Stress-strain behavior of $<0\,0\,1>$-oriented FIB'd gold pillars where flow stresses increase significantly for decreasing diameters in range less than $500nm$, but nearly unchange with diameters more than $1\mu m$. Then size effect by DS is insignificant at micron scale (*cf.* Greer *et al.* [72])

b) Classification and corresponding experimental results

At length scales within the range from a fraction of a micron to tens of microns, the size and boundary condition of the test specimen and the material microstructure significantly impacts on deformation and failure. Correspondingly, three groups of size as well as gradient effects commonly discussed in the literature roughly are: the first related to the loading and geometry size and the second to boundary condition of **microsystems** (first: thin wire torsion Figs. 2.3.a and 2.2, micro-foil bending Figs. 2.3.b and 2.4; second: micro-/nano-indentation or similarly micro-void growth Figs. 2.3.c and 2.5, stress field at the tip of a sharp crack Fig.2.3.d, thin film shearing Fig.2.6, etc.); the third associated with the **microstructure** of material (rigid particle in a metal-matrix composite Fig.2.3.e, grain structure of a polycrystal material Figs. 2.3.f and 2.7, etc.). All these groups relate to a term **"micro-mechanics"** that implies mechanics at **micro-scale**. At such a micro-level, both "size" and gradient effects generally become important and must be accounted for in the proposed model. Such terminology **"micro"** is understood in the sense of both **microsystems and microstructure** where the former will be our major object in the current study.

Group 1, 2: "size" and gradient effects related to microsystems

Once again let us come back the Fig.2.2 which corresponds to a set of experiments displaying strong size-dependence of plastic deformation in the micron range . Annealed copper wires of diameter ranging from 170 down to $12\mu m$ are twisted well into the plastic range. For each wire, the torque, Q, versus twist per unit length, κ,is plotted as Q/a^3 versus κa, where a is the radius of the wire (Fig. 2.2.b). Dimensional arguments allow to directly deduce that, if the wires strength is governed by a continuum theory with no

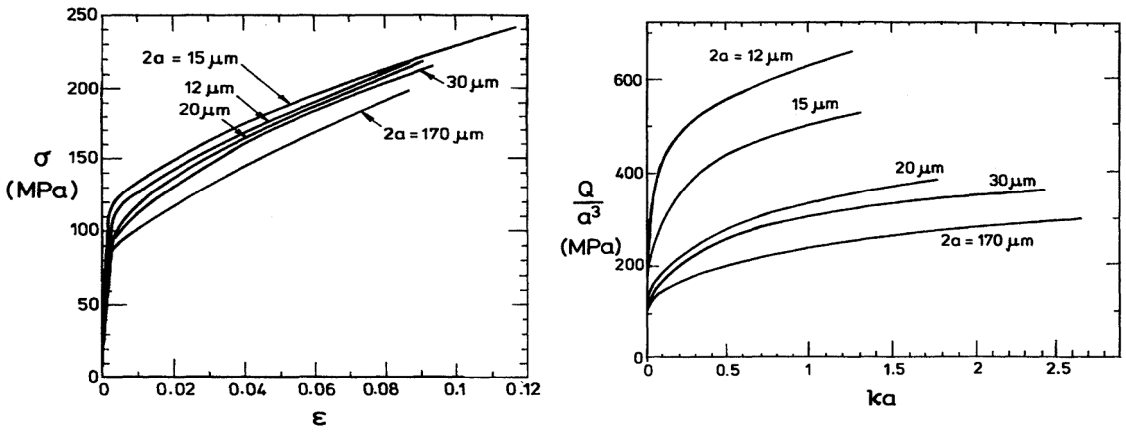

Figure 2.2 : *Data for tension and torsion of fine polycrystalline copper wires: (a) Uniaxial tension true stress σ versus logarithmic strain ε. Except experimental errors, a slight size effect (DS presumedly and pure size effects) is observed as the strain gradient is absent here; (b) Torque versus twist per unit length normalized. Both size and gradient effects exist where the latter is dominant and make largely different between the curves. In such way, the curves with no internal constitutive length scales must fall on top of one another.* (*cf.* Fleck *et al.* [55; 53])

constitutive length parameter, the curves of Fig.2.2.b should plot on top of one another. The difference in strength between the smaller wires over the largest wire reflects the "size effect". Besides, tensile stress-strain data for these same wire are plotted in Fig. 2.2.a. This displays a slight pure size effect apart from some experimental error. Accordingly, the strengthening effect at the micron scale appears to be more strongly associated with non-uniform deformation, as will be discussed in the next section.

A second set of experiments is plastic bending of a series of micron thick nickel films as in Fig.2.4. Strips of the film were bent around a series of fibers of different diameters. Elastic springback upon release of the film was measured providing the moment M associated with the curvature of the fiber κ. The bending data in Fig.2.4 is plotted as M/bh^2 versus the surface strain, $\varepsilon_b = \kappa h/2$, where h is the film thickness and b is the strip width. As in the case of wire torsion, the bending data presented this way should be independent of film thickness if there were no material length parameters operative. The large apparent strengthening of the thinner films over the thicker ones is similar to that observed for the wires in torsion.

A third set of experiments is indentation test which is a common means of assessing material yield strength. Instruments have been developed which permit measurement of indentation hardness at the micron and nano scales. A large size-dependence is observed in indentation tests on metals. Data for tungsten single crystals at three orientations relative to the indenter are shown in Fig.2.5. The hardness is defined as the indentation load divided by the area of the indent after unloading. The Vickers indenter is relatively shallow so that the indentation depth is a fraction of the indentation diagonal plotted in Fig.2.5. There is some dependence of hardness on crystal orientation, but the size-dependence is the predominant effect. Indents with diagonals longer than about $100\mu m$ cease to display any size-dependence. By simple

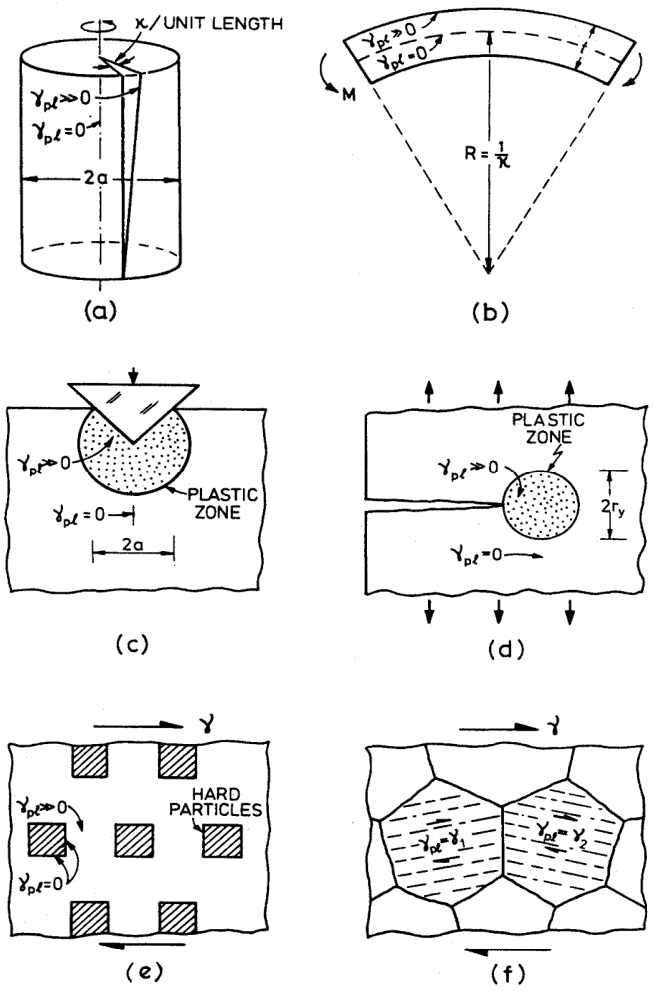

Figure 2.3 : *Plastic strain gradients are caused by the loading and geometry of deformation (a, b), by local boundary conditions (c, d), or by the microstructure itself (e, f).* (*cf.* Fleck *et al.* [55])

dimensional arguments, it follows that any classical plasticity theory (e.g. one that does not possess a constitutive length scale) necessarily implies indentation hardness would be size-independent. The strong size-dependence evident at the micron scale in Fig.2.5 and in data on other metals (Atkinson 1995 [14], Ma and Clarke 1995 [98]; De Guzman *et al.* 1993 [83]; McElhaney *et al.* 1998 [108]; Poole *et al.* 1996 [145]) constitutes the experimental evidence for the need of an extension of plasticity theory, i.e. SGP theory, to the micron scale.

To imagine how is the scope of the SGP theory, three following scales are considered in the light of dislocation theory. **(i)-At the micron scale**, the number of dislocations involved in the indentation zone is usually large - too large to be amenable at the present time to quantitative analysis using discrete dislocation mechanics. Problems in this range of length scales generally have sufficiently large numbers of dislocations that a continuum approach is essential for quantitative modeling; **(ii)-At even smaller scales**, by contrast, discrete dislocation mechanics is required to understand nucleation of dislocations

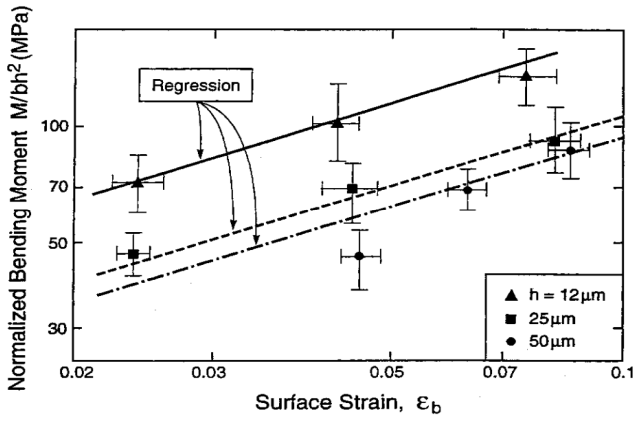

Figure 2.4 : *Normalized bending moment versus normalized curvature ($\varepsilon_b = \kappa_h/2$) for initially straight thin films of nickel subject to bending. The data is presented in such a way that responses for materials with no internal constitutive length scale would superimpose. In this way, the figure brings out the strength increase of thinner films relative to thicker films in bending.* (*cf.* Stolken and Evans [159])

at the indenter and the interaction between relatively small numbers of individual dislocations. That means problems tend to fall into the class where dislocations must be treated as discrete entities. Recent modeling efforts of nano scale indentation of single crystals based on discrete dislocation mechanics appear promising (Tadmore *et al.* 1998 [163]); **(iii)-At length scales above dozen microns**, classical plasticity theories which neglect gradient effects usually suffice.

Data for another common set of experiments, thin film shearing, is plotted in Fig.2.6. The normalized plastic strain decreases with the decrease of the normalized thickness, that means the strengthening is found. However this phenomenon is only observed if one or both surfaces of the thin film are passivated. By contrast, the strength of unpassivated thin films is relatively independent of film thickness and yield strength increases mainly as a result of grain size strengthening and then this belongs to the group 3 as follows.

Group 3: size effect related to microstructure

The well-known phenomenon in micro-mechanics is the so-called "Hall-Petch effect" which states that the yield strength of pure metals increases with diminishing grain size (see Fig.2.7).

On the other hand, after grain size, three categories of micro-grain-size materials can be enumerated as in the common literature: nanocrystalline (NC) metals ($< 100nm$); ultra fine-grained (UFG) metals ($100nm - 1\mu m$); and microcrystalline (MC) metals ($> 1\mu m$), also called coarse-grained (CG) metals. The last one is assumed maybe also in the validity range of the proposed model whose *material characteristic length scale* ℓ is directly related to the material grain size (as an example in Fig.2.8).

A similar phenomenon as "Hall-Petch effect", but for the metal-matrix composites of a given volume fraction of hard particles, in which the strengthening is observed with the decreased particles, as in the case of grain size.

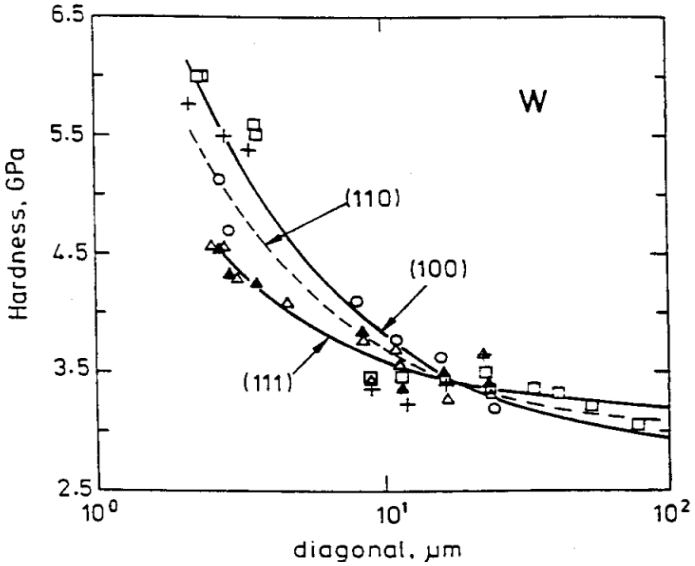

Figure 2.5 : *Hardness data for tungsten single crystals at three orientations relative to the Vickers indenter. The hardness (load divided by the area of the indent) is plotted against the diagonal of the four-sided pyramidal indent displaying the increase in hardness with decrease in indent size* (*cf.* Stelmashenso *et al.* [158])

2.2.2 Anisotropy effect

In micro-mechanics where mechanical behaviors are examined at small scales, the crystal structure (size, order, orientation, cleavage... of crystals) is of certain importance. From a microstructural point of view, the importance of this effect depends on the scale under consideration. In this thesis which is limited to problems related to microsystems (geometry dimension of micrometer) but not to microstructure, the anisotropy effect is not object of study.

2.2.3 Synthesis

The size and gradient effects are two distinct phenomena although they are frequently confused in the literature. The phenomenon "Smaller is Stronger" is attributed mainly to the gradient effect related to the size, and just a little part to the size effect (size effect by DS and pure size effect) in our cases; whereas "Higher Gradient is Stronger" is of course attributed to the gradient effect only. The phenomena become pronounced when the geometry size or microstructure size (indent size, grain size or particle spacing, etc.) lie below approximately $10\mu m$. With the negligibility of the size effect by DS and the pure size effect, it remains only the gradient effect to consider for both "Smaller is Stronger" and "Higher Gradient is Stronger". In this study, only cases where the gradient effect exists are considered. Then taking into account the gradient effect is considered enough to capture these both phenomena experimentally observed. Although the notation "size effect" is still used for "Smaller is Stronger", it is remarked that actually it implies gradient effect related to the size rather than the size effect.

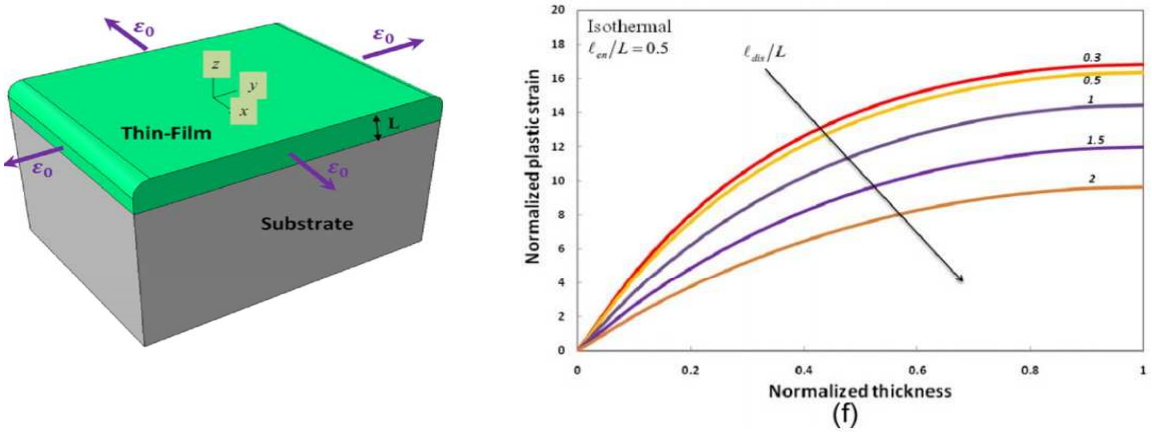

a) Biaxial loading of a thin film on an elastic substrate

b) Shearing test results for different thickness specimens

Figure 2.6 : *Thin-film shearing test: L-film thickness, l-material length scale* (*cf.* Voyiadjis *et al.* [174])

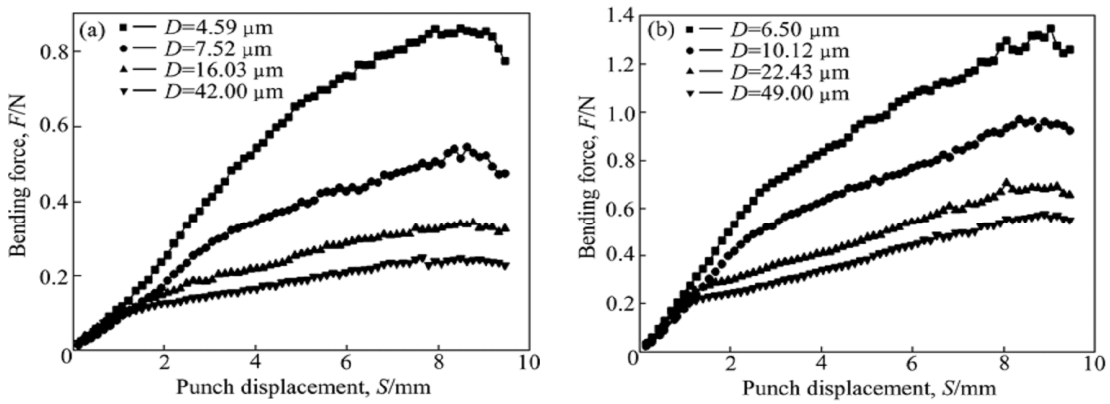

Figure 2.7 : *Curves of bending force-punch displacement under different grain sizes: (a)* $60\mu m$ *in foil thickness; (b)* $80\mu m$ *in foil thickness* (*cf.* Shan *et al.* [151])

The effects discussed above may not all have the same explanation, but it is clear that all require a length scale for their interpretation. A natural way to include "size effect" in the constitutive law is to postulate that the yield stress depends upon gradient. This point of view will be clarified by means of a synthesis of dislocation mechanism presented in the section 2.4 below.

2.3 Review of existing mechanical constitutive models in micro-mechanics

2.3.1 Overview

As aforementioned, when approaching sufficiently small scale, some relevant effects - especially "size" and gradient effects, become important and must be captured in the mechanical behavior models.

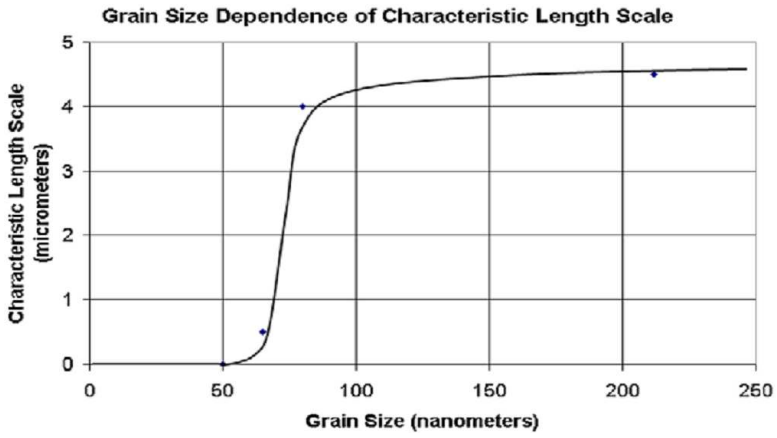

Figure 2.8 : *Evolution of the characteristic length scale with grain size* (*cf.* Haque and Saif [85])

However, classical theories of continuum plasticity possess no material length scale, thereby predict no "size effect" neither gradient effect. Using the classical approach, the material behavior is assumed to be the same even if its size is reduced ad infinitum. Otherwise, using this, common physical effects may be captured, but just available for each specific microstructure (e.g. grain size), and for each specific geometry, i.e. solely available at macroscopic aspect. In microscopic aspect, it requires a set of corresponding parameters for each microscopic scale under consideration (e.g. for each grain and geometry sizes).

For example, consider a Chaboche-type elasto-visco-plastic mechanical behavior model with nonlinear kinematic and isotropic hardening, accompanied with cyclic hardening, in which visco-parameters will be set equal to zero as from the stable cycles. This is applied to nano-copper making chip-to-package interconnections (Fig.2.9 - PhD thesis - Shubhra 2006 [155]) to predict mechanical behaviors of the material. At macroscopic level, a good agreement between experimental-numerical results is found (plasticity, viscosity, cyclicity, creep effects, etc.); at microscopic level, however, the need of a set of parameters corresponding to each grain size clearly proves that the microstructural effect is not captured and that is inherent defect of macroscopic classical models. In other word, changing the grain size (or more generally, microstructure) is equivalent to changing the material.

Therefore it leads to the need of a new class of constitutive models to predict mechanical behaviors at small scale. Basing on effects observed in micro-mechanics as just reviewed, a number of models/theories has been developed by many authors. In physics respect, two kinds of models have been often discussed in the literature. The first one concerns time-independent behaviors, i.e. non-viscous behaviors such as friction, incremental plasticity, brittle fracture or brittle damage. The other deals with time-dependent behaviors, also called viscous behaviors of the materials and is commonly discussed in Visco-Elasticity, Visco-Plasticity, in Phase change as in Damage Mechanics. In methodology respect, after the synthesis of Voyiadjis [176]), a number of theories which have been proposed in the literature for some recent decades to overcome the lack of a length scale in the classical theory of plasticity, are:

- Discrete dislocation dynamics simulations (Nicola *et al.* 2003 [120]; Espinosa *et al.* 2006 [48];

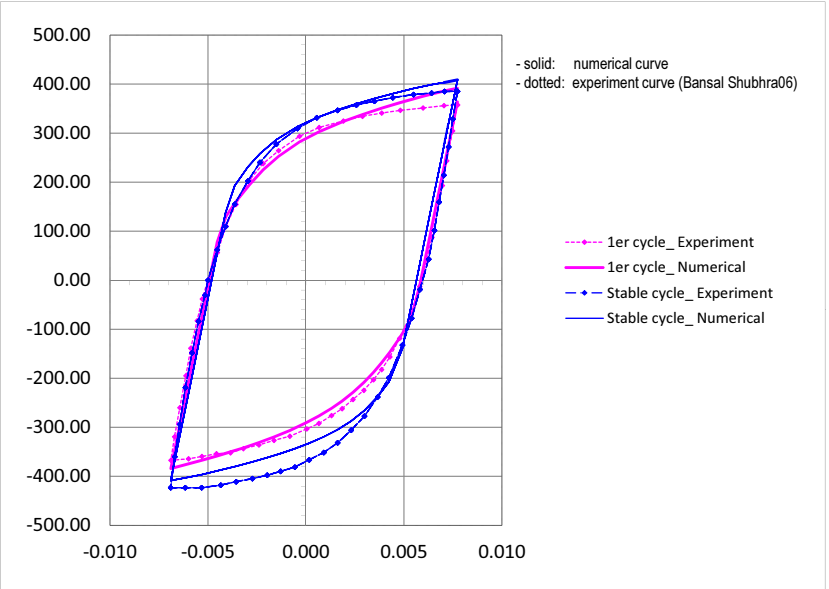

Figure 2.9 : *Chaboche-type elasto-visco-plastic cyclic mechanical behavior of nano-Cu at grain size of* $50nm$ (*cf.* Shubhra [155])

Balint *et al.* 2008 [15]; Kochmann and Le 2008 [92]);

- Molecular dynamics simulations (Schiotz *et al.* 1998 [150]; Warner *et al.* 2006 [178]; Groh *et al.* 2009 [73]; Nair *et al.* 2008 [113]);

- Crystal plasticity theories (Voyiadjis and Huang 1996 [175]; Bittencourt *et al.* 2003 [29]; Ohashi *et al.* 2007 [129]; Ohashi 2004, 2005 [127; 128]; Borg *et al.* 2008 [31]; Mayama *et al.* 2009 [107]; Liu *et al.* 2009 [95]);

- Gradient plasticity theory including two kinds commonly discussed in the literature: strain and stress gradient plasticity theories. In this work, a theory of **Strain Gradient Plasticity (SGP)** will be presented and applied. At this stage, the synthesis about SGP theory is temporarily ignored and will be back as well as detailed in the section (2.5) instead.

The first three classes have been termed "nonlocal models" after (Nilsson 1998 [121]; Stromberg and Ristinmaa 1996 [160]; de Sciarra 2008, 2009 [44; 45]; Polizzotto 2009 [142]). The terminology "nonlocal models" is here used in the sense that the evolution of a state variable (or tensor) at a particular point in the material, is dependent not only on the internal state of the point itself, but also on the state of the neighboring points. In general, this influence is weighed spatially, whereby the magnitude of the influence of a neighboring point is related to the proximity of the point.

The fourth class, SGP theory (i.e. SGP Constitutive Model), is a "coarse" model that has an embedded intrinsic length scale to capture discrete events that occur in the microstructure. The SGP Constitutive Model are our proposal in the current study.

2.3.2 Strain Gradient Plasticity (SGP) Models: promising candidate?

This subsection is devoted to answer a question "Why Gradient Constitutive Model is chosen?". The answer lies on the fact that, among the above classes, thanks to its simplicity and effectiveness in both mathematical formulation and numerical implementation, the SGP theory is much applied in micro-mechanics. Indeed, the gradient formulation is actually considered a higher-order extension of the classical plasticity theory. Thereby this still lies within the general framework of the *classical continuum thermodynamics (macro model)*.

2.4 Why size and gradient effects exist?

Let us recall that, the size effect relates to two sources: Dislocation Starvation and pure size effects; while the gradient concerns three sources: boundary condition, loading mode, and size. A very brief synthesis at this stage is that, the size effect is explained with the "Dislocation Starvation Theory" and with "Theory of Metallurgical defects and Heterogeneity of material"; whereas the gradient effect is interpreted by the "Crystallography Theory".

2.4.1 Dislocation Starvation Theory: not use for the SGP theory

Deshpande *et al.* 2005 [46] investigated the plasticity size effects in tension-compression test of single crystals where the gradients are zero using **discrete dislocation plasticity theory**. Greer *et al.* 2005 [72] addressed the size dependence of the gold at the micron scale in the absence of gradients (see Fig.2.1) using **atomistic simulations**. The same, Nix *et al.* 06 [125] studied the deformation at the nanometer and micrometer length scales in the light of the effects of the gradient and the dislocation starvation. However, as explained right from the Chapter 1, the size effect by Dislocation Starvation is negligible at micron scale and thereby this theory will not here discussed further.

In the framework of the SGP theory that the current study focuses on, gradient-free cases will be deliberately left out. In the next section, non-zero gradient cases will be considered from point of view of the Crystallographic Theory.

2.4.2 Crystallographic Theory: use for the SGP theory

a) Crystallographic basis

Crystallography Mechanism helps explaining the strain gradient effect as well as the role of material length scale in a consistent framework. A synthesis of discussions in [137; 52; 55; 53; 89] to recall crystallographic basis is here represented in this section along with some discussions. The motivation for the current research is provided by experimental results in the emerging fields of micro- and nanotechnology. In order to construct a mathematical formulation that properly models the observed effects, it is necessary to understand the behavior of the material at the most basic level that is relevant to plastic

deformation at this scale. In this section, we review the physical mechanism by which plastic deformation occurs. Physically, a dislocation is a crystallographic defect or irregularity in the crystal structure. The mathematical description implies that dislocations behave as stable particles; they can move, grow and annihilate each other. At the microscopic level, plastic deformation in metallic materials is the end result of the collective behavior of a vast number of dislocations. Hence, crystallographic dislocation densities are appropriate metrics of plastic deformation in metals. These densities can be defined by their magnitude ρ and are typically measured in line length per unit volume. Plastic strain is directly related to the motion of dislocations. Meanwhile, hardening in metals is attributed to the interaction among dislocations and the interaction with the crystal microstructure nearby. These phenomena are driven by dislocation multiplication mechanisms: cross-slip and double cross-slip, glide, climb, etc. Dislocations can also form loops, aggregate at grain boundaries, and arrange themselves into varied types of substructures commonly called dislocation networks. These networks in turn constitute obstacles to the motion of other dislocations. This effect provides the mechanism by which hardening occurs. It may therefore be said that the ease with which dislocation are able to move, determines the degree of hardening in the material. Hence, there are two types of dislocations which should be distinguished by even the simplest dislocation model: mobile and immobile dislocations. These basic types of dislocations correspond to the basic mechanics of plastic deformation, whereby plastic strain is carried by the motion of mobile dislocations, while plastic hardening is related to the resistance from immobile dislocations. As immobile dislocations accumulate, the mobile dislocations interact to an increasing degree with immobile dislocations and movement becomes more and more difficult. Consequently the threshold of stress required to produce additional plastic strain is continuously raised. This phenomenon relates to "hardening" of a material. That critical shear stress which is required to untangle the interacting dislocations and to induce a significant plastic deformation, is defined as the **Taylor flow stress** τ (Taylor 1938 [167]). The Taylor flow stress may also be viewed as the passing stress for a mobile dislocation to glide through a forest of immobile dislocations without being trapped or pinned. The related hardening law, i.e. the Taylor hardening law, relates the shear strength to the dislocation density, and provides a simple description of the dislocation interaction process at the microscale. One form of Taylor's hardening law which is generally accepted in literature is:

$$\tau = \tau_0 + CG\boldsymbol{b}\sqrt{\rho_i} \tag{2.1}$$

where ρ_i is the immobile forest dislocation density, G is the shear modulus, $\boldsymbol{b}$ is the magnitude of the Burgers' vector, and C is a material constant of order unity related to the crystal and grain structure and typically ranging from 0.1 to 0.5 (Ashby 1970 [12]). Meanwhile, τ_0 represents the stress extrapolated to a dislocation density of zero. The immobile forest dislocation density ρ_i is generally assumed to represent the total coupling between two types of dislocations (as elaborated later) that play significant roles in the hardening mechanism. Deformation in metals enhances the formation, motion, and storage of dislocations. Afterward, it is in turn storage of dislocations that is the cause of hardening in the material. On the two types of dislocations, they contain: stored dislocations which are generated by trapping each other in a random way are commonly referred to as statistically stored dislocations (SSDs); whereas

stored dislocations that maintain the plastic deformation incompatibilities within the polycrystal caused by nonuniform dislocation slip, are called geometrically necessary dislocations (GNDs). The presence of GNDs causes additional storage of metallurgical defects and increases the resistance to deformation by acting as an obstacle to the SSDs ([12]). A connection of SSDs to hardening by plastic strain, and of GNDs to that by plastic strain gradient which is regarded as the origin of the gradient effect (including "Smaller is Stronger" that is always confused as a "size effect"), will be analyzed in the next section.

b) Connection with SGP theory, size and gradient effects

The main physical arguments for a size effect within the context of continuum plasticity have already been presented by Fleck and Hutchinson 1993 [52] and Fleck *et al.* 1994 [55], and only a brief summary is reported here. The underlying idea is that material flow strength (or material hardening, more precisely) is controlled by the total density of dislocations stored ρ_i, part of which derives from, and is directly proportional to, the gradient of strain. This part is our main interest in the framework of SGP theory. In this approach, the size-dependence yield strength displayed in each of the cases-studies above is believed to be associated with GNDs generated by non-uniform (non-zero gradient) straining. The distinction between dislocations stored during uniform straining (i.e. SSDs) and those necessitated by gradients of strain (i.e. GNDs) is as follows. Attention is directed to distributions of large numbers of dislocations, and not with individual dislocation interactions.

Dislocation theory suggests that the plastic flow strength of a solid depends on strain gradients in addition to strains (as explained later). Hardening is due to the combined presence of GNDs associated with a plastic strain gradient, and SSDs associated with plastic strain. In general, strain gradients are inversely proportional to the **length scale over which plastic deformations occur**. Thus, gradient effects become important for plastic deformations taking place at small scales. Experimental evidence suggests that flow strength increases with diminishing size, at length scales on the order of several microns or less (as analyzed below by means of the data in Fig.2.10).

When a plastic crystal is deformed, dislocations are generated, move, and are stored; the storage causes the material to work harden. According to the Crystallographic Theory, dislocations are stored for two reasons:

(i) In principle, uniform straining of a single crystal could occur without any dislocations being stored. However dislocations do accumulate by random trapping each other due to statistical interaction with one another and with the microstructural features such as precipitates. These are referred to as SSDs whose density, ρ_S, increases with strain in a complex manner (Ashby 1970, 1971 [12; 13]). As yet, there is no simple theory to predict the density ρ_S as a function of strain, although it has been measured by numerous investigators (see, e.g. Basinski and Basinski 1966 [20]).

(ii) When a crystal is subjected to nearly any gradient of plastic strain, apart from SSDs, GNDs must be stored for compatible deformation of various parts of the crystal. That means GNDs results from gradients of plastic strain which appear either because of the geometry of the solid, or because the material itself is plastically inhomogeneous (containing non-deforming phases, e.g.). As examples:

in the plastic twisting of a cylinder or bending of a beam, the strain is finite at the surface but zero along the axis of twist or of bending [Fig.2.3(a, b)]; in the hardness test the strain is large immediately beneath the indenter but zero far from it; and in the plastic zone at the tip of a crack in an elastic medium steep gradients of plastic strain appear [Fig.2.3(c, d)]; in the deformation of plastic crystals containing hard, non-deforming particles local strain gradients are generated between particles; and in the plastic deformation of polycrystals, the mismatch of slip at the boundaries of the grains can induce gradients of plastic strain there [Fig.2.3(e, f)]. In approximate terms, the magnitude of the plastic strain gradient is of the order of the average shear strain in the crystal divided by the local length scale λ of the deformation field. The density of GNDs, ρ_G, is directly proportional to this plastic strain gradient, and in principle, can be calculated if the gradient of plastic slip on crystal planes is known. In brief, strain gradients require, for compatibility reasons, the presence of GNDs of density ρ_G in addition to that of SSDs, where (*cf.* [12]):

$$\rho_G \approx \frac{4\gamma}{\boldsymbol{b}\lambda} \tag{2.2}$$

Here, γ is the macroscopic plastic shear strain and $\boldsymbol{b}$ is again the magnitude of the Burger's vector.

Some illustrations of the calculation of ρ_G in which each type of dislocation storage mechanism operates can be found at ([55; 53] (e.g. uniaxial straining of a metallic single-crystal bar, plastic bending of an initially straight single-crystal beam to a macroscopic curvature κ, etc.).

It is assumed that the flow strength for a single-slip system of a single crystal depends upon the sum of the densities SSDs, ρ_S, and GNDs, ρ_G, i.e upon $\rho_i = \rho_S + \rho_G$. The simplest possible dimensionally correct relationship between the flow strength τ_γ on the slip plane and total dislocation density is, in accord with Taylor's relation (eq. 2.1),

$$\tau_\gamma = CG\boldsymbol{b}\sqrt{\rho_S + \rho_G} \tag{2.3}$$

where $G, C, \boldsymbol{b}$ as defined before, but C here is taken to be 0.3 by Ashby 1970 [12].

Other couplings between ρ_S and ρ_G to form ρ_i are possible, but anyway the contribution of each one is impossible to deny. And it is now worthy to recall that, among two components of ρ_i, the density of dislocations ρ_S is inherently and always already included in the classical plasticity theory as well-known. Hence, in the case where the length scale λ of deformation field is large enough such that the gradient of plastic strain is small enough, and as a result $\rho_G \ll \rho_S$, the classical plasticity theory is still valid. In other word, classical plasticity laws tacitly assume that $\rho_G \ll \rho_S$ and no length scale enters. Otherwise a modified plasticity theory is then needed to include the important contribution of ρ_G, i.e. of the plastic strain gradient. Accordingly we must now determine in what case the density ρ_G associated with the plastic strain gradient becomes important and must be considered too.

Consider now the order of λ in comparing the magnitudes of ρ_S and ρ_G. In the torsion test, λ is simply the radius of the cylinder; in bending it is the half thickness of the beam; in the hardness test it is related to the indent size; at the crack tip, to the plastic zone size; and in metals containing non-deforming particles λ is related to the particle separation, approximately r/f, where r is the radius and f is the volume fraction of the particles. In polycrystals one might expect it to be related to the grain size.

Figure 2.10 shows a comparison of ρ_S and ρ_G as a function of shear strain γ for a variety of microstructural length scales λ for pure copper. The shaded band marked "Single Crystal" is the measured density ρ_S in single crystal copper, oriented for (initial) easy glide, with three stages as represented in ([55]). In polycrystals, stages I and II are absent as shown in the shaded band labeled "Polycrystal". It is to be emphasized that these are the densities of dislocations which characterize macroscopically uniform deformation - that is, one in which no gradients of strain are imposed. When gradients are present, additional dislocations are required to accommodate them. The figure shows this contribution, calculated from eq. (2.2) for various length scales λ set, as explained, by the particular aspect of geometry (wire radius or beam thickness), imposed displacements (the hardness test) or microstructural feature (particles or grain boundaries) which induce them. We note that at 10% strain $\rho_G \gg \rho_S$ for $\lambda < 50\mu m$ in single crystals and for $\lambda < 20\mu m$ in polycrystals. Thus, there exists a threshold where the density of GNDs swamps the SSDs and hardening is strongly dependent upon strain gradient effects. The smaller the length scale λ of the gradients, the more important the effects become. Finally, the fact that the order of length scale is roughly micron is now confirmed.

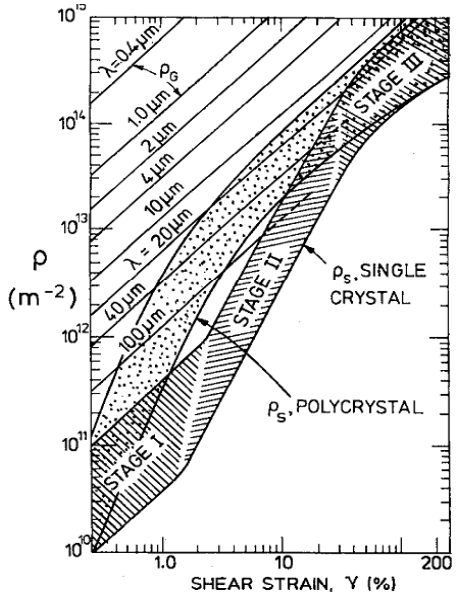

Figure 2.10 : *The density of SSDs ρ_S, and GNDs ρ_G plotted against shear strain. The single crystal density ρ_S (shaded band) is taken from the experimental data (*cf. *Basinski and Basinski [20]); that for polycrystals is inferred from stress-strain curves. The density ρ_G is shown as a set of parallel lines for assumed values of microstructural length scale λ, using eq. (2.2) (cf.* Fleck *et al.* [55])

2.4.3 Synthesis

- Methodology of theory: The main idea here is to develop a continuum theory of plasticity which assures a transition from a behavior independent from strain gradients to that dominated by strain gradient effects. Only non-zero gradient cases are considered, thereby Crystallographic Theory is applied. There

have been attempts to include strain gradients within a plasticity formulation. An approach usually used is to bring in a length scale associated with localization phenomena. To the best of the authors' knowledge, the theories proposed until now have not directly involved GNDs, but are mainly based upon ideas on the thermally activated diffusion of dislocations under a potential gradient. Here we will take the same idea by introducing some gradient hardening terms into the expression of the energy and dissipation potentials as seen in the Chapter 3.

- Validity range of theory: Phenomenological theories of SGP reported in this work are intended for applications to materials and multilayers, whose dimensions controlling plastic deformation fall roughly within the range from a tenth of a micron to ten microns. Problems in this range of length scales generally have sufficiently large numbers of dislocations so that a continuum approach is appropriate for quantitative modeling. At smaller scales, problems tend to fall into the class where dislocations must be treated as discrete entities (e.g. discrete dislocation mechanics). At length scales of dozen microns, classical plasticity theories which neglect gradient effects usually suffice.

2.5 Survey of existing typical SGP Constitutive Models

2.5.1 Overview

Pioneered by Aifantis throughout 1984-2009 with typical works 1984 [4] and 1987 [5], the gradient plasticity theory has been much developed and largely applied by many other authors. It involves typical authors who have developed the theory for a long time such as Fleck and Hutchinson *et al.* 1993-2009 [52; 55; 53; 54; 56; 57], Gurtin *et al.* 2000-2010 with typical ones [76; 80], Voyiadjis *et al.* 2001-2011 with [176; 174], Polizzotto *et al.* 1998-2011 with [141; 144], Willis 1996-2011, Gudmundson *et al.* 2004-2009 with [74], de Borst and Muhlhaus [43], Q.S. Nguyen 2000-2012 [117; 119; 118; 116], etc.

In this section, reviews of Pekmezi 2008 [137], Voyiadjis *et al.* 2010 [176] and Fleck 2001 [54] are here reported to present in a consistent view the state of the art of the gradient plasticity theory.

The gradient formulation may be considered an extension of the local plasticity theory. The introduction of strain gradients into the local theory formulations leads to boundary value problems governed by partial differential equations of higher order with non-standard boundary conditions. There are essentially two strategies for the strain gradient theory formulations: **(1)**- one consists in heuristically introducing the gradient dependence directly into the constitutive equations of the local-type material. This framework of SGP theories does not involve the higher-order stress, and requires no additional boundary conditions. The plastic strain gradient comes into play through the incremental plastic modulus. Examples in this class include the works by (Acharya 2000 [1], Acharya and Beaudoin 2000 [2], Acharya *et al.* 2004 [3], Dai and Parks 1997 [40]). It was concluded that the only possible formulation is a flow theory with strain gradient effects represented as an internal variable which acts to increase the current tangent hardening modulus. These theories are straightforward to implement in standard FE codes. This particular approach was used in predicting polycrystal size effect and cleavage/orientation dependence in the fracture of ductile single crystals. However, criticism has been directed on the model's capability due

to the nonstandard boundary conditions (Niordson and Hutchinson 2003 [122], Volokh and Hutchinson 2002 [170]) and the lack of systematic construction of the tangent modulus (Gao *et al.* 1999 [69]). **(2)**- In another class of SGP theory, formulations are derived by means of suitable energy arguments. A classical example of this strategy is the second strain gradient elasticity theory by Mindlin 1964 [109] in which the higher order stresses are defined as the work conjugate of strain gradient by implying the virtual work principle and a strain energy potential incorporating the strain gradients. Along with the standard equilibrium equations, higher order nonlocal micro force balance equations are retrieved from the variational formulation of the virtual work principle. This additional equation requires the extra boundary conditions. Examples in this class include the works of Fleck and Hutchinson 1997 [53], Fleck and Hutchinson 2001 [54] and Fleck *et al.* 1994 [55] where experimentally observed size effects have been modeled successfully. From a dimensional, an internal constitutive length parameter was introduced to scale the rotational gradient terms in the couple stress theory of the SGP. The physical basis of the length scale is connected to the storage of GNDs (Ashby 1970 [12], Nye 1953 [126]).

Chen and Wang 2002 [38] proposed a new strain gradient theory, based on the general concept of couple stress theory. They implemented their new formulation to solve thin metallic wires in torsion and ultra thin metallic beam bending problems. It was concluded that if the boundary conditions are properly taken in their new theory, the results of the solution will predict the experimental findings provided by Fleck *et al.* 1994 [55] and Stolken and Evans 1998 [159]. Still for problems related to the boundary condition, Xiang *et al.* 2006 [181] used Fleck *et al.* 1994 [55] SGP to capture the Bauschinger effect that is observed in the experimental investigations on Cu thin films with a passivated layer. From these experiments they found that thin films yield strength increased significantly with decreasing film thickness if one or both surfaces are passivated. By contrast, unpassivated thin films are relatively independent of film thickness and yield strength increases mainly as a result of grain size strengthening, a manifestation of Hall-Petch effect.

Gao *et al.* 1999 [69], and Huang *et al.* 2000 [88] proposed a Taylor based nonlocal theory of plasticity to account for the size dependency of the plastic deformation at the micron and submicron scales. The length scale is related to the density of the GNDs as introduced into the constitutive equations via the nonlocal variables which are expressed as an integral of local variables over all material points in the body. Gao and Huang 2001 [68], Zhang *et al.* 2007 [183], and Shi *et al.* 2008 [154] applied this theory to micro- bending, micro tension, void growth, cavitations' instabilities and particle reinforced composites. Their analyses results in identical predictions as in the mechanism-based strain gradient (MSG) plasticity. This higher order strain gradient theory is established from a multiscale, hierarchical framework to connect with the Taylor model in dislocation mechanics (Taylor 1934, 1938 [166; 167]). Results obtained using the MSG model agrees well with the work of McElhaney *et al.* 1998 [108] on micro-indentation experiments of bulk copper, Gao *et al.* 1999 [69] and Saha *et al.* 2001 [149] on indentation experiments of aluminum thin film on a glass substrate, Fleck *et al.* 1994 [55] on micro-torsion, Stolken and Evans 1998 [159] on micro-bending experiments (see Gao *et al.* 1999 [69]), and on metal-matrix composites (Xue *et al.* 2002 [182]). It has also been successfully applied to study a few

important problems at the micron and submicron scales, including micro-electro-mechanical systems (Saha *et al.* 2001 [149]), plastic flow localization (Shi *et al.* 2000 [152]), and fracture (Jiang 2001 [91]; Lu *et al.* 2000 [164]).

Shi and Gao 2001 [153] recently used the singular perturbation method to investigate a solid subjected to a constant body force, and showed that the effect of the higher-order stresses is significant only within a thin layer near the boundary of the material. Comparing the material length scale used in strain gradient theories, the thickness of the boundary layer is much smaller and is on the order of $10nm$. These results are interpreted by Huang *et al.* 2000 [88] and Saha *et al.* 2001 [149] as the higher-order stress has little or essentially no effect on material properties that represent an average over the micron scale and above, such as the micro-indentation hardness. Therefore, they distinguished the effect of higher-order stress from the strain gradient effect by defining the former is within a thin boundary layer (thickness on the order of $10nm$) and the latter comes from the Taylor dislocation model and is important at the micron scale. As part of this separation they concluded that the effect of higher-order stress is negligible away from the thin boundary layer, and argued the possibility to develop a SGP theory based on the dislocation model to incorporate the strain gradient effects without the higher-order stress. The reason to eliminate the effect of higher order stress from the governing equations in such a theory is to avoid from the additional boundary conditions and to have essentially the same boundary conditions as in the classical plasticity theories.

Gurtin 2004 [78] developed a gradient theory of small deformation viscoplasticity based on the system of micro forces consistent with its peculiar balance, a mechanical version of the second law and a constitutive theory that includes Burgers vector through a free energy dependence on where represents the plastic part of the elastic plastic decomposition of the displacement gradient. Later Anand *et al.* 2005 [10] studied the one dimensional theory of the SGP by performing analytical and numerical analyses by means of nonlocal finite element on three distinct physical phenomena such as internal variable hardening, energetic hardening with back stress associated with plastic strain gradient and dissipative strengthening associated with plastic strain rate and resulting in a size dependent increase in yield strength.

Gudmundson 2004 [74] formulated the small SGP for isotropic materials based on the balance law and dissipation inequality. He addressed boundary conditions and concluded that there is a close connection between surface energy of an interface and boundary conditions in terms of plastic strain and moment stress. A simple version of the theory was applied to a few examples such as biaxial loading of a thin film on thick substrate, torsion of thin wire and spherical void under remote hydrostatic tension in order to investigate the effect of varying length scales. This formulation is later used to analyze the size dependent yield strength of thin films by Fredriksson and Gudmundson 2005 [63]. The results of their numerical analysis from these studies reveals that boundary layer is developed in the thin film for both biaxial and shear loading giving rise to size effects. These size effects are strongly connected to the buildup of surface energy at the interface. These effects of interface surface energy on the plastic deformation at the micron scale were motivated by Fredriksson and Gudmundson 2007 [64] in order

to conduct a detailed study on modeling of the interface between a thin film and a substrate. They addressed this issue within the framework of SGP and proposed two kinds of interface models for isotropic materials. First kind is based on the assumption that plastic work at the interface is completely stored as a surface energy and no dissipation occurred due to plasticity at the interface. In the second type it is assumed that the plastic work is completely dissipated and there is no build up of a surface energy. Two types of length scales are introduced, one is for the behavior of the bulk material the other is for the interface. Their model can be considered in the same class of the existing interface models proposed by Cermelli and Gurtin 2002 [37], Gurtin and Needleman 2005 [82], Sun *et al.* 2000 [161], Gurtin 2008 [79], and Borg and Fleck 2007 [30]. Gurtin and Needleman 2005 [82] and Cermelli and Gurtin 2002 [37] addressed in their work the application of SGP for the case of crystal plasticity. In the case of Gurtin and Needleman 2005 [82] they assumed continuity of the conjugate higher-order stresses on both sides of the interface. However, Cermelli and Gurtin 2002 [37] assumed a jump at the interface of the conjugate higher order stresses. Both Gurtin and Needleman 2005 [82] and Cermelli and Gurtin 2002 [37] used dissipative mechanisms to model the interface (grain boundaries) using a viscoplastic model that involved plastic slip rates at both sides of the interface as well as conjugate higher order stresses on both sides of the interface. In both cases they included discontinuities in plastic strains over the interface.

Willis and co-workers (Aifantis and Willis 2005 [7], Aifantis *et al.* 2006 [6]) modeled the interface by a surface contribution to the strain energy that depends on the plastic strain at the interface. The distinct feature of this formulation is to introduce an interfacial yield stress that allows the interface to follow its own yield behavior. This interfacial yield stress is then described via dislocation transfer phenomena where its physical justification is made from observations of the nano-indentation near grain boundaries of body-centered cubic (bcc) metals. The main distinction of the work of Willis and co-workers from that of Gurtin and coworkers is that Willis and co-workers assumed a continuity in the plastic strain over the interface with a jump in the conjugate higher-order stresses.

One of the open issues of the SGP is the ongoing discussion of the energetic and dissipative nature of the dislocation network that accounts for many plasticity phenomena. Gurtin argued that the density of geometrically necessary dislocations is quantified by Nye's tensor, which leads to an increase in the free energy. However, Fleck and Willis 2009a,b [56; 57] discussed this issue by questioning whether the additional strengthening is mainly energetic or dissipative. They assumed that the core energy of dislocations stored during plastic deformation is much smaller than the plastic work dissipated during dislocation motion. Based on this observation they concluded that both SSDs stored and GNDs contribute more to the plastic dissipation than to a change in energy. Bardella 2006, 2007 [18; 19]pointed out that modeling involving only energetic material length scales may not be sufficient to describe the size effects exhibited in metals. He reasoned the fact that energetic length scales, defined through a function of Nye's dislocation density tensor, allows the description of the increase in strain hardening accompanied with diminishing size, but they do not help in capturing the related strengthening.

Recently, Gurtin and Anand 2009 [81] revisited the theories of Aifantis and Fleck and Hutchinson to discuss the physical nature of their flow rules based on thermodynamic principles. In their study they

arrived to the following conclusions: (i) the flow rule of the Aifantis theory obeys the thermodynamic constraints if the nonlocal term, which was defined as the Laplacian of the accumulated plastic strain is energetic; (ii) the flow rule of Fleck and Hutchinson 2001 [54] is inconsistent with thermodynamics unless its nonlocal term is ignored. Voyiadjis and Deliktas 2009a,b [172; 173] investigated the interfacial effect in parallel with the works of Willis and coworkers (Aifantis and Willis 2005 [7]; Fleck and Willis 2009a,b [56; 57]) and Gudmunsond and coworkers (Gudmundson 2004 [74]; Fredriksson and Gudmundson 2005 [63]; Fredriksson and Gudmundson 2007 [64]) by using the higher-order gradient dependent plasticity theory (AbuAl-Rub *et al.* 2007 [8]; Voyiadjis and Abu Al-Rub 2007 [171]) where microstress boundary conditions at the interface and free surfaces are enforced. In these works (Voyiadjis and Deliktas, 2009a,b [172; 173]) they assumed that the total strain energy stored at the interface can be expressed in terms of the plastic strain state at the interface (Gudmundson 2004 [74]; Gurtin 2002 [77]; Benallal 1995, 2001, 2007 [27; 25; 26], Fredriksson and Gudmundson 2007 [64]; Gurtin and Anand 2009 [81]; Fleck and Willis 2009a,b [56; 57]).

2.5.2 Typical works

It can be listed here some typical works until now such as:

- Gradient-dependent plasticity model: de Borst and Muhlhaus 1992 [43];
- A reformulation of strain gradient plasticity: Fleck and Hutchinson 2001 [54];
- A unified treatment of strain gradient plasticity: Gudmundson 2004 [74];
- Strain gradient plasticity with strengthening effects and plastic limit analysis: Polizzotto 2010 [144];
- Nonlocal gradient-dependent modeling of plasticity with anisotropic hardening: Voyiadjis *et al.* 2010 [176];
- Nonlocal continuum effects on bifurcation in the plane strain tension-compression test: Benallal and Tvergaard 1995 [27];
- Standard Gradient Models and Gradient Plasticity: Q.S. Nguyen 2005, 2011, 2012 [119; 118; 116];
- And many other works...;

2.6 Strain Standard Gradient Plasticity (SSGP) Constitutive Model

2.6.1 Why SSGP Constitutive Model? Formulation and numerical implementation

In the same spirit as in the section 2.3.2, it needs to make clear "Why Standard Gradient Constitutive Model is chosen?". The reason again lies on its simplicity and effectiveness in both formulation and numerical implementation aspects.

Among SGP theories inherently based on classical laws of continuum thermodynamics, the SSGP theory is built in the framework of the generalized standard materials (Halphen and Q.S. Nguyen 1975 [84], Q.S. Nguyen [117]) using an extended version of virtual work principle (Frémond 1985 [65] or Gurtin 1996 [76]) and the development of Q.S. Nguyen 2005, 2011, 2012 ([119; 118; 116]). The standard

gradient of internal parameters are directly introduced in the energy and dissipation potentials of the model. The thermodynamically consistent equations of the **"SSGP Constitutive Model"** or briefly **Gradient Model**, are derived for the standard gradient plasticity yield criterion and associated flow rule. The Gradient Model of such formulation is considered a higher-order extension of the classical plasticity theory, then still lies within the general framework of the classical macro model. This therefore possesses the simplicity as well as effectiveness in both formulation and numerical implementation, then is chosen in the thesis.

Apart from the characteristics as in classical models, there are also obviously some new features, actually some difficulties. That is, in addition to the inherent boundary conditions of classical plasticity, *secondary boundary condition (insulation boundary condition*, *cf.* Polizzotto 2003 [141]), is introduced. The introduction of strain gradients into the local theory formulations leads to a *Laplacian equation* solved at *global level*, and to *boundary value problem* governed by partial differential equations of higher order with *non-standard boundary conditions*, therefore much more difficult to solve. However, these difficulties are treated with a computational method based on diffusion like-problem spirit. Indeed, the **Laplacian equation at global level** is here easily solved numerically with UMATs built in usual available FE codes (*cf.* CAST3M for example).

The thesis actually discusses not only the standard gradient plasticity theory but also higher-gradient version where the presence of higher gradients of the internal parameters can also be taken into account ($\nabla\phi$, $\nabla\nabla\phi$, etc.). However the numerical implementation of the latter is ignored and its effectiveness is still and open question.

2.6.2 Framework

In this work, only cases with the presence of the gradient effect besides the inherent pure size effect, are considered. Cases without gradient effect are here not our object of study. In such a condition, the SSGP model is considered enough to capture the "size" and gradient effects as principles stated in Section (2.4) and as proved via a good validation in Section (3.2.2).

The size effect in gradient-free cases may be taken into account not via SSGP theory, but via other theories such as discrete dislocation plasticity theory Deshpande *et al.* 2005 ([46]), atomistic simulations Greer 2005 *et al.* ([72], Nix *et al.* 2006 [125]), etc.

Besides, basing on available reference data, the "size" and gradient effects concerning the **microsystems' geometry size** (groups 1,2) will be confirmed to be successfully and directly captured with the adopted models. As for those concerning the **material microstructure size** (group 3), it is assumed that these effects may be also captured by the models thanks to the presence of the material internal length scale related to the microstructure size. Nevertheless, the validation for these cases has been left out due to the lack of experimental database.

2.6.3 Application

In this thesis, the Gradient Model is used to examine the three first ones of some typical problems for the gradient theory. Those are:

1. **Micro-void growth test** under remote spherically symmetric tension/pressure (plotting curves of "remote spherically symmetric tension versus volume expansion of a micron spherical void", and of "plastic shear versus radius of the micron spherical void") ([54] and [74]).

2. **Thin wire torsion test** (plotting curves of "torque versus twist of a micron solid cylindrical wire", and of "plastic shear versus radius of the micron solid cylindrical wire") ([54] and [74]).

3. **Thin film shearing test**, some typical problems as follows:
   - Biaxial/shear loading of a thin film on a substrate (plotting curves of "biaxial/shear plastic strain across the thin film thickness", "biaxial/shear stress across the thin film thickness", "average biaxial stress versus biaxial strain of the thin film", and of "average biaxial stress versus normalized length scale of the thin film") ([176]);
   - Shear loading of a thin film sandwiched between two substrates (plotting curves of "distribution of plastic shear strain across the thickness of thin film", and of "shear stress versus shear displacement of the thin film") ([54]).

4. **Micro-indentation test** (plotting a curve of "hardness versus diameter of micron indenter") ([93], [23], [89], [180]).
   This problem is actually very related to the micro-void growth. In the literature, one even uses micro-indentation problem result as approximate result of the micro-void growth problem.

5. **Micro-bending test** of thin beams or thin metal sheets/foils (plotting a curve of "normalized bending moment versus the normalized curvature") ([159], [177], [90], [143], [151]).

It will be shown in this study that, using the Gradient Model for these problems, the "size" and gradient effects are well captured to represent both phenomena "Smaller is Stronger" and "Higher Gradient is Stronger".

2.7 Conclusion

At small scales, some effects such as the size, gradient,...and anisotropy effects become important and must be taken into account. Only the **size and gradient effects at the micron scale** are here investigated in the context that the pure size effect, the size effect by DS are negligible; and the anisotropy effect is ignored. Experimental evidences show that the size and gradient effects are actually two distinct phenomena. There is also a correlation between them in many cases. The phenomenon "Higher Gradient is Stronger" is related to the gradient effect only, while "Smaller is Stronger" is related to both size and gradient effects where the latter is dominant. Taking into account only the gradient effect (related to all

its sources) is enough to capture both "size" and gradient effects on plastic behavior, thereby capture both "Higher Gradient is Stronger" and "Smaller is Stronger". Three groups of the "size" and gradient effects commonly discussed are: the first associated with the loading mode and geometry size, and the second with boundary condition of **microsystems**; the third related to the **microstructure** of material and left out in this work.

Classical theories of continuum plasticity predict however no "size effect" neither gradient effect. It leads to the need of a new class of constitutive models to predict mechanical behaviors at small scale. A number of theories has been developed by many authors (discrete dislocation dynamics simulations, molecular dynamics simulations, etc.). Among these theories, the **SGP theory**, is chosen because of its simplicity and effectiveness in both formulation and numerical implementation. The gradient formulation is in fact an extension of the classical plasticity theory and still lies within the general framework of the *classical continuum thermodynamics*.

The effectiveness of the SGP Model in capturing the "size" and gradient effects whereby both phenomena "Smaller is Stronger" and "Higher Gradient is Stronger" are captured, lies on the mechanism of these phenomena. This mechanism states that material hardening is due to the combined presence of GNDs associated with a plastic strain gradient, and SSDs associated with plastic strain. The role of SSDs is already taken into account in classical models, but that of GNDs is just captured with the new model by means of the gradient terms and the internal length scale. With such an approach, SGP Constitutive Model is only used to treat the non-null gradient problems.

Among SGP theories, the **SSGP theory** is chosen also due to its most simplicity and similarity to classical continuum thermodynamics ones. Although there are also some difficulties, the final equation i.e. **Laplacian equation at global level**, can be numerically solved based on diffusion like-problem spirit.

Only the "size" and gradient effects concerning the **microsystems** are considered here. A few applications (thin wire torsion, thin film shearing, micro void growth) are given.

CHAPTER 3

Standard Gradient Constitutive Models

The outline of the work is as follows. In Section (3.1), formulation, variational inequality and some applications of SSGP Constitutive Models are given; Section (3.2) is devoted to numerical implementation; Sections (3.3) are conclusions and comments; and finally, more details about numerical implementation are given in Appendix .1

3.1 Standard Gradient Models: formulation, variational inequality and application

3.1.1 Introduction

The introduction of the gradients of the state variables such as the strain, the internal parameter and even the temperature in Solid Mechanics has been much discussed in the literature since the pioneering works of Mindlin and Toupin in second-gradient elasticity. Especially, in the two last decades, standard gradient theories has been considered in many papers, *cf.* for example [65], [67], [106], [76], [141], [60], for the modeling of phase change and solids with microstructures. In particular, in Frémond or Gurtin's approach (cf. [65], [76]), the governing equations have been originally derived from an additional virtual work equation. These models have been applied in various applications such as **gradient plasticity** and **gradient damage**.

The developments undertaken in this section are based on Q.S. Nguyen published works [119; 118] and private communication [116]. A particular case of Gradient Model of accumulated plasticity γ with isotropic and kinematic hardening [116] will be focused on.

The objective of this work is to revisit the proposed approach by Q.S. Nguyen 2005 and 2011 (*cf.* [119] and [118]). Using the formalism of the generalized standard materials, a dissipation analysis is considered in order to derive the general expression of the governing equations for the internal parameters in terms of the energy and dissipation potentials. Gradient and higher-gradient models can be discussed in the same spirit. In particular, the governing equations for the Standard Gradient Models can be written as a generalized Biot equation.

For a time-independent behavior such as incremental plasticity or brittle fracture or brittle damage, our attention is focussed on the derivation of some theoretical results, which are well known in classical plasticity, such as the governing equations of the global response and the determination of the rate response and the associated variational principles. After all, a consistent mathematical description of the

theory of Gradient Plasticity is proposed and is illustrated with some particular cases in the application section.

3.1.2 Standard Gradient Models

In the internal variable framework, the thermo-mechanical response of a solid V in a reference configuration is described by the fields of displacement u, internal parameter ϕ and temperature T. The internal parameter is a scalar or a tensor and represents physically hidden parameters such as micro-displacements or phase proportions or inelastic strains, etc.

Standard Gradient Models for the internal parameter assume that the set of state variables $(\nabla u, \phi, \nabla\phi, T)$ is necessary and sufficient to describe the material behavior. The constitutive equations can be given in the following way (cf. Fremond , Gurtin,...) in an isothermal transformation.

a) Generalized Forces and Virtual Work Equation

It is first accepted that the state variables $(\nabla u,\ \phi,\ \nabla\phi)$ are associated with the generalized forces $\boldsymbol{\sigma}, X, \boldsymbol{Y}$ such that a **generalized virtual work equation** holds:

$$P_i + P_j = P_e \quad \forall \quad \delta u, \delta\phi \tag{3.1}$$

with

$$\begin{cases} P_i = \int_V (\boldsymbol{\sigma} \cdot \nabla\delta u + X \cdot \delta\phi + \boldsymbol{Y} \cdot \nabla\delta\phi)\, dV \\ P_j = \int_V \rho\ddot{u} \cdot \delta u\, dV \\ P_e = \int_V (f_{vu} \cdot \delta u + f_{v\phi} \cdot \delta\phi)\, dV + \int_{\partial V} (f_{su} \cdot \delta u + f_{s\phi} \cdot \delta\phi)\, da \end{cases} \tag{3.2}$$

where (f_{vu}, f_{su}) and $(f_{v\phi}, f_{s\phi})$ are respectively external body and surface forces associated with the displacement and the internal parameter. This leads, after integration by parts, to the *mechanical equilibrium equation* (also called the **Biot equilibrium equation** [28]) and the associated boundary condition equations:

$$\begin{cases} \nabla \cdot \boldsymbol{\sigma} + f_{vu} = \rho\ddot{u} \ \text{ on } \ V & (a) \\ \boldsymbol{\sigma} \cdot \boldsymbol{n} = f_{su} \ \text{ on } \ \partial V_{fu}, \ \ u = u_d \ \text{ on } \ \partial V_u; \ \ \partial V_{fu} \cap \partial V_u = \partial V & (b) \end{cases} \tag{3.3}$$

and the following *constitutive equilibrium equations* (also termed the **extended Biot equilibrium equation**) together with the corresponding boundary condition, holding for internal parameter:

$$\begin{cases} \nabla \cdot \boldsymbol{Y} - X + f_{v\phi} = 0 \ \text{ on } \ V & (a) \\ \boldsymbol{Y} \cdot \boldsymbol{n} = f_{s\phi} \ \text{ on } \ \partial V & (b) \end{cases} \tag{3.4}$$

These equations are easily understood when $\boldsymbol{Y}$ is a micro-stress, ϕ is a micro-displacement and X is then an internal volume force, homologous with the stress $\boldsymbol{\sigma}$, displacement u and external body force f_{vu}.

b) Energy and Dissipation Potentials: State and Complementary Laws

Standard Gradient Models also assume that there exists an energy potential $W(\nabla u, \phi, \nabla\phi)$ and a dissipation potential $D(\nabla\dot{u}, \dot{\phi}, \nabla\dot{\phi}, \nabla u, \phi)$ per unit reference volume. The energy potential $W(\nabla u, \phi, \nabla\phi)$ gives the state law, i.e. the non-dissipative thermodynamic forces associated with the *state variables*. The dissipation potential $D(\nabla\dot{u}, \dot{\phi}, \nabla\dot{\phi}, \nabla u, \phi)$ brings the **complementary law** i.e. the dissipative thermodynamic forces associated with the *state variables rates*. These equations are written as:

$$\begin{cases} W = W(\nabla u, \phi, \nabla\phi), \quad D = D(\nabla\dot{u}, \dot{\phi}, \nabla\dot{\phi}, \nabla u, \phi) \\ \boldsymbol{\sigma} = \boldsymbol{\sigma}_e + \boldsymbol{\sigma}_d, \quad \boldsymbol{\sigma}_e = W_{,\nabla u}, \quad \boldsymbol{\sigma}_d = D_{,\nabla\dot{u}} \\ X = X_e + X_d, \quad X_e = W_{,\phi}, \quad X_d = D_{,\dot{\phi}} \\ \boldsymbol{Y} = \boldsymbol{Y}_e + \boldsymbol{Y}_d, \quad \boldsymbol{Y}_e = W_{,\nabla\phi}, \quad \boldsymbol{Y}_d = D_{,\nabla\dot{\phi}} \end{cases} \tag{3.5}$$

where: the low indexes "e" and "d" imply elastic (non-dissipative rather) and dissipative forces. When the potentials W and D are smooth functions of their arguments (the dissipation potential may be state-dependent via the current value of the variable ϕ), the relationships $X_d = D_{,\dot{\phi}}$, $\boldsymbol{Y}_d = D_{,\nabla\dot{\phi}}$ describe a time-dependent behavior of the materials and are commonly discussed in Visco-Elasticity, Visco-plasticity, Phase change as Damage Mechanics.

The case of convex but non-smooth dissipation potentials is also interesting. For example, D is a convex, positive homogeneous of degree 1 in *time-independent processes* such as *friction, plasticity, brittle fracture and brittle damage*. This case will be further discussed.

c) Governing Equations

The equations (3.3), (3.4), (3.5) are the governing equations of a Standard Gradient Model. In terms of the two potentials, the governing equations for the fields of unknown $\mathbf{u}, \boldsymbol{\phi}$ are:

$$\begin{cases} \nabla \cdot (w_{,\nabla u} + D_{,\nabla\dot{u}}) + f_{vu} = \rho\ddot{u} & \forall x \in V \quad (a) \\ (w_{,\nabla u} + D_{,\nabla\dot{u}}) \cdot n = f_{su} \quad \forall x \in \partial V_{fu} \ , \quad u = u_d \ \forall x \in \partial V_u & (b) \\ \nabla \cdot (w_{,\nabla\phi} + D_{,\nabla\dot{\phi}}) - \ w_{,\phi} - D_{,\dot{\phi}} + f_{v\phi} = 0 & \forall x \in V \quad (c) \\ (w_{,\nabla\phi} + D_{,\nabla\dot{\phi}}) \cdot n = f_{s\phi} & \forall x \in \partial V \quad (d) \end{cases} \tag{3.6}$$

These equations describe the response of the solid from an initial position of state and velocity. The forces $f_{v\phi}$ and $f_{s\phi}$ appears as physical data. In this spirit, the condition $f_{v\phi} = 0$ and $f_{s\phi} = 0$ has been denoted as the **constitutive insulation condition** following a terminology due to Polizzotto [141]. The response of a solid under insulation condition has been discussed by several authors, *cf.* [65], [141], [60], [96].

3.1.3 Generalized Standard Formalism

The governing equations (3.6) can be also derived directly from the formalism of generalized standard materials [84]. This formalism states that the dissipative forces, obtained from the expression of the

dissipation, are also derived from the dissipation potential.

a) Dissipation Analysis

Indeed, the solid V admits as energy and dissipation potentials:

$$\mathbf{W}(\mathbf{U}) = \int_V W(\nabla u, \phi, \nabla\phi)\, dV \quad , \quad \mathbf{D}(\dot{\mathbf{U}}, \mathbf{U}) = \int_V D(\dot{\phi}, \nabla\dot{\phi}, \phi)\, dV \tag{3.7}$$

where $\mathbf{U} = (\mathbf{u}, \boldsymbol{\phi})$ denotes the fields of displacement and internal parameter. Under the applied forces [1]

$$\mathbf{F} \cdot \delta\mathbf{U} = \int_V f_{vu} \cdot \delta u\, dV + \int_{\partial V} f_{su} \cdot \delta u\, da \tag{3.8}$$

and insulation condition, the dissipation of the solid is by definition the unrecoverable part of the received energy per unit time

$$D_V = \mathbf{F} \cdot \dot{\mathbf{U}} - \frac{d}{dt}\big(\mathbf{W}(\mathbf{U}) + \mathbf{K_t}\big) \tag{3.9}$$

where $\mathbf{K_t} = \int_V \frac{1}{2}\rho\dot{u}^2\, dV$ denotes the kinetic energy. As the dissipation is positive, taking account of the fundamental law of dynamics leads to:

$$D_V = \int_V ((\boldsymbol{\sigma} - w_{,\nabla u}) : \nabla\dot{u} - w_{,\phi} \cdot\dot{\phi} - w_{,\nabla\phi} \cdot\nabla\dot{\phi})\, dV \quad \geq \quad 0 \tag{3.10}$$

b) Generalized Standard Formalism

The dissipation D_V is a product of forces and fluxes. For any field of fluxes $(\delta\mathbf{u},\ \delta\boldsymbol{\phi})$ defined on V, the power of the dissipative forces $\mathbf{F_d}$ is:

$$\mathbf{F_d} \cdot\ \delta\mathbf{U} = \int_V \big((\boldsymbol{\sigma} - w_{,\nabla u}) : \nabla\delta u - w_{,\phi} \cdot\delta\phi - w_{,\nabla\phi} \cdot\nabla\delta\phi\big)\, dV \tag{3.11}$$

The generalized standard formalism consists of admitting that

$$\mathbf{F_d} \cdot\ \delta\mathbf{U} = \mathbf{D}_{,\dot{\mathbf{U}}} \cdot \delta\mathbf{U} \quad \forall\ \delta\mathbf{U} \tag{3.12}$$

Thus

$$\begin{cases} \int_V (D_{,\nabla\dot{u}} \cdot\nabla\delta u + (D_{,\dot{\phi}} - \nabla \cdot D_{,\nabla\dot{\phi}}) \cdot\ \delta\phi)\, dV + \int_{\partial V} n \cdot D_{,\nabla\dot{\phi}} \cdot \delta\phi\, da \\ = \int_V ((\boldsymbol{\sigma} - w_{,\nabla u}) : \nabla\delta u - (w_{,\phi} \cdot - \nabla \cdot w_{,\nabla\phi}) \cdot\ \delta\phi\ )\, dV + \\ - \int_{\partial V} n \cdot w_{,\nabla\phi} \cdot \delta\phi\, da \qquad \forall\ \delta u,\ \delta\phi \end{cases} \tag{3.13}$$

It results from a classical argument (Haar lemma in Variational Calculus) [2] that the following equations hold:

$$\begin{cases} \nabla \cdot (\boldsymbol{\sigma} - w_{,\nabla u} - D_{,\nabla\dot{u}}) = 0 \\ w_{,\phi} - \nabla \cdot w_{,\nabla\phi} + D_{,\dot{\phi}} - \nabla \cdot D_{,\nabla\dot{\phi}} = 0 \quad \in V, \quad and \\ (\boldsymbol{\sigma} - w_{,\nabla u} - D_{,\nabla\dot{u}}) \cdot n = 0 \quad \forall x \in \partial V_{fu}\ ,\ \ u = u_d \quad \in \partial V_u \\ (w_{,\nabla\phi} + D_{,\nabla\dot{\phi}}) \cdot n = 0, \qquad \in \partial V \end{cases} \tag{3.14}$$

[1] Bold face letters for $\boldsymbol{\phi}$ or $\mathbf{u}$ refer to fields whereas normal letters ϕ and u refer to local values. This convention is just available for ϕ and u

[2] For any tensor fields F and G, the variational condition $\int_V (F \cdot \delta\phi + G : \nabla\delta\phi)\, dV = 0$ for all $\delta\phi$, which can be written as $\int_V (F - \nabla \cdot G) \cdot \delta\phi\, dV + \int_{\partial V} (G \cdot n) \cdot \delta\phi\, da = 0$ for all $\delta\phi$, implies after Haar lemma that $F - \nabla \cdot G = 0$ in V and that $G \cdot n = 0$ on ∂V

It is then clear that the governing equations (3.6) are recovered.

c) Generalized Extended Biot Equation

In the same spirit but more general, the current work will present a Gradient Model in which the presence of standard and higher gradients of the internal parameter are taken into account in governing equations. For example, if the expression of the energies include the standard and second gradients, i.e the energy potential $W(\nabla u, \phi, \nabla\phi, \nabla\nabla\phi)$ and the dissipation potential $D(\nabla\dot{u}, \dot{\phi}, \nabla\dot{\phi}, \nabla\nabla\dot{\phi}, \nabla u, \phi)$, then the **generalized version** of the Biot equilibrium (Eq. 3.3) and of the extended ones (Eq. 3.4) can be written under the **local form**:

$$\begin{cases} \bullet\ \forall x \in V \\ \qquad \frac{\delta W}{\delta u} + \frac{\delta D}{\delta \dot{u}} = f_{vu} - \rho\ddot{u}, \qquad \text{after } (3.6.a) \\ \qquad \frac{\delta W}{\delta \phi} + \frac{\delta D}{\delta \dot{\phi}} = f_{v\phi}, \qquad \text{after } (3.6.c) \\ \bullet\ \forall x \in \partial V : \qquad \text{appropriate condition after } (3.6.b) \text{ and } (3.6.d) \end{cases} \tag{3.15}$$

with the popular notation (notation of variational derivation):

$$\frac{\delta G}{\delta x} = G_{,x} - \nabla \cdot G_{,\nabla x} + \nabla\nabla \cdot G_{,\nabla x} - \dots \tag{3.16}$$

Using the notation (3.16) and the state and complementary laws (3.5), to consider for example the case of standard gradient of the internal parameter, the following extended forces A_e^ϕ and A_d^ϕ are defined:

$$\begin{cases} A_e^\phi = \frac{\delta W}{\delta \phi} = W_{,\phi} - \nabla \cdot W_{,\nabla\phi} = X_e - \nabla \cdot \boldsymbol{Y}_e \\ A_d^\phi = \frac{\delta D}{\delta \dot{\phi}} = D_{,\dot{\phi}} - \nabla \cdot D_{,\nabla\dot{\phi}} = X_d - \nabla \cdot \boldsymbol{Y}_d \end{cases} \tag{3.17}$$

Using (3.15) together with the constitutive insulation condition after Polizzotto $f_{v\phi} = 0$, the relationship between two extended forces A_e^ϕ and A_d^ϕ can be made:

$$A_e^\phi + A_d^\phi = f_{v\phi} = 0 \Longrightarrow (X_e - \nabla \cdot \boldsymbol{Y}_e) + (X_d - \nabla \cdot \boldsymbol{Y}_d) = 0 \tag{3.18}$$

On the other hand, in terms of the global energy function **W(U)** and of the global dissipation function $\mathbf{D}(\dot{\mathbf{U}}, \mathbf{U})$, the **global form** of (3.15) for the displacement and the internal parameter of the solid subjected to a loading path $\mathbf{F(t)} = \big(\mathrm{f}_{vu}(t), \mathrm{f}_{su}(t)\big)$, is given:

$$\mathbf{W}_{,\mathbf{U}} + \mathbf{D}_{,\dot{\mathbf{U}}} = \mathbf{F} \tag{3.19}$$

These have been derived under the assumption of smoothness of the two potentials with respect to their arguments and are thus available only to *time-dependent processes*. However, *time-independent behavior* such as plasticity and brittle damage are associated with a dissipation potential **D** which is convex but positively homogenous of degree 1 of the rates $\dot{\mathbf{U}}$, i.e:

$$\mathbf{D}(\mu\dot{\mathbf{U}}, \mathbf{U}) = \mu\mathbf{D}(\dot{\mathbf{U}}, \mathbf{U}), \quad \forall \mu \geq 0 \tag{3.20}$$

thus non-differentiable at $\dot{\mathbf{U}} = 0$. In this case, the function $\mathbf{D}$ is also called a **pseudo-potential** and the governing equations in terms of the global energy functions can be written again, in the most general form, with a bit change compared to the previous one (3.19):

$$\mathbf{W}_{,\mathbf{U}} + \partial \mathbf{D}_{\dot{\mathbf{U}}} = \mathbf{F} \tag{3.21}$$

where $\partial \mathbf{D}_{\dot{\mathbf{U}}}$ denotes a sub-gradient of the convex function $\mathbf{D}$ at point $\dot{\mathbf{U}}$.

3.1.4 Time-Dependent Processes

The considered governing equations are derived under the assumption of smoothness of the two potentials. Gradient Models have been much considered in *visco-plasticity* as well as in *damage mechanics*, *cf.* [4], [43], [53], [57], [96; 97], [80], [99]. In particular the phase-field method, which is very popular in the study of different phenomena of diffusion and phase change, deals principally with gradient models of visco-elasticity, *cf.* for example [86]. Many discussions have been devoted to the problem of strain localization and fracture, especially in the numerical computation of elastic-plastic solids. These works principally address the insulation case $f_{v\phi} = 0$ and $f_{s\phi} = 0$ because of the difficulty to define physically these actions. Some interesting discussions from the literature are reported here in order to obtain some examples on the physical nature of the internal parameters and on the practical interest of Gradient Models in the modeling of multi-physics phenomena in solids.

The modeling of the damage of an elastic solid is an important subject in Solid Mechanics, *cf.* for example [117], [162], [24], [42], [94]. In particular, the case of viscous damage is here reported because of its connection with the problem of strain localization and with the phase field method, *cf.* [32], [62], [86].

As an example, we consider the case of damage, with an internal parameter ϕ, $0 \leq \phi \leq 1$ representing the damage proportion. $\phi = 0$ if no damage and $\phi = 1$ if full damage. A simple viscous model of damage is obtained with the following expression of the energy and of the dissipation potentials:

$$w(\nabla u, \phi, \nabla\phi) = (1-\phi)\, w_{e\ell}(\nabla u) + \frac{h}{2}\phi^2 + \frac{g}{2}|\nabla\phi|^2, \quad D(\dot{\phi}) = \frac{1}{2}\boldsymbol{\xi}\dot{\phi}^2 + \frac{1}{2}\eta\nabla\dot{\phi}^2$$

where $w_{e\ell}$ is the classical elastic energy, h, g and $\boldsymbol{\xi}$, η are constants. The governing equations for the variation of the damage are:

$$(\boldsymbol{\xi} I - \eta\Delta)\,\dot{\phi} = -h\phi + g\Delta\phi + w_{e\ell}(\nabla u) \quad \forall\, x \in V \quad \text{and} \quad \phi_{,n} = 0 \quad \forall x \in \partial V$$

In particular, a full-equilibrium state for the solid under a displacement control loading is a stationary point of the energy functional, *cf.* [117]. The model is particularly interesting when $h = \frac{G_c}{2\varepsilon}$, $g = G_c\,\varepsilon$, cf. [32]. For vanishing ε, the search for full-equilibrium states has a strong connection with the apparition of Griffith cracks of surface energy G_c. This model gives an interesting method to detect the apparition of Griffith cracks as the limit of damage zones, *cf.* [32], [66], [97].

3.1.5 Time-Independent Processes and Gradient Plasticity

For time-independent processes such as *friction, plasticity, brittle fracture, and brittle damage*, the dissipation potential D is convex, positively homogeneous of degree 1 of the rates $\dot{\phi}$.

$$D(\mu\dot{\phi}, \mu\nabla\dot{\phi}, \phi) = \mu D(\dot{\phi}, \nabla\dot{\phi}, \phi) \quad \forall \quad \mu > 0. \tag{3.22}$$

Because of the loss of differentiability with respect to $(\dot{\phi}, \nabla\dot{\phi}) = (0, 0)$, the sub-gradient is used to define the forces X_d and $\boldsymbol{Y}_d$ appearing in Eq. (3.6), by :

$$X_d = \partial_{\dot{\phi}} D \quad \text{and} \quad \boldsymbol{Y}_d = \partial_{\nabla\dot{\phi}} D$$

a) Force-Flux Relationships

1/ Model I: Gradient-independent pseudo-potential

The case of particular models admitting a gradient-independent dissipation potential

$$D = D(\dot{\phi}, \phi) \tag{3.23}$$

is first considered. In this case, the *force-flux* relationship, in the sense of sub-gradient, *cf.* [111], [70], [117], is:

$$X_d = \partial_{\dot{\phi}} D(\dot{\phi}, \phi) \quad , \quad \boldsymbol{Y}_d = 0 \tag{3.24}$$

This means that the force X_d must belong to a convex domain of admissible forces $C_{X_d;\phi}$ and that the normality law is satisfied by the rate $\dot{\phi}$. Although X_d cannot be uniquely determined at $(\dot{\phi}, \phi) = (0, \phi)$ directly via (3.24.a), there is no indetermination difficulty as, from (3.24.b) and (3.4), or more precisely, from (3.18), $X_d = -X_e + \nabla\cdot\boldsymbol{Y}_e$ is still known at the present state. Such a particular model will be denoted as model I.

For example, if a process described with a dissipation potential

$$D(\dot{\phi}, \phi) = k(\phi)\|\dot{\phi}\| \tag{3.25}$$

then the set of admissible forces is described by the plastic criterion

$$f(X_d, \phi) = \|X_d\| - k(\phi) \leq 0 \tag{3.26}$$

and the rate $\dot{\phi}$ must satisfy the normality law:

$$\dot{\phi} = \lambda \frac{\partial f}{\partial X_d} \text{ with } \lambda \geq 0 \ , \ \lambda f = 0 \tag{3.27}$$

2/ Model II: Gradient-dependent pseudo-potential

In the general case (models II), $D = D(\dot{\phi}, \nabla\dot{\phi}, \phi)$ and the force-flux relationship can be written as

$$X_d = \partial_{\dot{\phi}} D(\dot{\phi}, \nabla\dot{\phi}, \phi) \quad , \quad \boldsymbol{Y}_d = \partial_{\nabla\dot{\phi}} D(\dot{\phi}, \nabla\dot{\phi}, \phi) \tag{3.28}$$

This means that the force $(X_d, \boldsymbol{Y}_d)$ must belong to a convex set of admissible forces $C_\phi(X_d, \boldsymbol{Y}_d, \phi)$ and that the normality law is satisfied by the rates $(\dot\phi,\ \nabla\dot\phi)$.

For example, if

$$D = k(\phi)\|\dot\phi\| + \kappa(\phi)\|\nabla\dot\phi\| \tag{3.29}$$

then the convex of admissible forces is given by two inequalities

$$f(X_d,\phi) = \|X_d\| - k(\phi) \le 0 \quad , \quad \varphi(\boldsymbol{Y}_d,\phi) = \|\boldsymbol{Y}_d\| - \kappa(\phi) \le 0 \tag{3.30}$$

and the rates $\dot\phi,\ \nabla\dot\phi$ must satisfy the normality law

$$\dot\phi = \lambda\frac{\partial f}{\partial X_d} \ \text{ with } \ \lambda \ge 0\ ,\ \lambda f = 0\ , \quad \nabla\dot\phi = \mu\frac{\partial\varphi}{\partial \boldsymbol{Y}_d}\ , \quad \mu \ge 0\ ,\ \mu\varphi = 0 \tag{3.31}$$

The force pair $(X_d,\ \boldsymbol{Y}_d)$ cannot be uniquely determined at $(\dot\phi, \dot\nabla\phi) = (0,0)$ directly via (3.28). From (3.4), or more precisely from (3.18), these forces must also satisfy the constitutive equilibrium equations $(X_e + X_d) - \nabla\cdot(\boldsymbol{Y}_d + \boldsymbol{Y}_e) = 0$ and appropriate boundary conditions. However, even these relationships are still not enough to determine $(X_d, \boldsymbol{Y}_d)$ at $(\dot\phi, \nabla\dot\phi) = (0,0)$, even if the present state is known. This indetermination is the main difficulty of the models II, but that can be overcome by *Energy Regularization* method proposed by Q.S. Nguyen [116], as discussed in section 3.1.6.e.

The following case is also considered in the literature, *cf.* for example [54], [57]

$$D = k(\phi)(\|\dot\phi\|^2 + \ell^2\|\nabla\dot\phi\|^2)^{1/2} \tag{3.32}$$

and leads to a Mises-like plastic criterion and the normality law:

$$\begin{cases} f = (\|X_d^\phi\|^2 + \dfrac{1}{\ell^2}\|\boldsymbol{Y}_d^\phi\|^2)^{1/2} - k(\phi) \\ \dot\phi = \lambda\dfrac{\partial f}{\partial X_d} \quad , \quad \nabla\dot\phi = \lambda\dfrac{\partial f}{\partial \boldsymbol{Y}_d} \end{cases} \qquad f \le 0\ ,\ \lambda \ge 0\ ,\ f\lambda = 0 \tag{3.33}$$

It is classical that the dissipation potential is obtained from the elastic domain by the maximum dissipation principle

$$D = D(\dot\phi, \nabla\dot\phi, \phi) = \max_{(X_d^*, \boldsymbol{Y}_d^*)\in C_\phi} \{X_d^*\cdot\dot\phi + \boldsymbol{Y}_d^*\cdot\nabla\dot\phi\} \tag{3.34}$$

b) Governing Equations

Under the insulation condition, the governing equations, given by (3.1), (3.4), (3.28), are

$$\begin{cases} \boldsymbol{\sigma} = W_{,\nabla u} \quad , \qquad X_e = W_{,\phi} \quad , \qquad \boldsymbol{Y}_e = W_{,\nabla\phi} \\ X = X_e + X_d \quad , \quad \boldsymbol{Y} = \boldsymbol{Y}_e + \boldsymbol{Y}_d \quad , \quad (X_d, \boldsymbol{Y}_d) = \partial D(\dot\phi, \nabla\dot\phi, \phi) \\ P_i + P_j = P_e \quad \forall \quad \delta u, \delta\phi \\ P_i = \int_V (\boldsymbol{\sigma}\cdot\nabla\delta u + X\cdot\delta\phi + \boldsymbol{Y}\cdot\nabla\delta\phi)\, dV \\ P_j = \int_V \rho\ddot u\cdot\delta u\, dV \\ P_e = \int_V f_{vu}\cdot\delta u\, dV + \int_{\partial V} f_{su}\cdot\delta u\, da \end{cases} \tag{3.35}$$

3.1.6 Gradient Plasticity and Evolutionary Variational Inequality

In quasi-static transformations, a variational form of the governing equations also exists and is given by the following evolutionary variational inequality, as in Classical Plasticity, *cf.* for example [47], [117], [61].

Proposition 1 *The response* $\mathbf{U}(\mathbf{t})$ *of a solid under a quasi-static loading* $\mathbf{F}(\mathbf{t})$ *is a solution of the evolutionary variational inequality* (cf. *[116]*)

$$\mathbf{W}_{,\mathbf{U}} \cdot (\delta\mathbf{U} - \dot{\mathbf{U}}) + \mathbf{D}(\delta\mathbf{U}, \mathbf{U}) - \mathbf{D}(\dot{\mathbf{U}}, \mathbf{U}) - \mathbf{F} \cdot (\delta\mathbf{U} - \dot{\mathbf{U}}) \geq \mathbf{0} \quad \forall\, \delta\mathbf{U} \tag{3.36}$$

From the expression (3.22) of the dissipation, this variational inequality can be written in the form of a mechanical energy balance and a minimum principle

$$\begin{cases} \int_V (w_{,\nabla u} : \nabla\delta u - f_{vu} \cdot \delta u)\, dV - \int_{\partial V} f_{su} \cdot \delta u\, da = 0 \\ \int_V (X_e \cdot \dot{\phi} + \boldsymbol{Y}_e \cdot \nabla\dot{\phi} + D(\dot{\phi}, \nabla\dot{\phi}, \phi))\, dV = 0 \\ = \min_{\delta\boldsymbol{\Phi}} \int_V (X_e \cdot \delta\phi + \boldsymbol{Y}_e \cdot \nabla\delta\phi + D(\delta\phi, \nabla\delta\phi, \phi))\, dV \end{cases} \tag{3.37}$$

a) Minimum Principle and Admissible Rates

For a given couple of non-dissipative forces $(X_e, \boldsymbol{Y}_e)$, let us consider the solutions of the minimum problem

$$m = \min_{\mathrm{r}} \ \mathcal{L}(\mathbf{r}) \quad , \quad \mathcal{L}(\mathbf{r}) = \int_V (X_e \cdot r + \boldsymbol{Y}_e \cdot \nabla r + D(r, \nabla r, \phi))\, dV \tag{3.38}$$

where r is an arbitrary rate of internal parameter. It is clear that

i- When $m = 0$, if $\mathbf{r_o} \neq \mathbf{0}$ is a solution then $a\, \mathbf{r_o}$ is also a solution for all number $a > 0$.

ii- If $\mathbf{r_o} \neq \mathbf{0}$ and $\mathbf{r'_o} \neq \mathbf{0}$ are two different solutions, then $\alpha\mathbf{r_o} + (1-\alpha)\mathbf{r'_o}$ is also a solution since D is a convex function.

From (3.37), it is also clear that $\dot{\boldsymbol{\Phi}}$ must belong to the set $\mathcal{R}$ of solutions of (3.38) with $m = 0$.

The proof of Proposition 1 is straightforward for the particular case of models I. The dissipation potential $D(\dot{\phi}, \phi)$ leads to a convex elastic domain C in the force space X_d and the associated minimum principle is

$$m = \min_{r} \left\{ \int_V (X_e - \nabla \cdot \boldsymbol{Y}_e) \cdot r + D(r, \phi))\, dV + \int_{\partial V} (\boldsymbol{Y}_e \cdot n) \cdot r\, da \right\} \tag{3.39}$$

Thus the minimum m is

$$\begin{cases} m = -\infty \quad if\ X_d = X_e - \nabla\cdot\boldsymbol{Y}_e \notin C \ \ \forall\, x \in V \ \text{ or } \ \boldsymbol{Y}_e \cdot n \neq 0 \ \ \forall\, x \in \partial V \\ m = 0 \quad if \quad X_d = X_e - \nabla\cdot\boldsymbol{Y}_e \in C \ \ \forall\, x \in V \ \text{ and } \ \boldsymbol{Y}_e \cdot n = 0 \ \ \forall\, x \in \partial V \end{cases} \tag{3.40}$$

It is clear that the set $\mathcal{R}$ of solutions is composed of admissible rates defined on the current plastic zone. For example:

$$\Omega = \left\{\, x \in V \mid \ f(X_d(x), \phi(x)) = 0 \,\right\} \tag{3.41}$$

when the elastic domain C is defined by the criterion $f(X_d, \phi) \leq 0$.

For models II, the proof of Proposition 1 is also straightforward in the sense $\Rightarrow$, a solution of the governing equations is a solution of the evolutionary variational inequality. In the inverse sense $\Leftarrow$, some open questions remain concerning the dissipative forces outside the present plastic zone.

Since the integrants in (3.38) consists of linear or degree-1 functions, it is interesting to compute the value m_1 of the quotient

$$m_1 = \max_{\mathbf{r}} \frac{\int_V -(X_e \cdot r + \boldsymbol{Y}_e \cdot \nabla r)}{\int_V D(r, \nabla r, \phi))\, dV}$$

It follows that if $m_1 < 1$, then $m = 0$ and $\mathbf{r} = \mathbf{0}$ is the only solution. If $m_1 = 1$, then $m = 0$ and one or many solutions $\mathbf{r_o} \neq \mathbf{0}$ exist. If $m_1 > 1$, then $m = -\infty$ and there is no solution. Thus, if $m_1 < 1$, then $\dot{\mathbf{\Phi}} = \mathbf{0}$ and the incremental behavior is purely elastic. If $m_1 > 1$, the non-dissipative forces $(\mathbf{X_e}, \mathbf{Y_e})$ are not allowable by the constitutive equations. If $m_1 = 1$, the response $\dot{\mathbf{\Phi}}$ is to be found in $\mathcal{R}$, the set of solutions of the minimum principle.

The model (3.32) is considered here for example. Let $\mathbf{r_o} \neq \mathbf{0}$ be a solution of the minimum principle and $\mathbf{V_{r_o}}$ the loading zone associated with this solution:

$$x \in \mathbf{V_{r_o}} \quad \Leftrightarrow \quad \big(r_o(x), \nabla r_o(x)\big) \neq (0, 0) \tag{3.42}$$

and V^p the reunion of all loading zones associated with the solutions of the minimum principle:

$$V^p = \bigcup_{\mathbf{r_o} \in \mathcal{S}} \mathbf{V_{r_o}} \tag{3.43}$$

Since the criterion (3.32) is strictly convex, the following proposition holds

Proposition 2 *The dissipative forces $(X_d, \boldsymbol{Y}_d)$ are uniquely defined in V^p, the reunion of all loading zones associated with the solutions of the minimum principle and satisfy in V^p the local equation $X - \nabla \cdot \boldsymbol{Y} = 0$ (*cf. *[116]).*

The proof is quite simple as in rigid plasticity, *cf.* Mandel [103], and based upon the strict convexity of the elastic domain C. As in rigid plasticity however, it is not clear that an extension of these forces could exist in $V - V^p$ satisfying the constitutive equilibrium equations (3.4) and the strict inequality of the plastic criterion $f(X_d, \boldsymbol{Y}_d, \phi) < 0$.

The set $\mathcal{R}$ can also be described in the following way:

By definition, a rate $\delta\mathbf{\Phi}$ is admissible if locally, $(\delta\phi, \nabla\delta\phi)$ belongs to the normal cone of the elastic domain C at $(X_d, \boldsymbol{Y}_d)$ for all $x \in \Omega$

$$\delta\mathbf{\Phi} \text{ admissible} \quad \Leftrightarrow \quad \big(\delta\phi(x), \nabla\delta\phi(x)\big) \in N_C(X_d, \boldsymbol{Y}_d) \quad \forall\ x \in V^p \tag{3.44}$$

For example, in terms of the criterion $f(X_d, \boldsymbol{Y}_d, \phi) \leq 0$

$$\begin{cases} \delta\mathbf{\Phi} \text{ admissible} \quad \Leftrightarrow \quad \delta\phi = \lambda \frac{\partial f}{\partial X_d} \quad , \quad \nabla\delta\phi = \lambda \frac{\partial f}{\partial X_d} \\ \qquad\qquad\qquad\qquad f \leq 0, \quad \lambda \geq 0, \quad \lambda\, f = 0 \quad \forall\, x \in V^p \end{cases} \tag{3.45}$$

The following statement holds:

Proposition 3 *An admissible rate is a solution of the minimum principle* (cf. *[116]*)

$$\delta\mathbf{\Phi} \ \textit{admissible} \quad \Leftrightarrow \quad \delta\mathbf{\Phi} \in \mathcal{R} \tag{3.46}$$

Indeed, from (i) and (ii), it is possible to combine different solutions $\mathbf{r_o}$ to construct a solution φ such that $\varphi \neq 0$ for all $x \in V^p$. This solution admits as loading zone V^p and the forces $(\mathbf{X_d}, \mathbf{Y_d})$ can be completed in $V - V^p$ to obtain an admissible force system $(\mathbf{X_d}, \mathbf{Y_d})$ in the whole volume V since φ is a solution. This system of force $(\mathbf{X_d}, \mathbf{Y_d})$ is associated with any admissible rate $\delta\mathbf{\Phi}$. It is clear that V^p can be identified as the current plastic zone, where the criterion of plasticity is satisfied $f(X_d, \boldsymbol{Y}_d, \phi) = 0$.

b) Rate Problem: Rate Equations

It is however necessary to check that equations (3.36) defines effectively an incremental process for a solid submitted to a loading path. At a current time t, if the present state $(\mathbf{u}, \mathbf{\Phi})$ is assumed to be known, it must be possible to determine the rate of the unknowns (displacement and internal parameter) $(\dot{\mathbf{u}}, \dot{\mathbf{\Phi}})$ in terms with the rate of the data $\dot{\mathbf{F}} = (\dot{\mathbf{f}}_{\mathbf{vu}}, \dot{\mathbf{f}}_{\mathbf{su}})$. This is a necessary condition in order to follow step-by-step the response of the solid along the loading path.

The rate equations describe the system of equations satisfied by the rate of the unknowns (displacement and internal parameter) $(\dot{\mathbf{u}}, \dot{\mathbf{\Phi}})$ in terms with the rate $\dot{\mathbf{F}}$. The following statement holds:

Proposition 4 *The rate response* $\dot{\mathbf{U}} = (\dot{\mathbf{u}}, \dot{\mathbf{\Phi}})$ *is a solution of the variational inequality* (cf. *[116]*)

$$\begin{cases} \mathbf{W}_{,\mathbf{UU}}\left[\dot{\mathbf{U}}, \delta\mathbf{U} - \dot{\mathbf{U}}\right] + \dot{\mathbf{U}} \cdot \left(\mathbf{D}_{,\mathbf{U}}\left(\delta\mathbf{U}, \mathbf{U}\right) - \mathbf{D}_{,\mathbf{U}}\left(\dot{\mathbf{U}}, \mathbf{U}\right)\right) \\ -\dot{\mathbf{F}} \cdot \left(\delta\mathbf{U} - \dot{\mathbf{U}}\right) \geq 0 \quad \forall \ \text{admissible rates} \ \ \delta\mathbf{U} \end{cases} \tag{3.47}$$

This proposition shows how the rate $(\dot{\mathbf{u}}, \dot{\mathbf{\Phi}})$ can be selected among the admissible rates. For this, the definitions $\dot{\mathbf{u}} = \lim_{\mathbf{\Delta t} \to \mathbf{0}} \frac{\mathbf{\Delta u}}{\mathbf{\Delta t}}$ and $\dot{\mathbf{\Phi}} = \lim_{\mathbf{\Delta t} \to \mathbf{0}} \frac{\mathbf{\Delta \Phi}}{\mathbf{\Delta t}}$ must be introduced.

The proof of this proposition can be obtained for example from (3.36) by an implicit time-discretization. The present state is assumed to be given, an increment of the response $\Delta U = \dot{U}\Delta t$ associated with an increment of load must satisfy (3.36) at the next step:

$$\begin{cases} \mathbf{W}_{,\mathbf{U}}\left(\mathbf{U}+\mathbf{\Delta U}\right)\cdot\left(\delta\mathbf{U}-\mathbf{\Delta U}\right) + \mathbf{D}(\delta\mathbf{U}, \mathbf{U}+\mathbf{\Delta U}) - \mathbf{D}(\mathbf{\Delta U}, \mathbf{U}+\mathbf{\Delta U}) \\ -\mathbf{F} + \mathbf{\Delta F} \cdot \left(\delta\mathbf{U}-\mathbf{\Delta U}\right) \geq 0 \quad \forall \quad \delta\mathbf{U} \end{cases} \tag{3.48}$$

with

$$\begin{cases} \mathbf{W}_{,\mathbf{U}}\left(\mathbf{U} + \mathbf{\Delta U}\right) = \mathbf{W}_{,\mathbf{U}}\left(\mathbf{U}\right) + \mathbf{W}_{,\mathbf{UU}}\left(\mathbf{U}\right) \cdot \mathbf{\Delta U} + h.o.t. \\ \mathbf{D}(\delta\mathbf{U}, \mathbf{U} + \mathbf{\Delta U}) = \mathbf{D}(\delta\mathbf{U}, \mathbf{U}) + \mathbf{D}_{,\mathbf{U}}\left(\delta\mathbf{U}, \mathbf{U}\right) \cdot \mathbf{\Delta U} + h.o.t. \end{cases} \tag{3.49}$$

The special choice ΔU and δU are admissible rates ensures that

$$\mathbf{W}_{,\mathbf{U}}\left(\mathbf{U}\right) \cdot \delta\mathbf{U} + \mathbf{D}(\delta\mathbf{U}, \mathbf{U}) - \mathbf{F} \cdot \delta\mathbf{U} = 0 \quad \forall \ \ \delta\mathbf{U} \ \text{admissible}$$

In (3.48), the first order term is zero thus the second order terms must be positive and the variational inequality (3.47) follows.

Since $D = D(\dot{\phi}, \nabla\dot{\phi}, \phi)$, this variational inequality can be detailed as

$$\begin{cases} \mathbf{W}_{,\mathbf{uu}}\left[\dot{\mathbf{u}}, \delta\mathbf{u}\right] + \mathbf{W}_{,\mathbf{u\Phi}}\left[\dot{\mathbf{\Phi}}, \delta\mathbf{u}\right] - \dot{\mathbf{F}} \cdot \delta\mathbf{u} = 0 \quad \forall \ \delta\mathbf{u} \\ \mathbf{W}_{,\mathbf{\Phi u}}\left[\dot{\mathbf{u}}, \delta\mathbf{\Phi} - \dot{\mathbf{\Phi}}\right] + \mathbf{W}_{,\mathbf{\Phi\Phi}}\left[\dot{\mathbf{\Phi}}, \delta\mathbf{\Phi} - \dot{\mathbf{\Phi}}\right] \\ + \dot{\mathbf{\Phi}} \cdot \left(\mathbf{D}_{,\mathbf{\Phi}}\left(\delta\mathbf{\Phi}, \mathbf{\Phi}\right) - \mathbf{D}_{,\mathbf{\Phi}}\left(\dot{\mathbf{\Phi}}, \mathbf{\Phi}\right)\right) \geq 0 \\ \quad \forall \quad \delta\mathbf{\Phi} \quad \text{admissible} \end{cases} \tag{3.50}$$

The variational inequality (3.47) is symmetric if the following symmetry

$$\delta\mathbf{U} \cdot \mathbf{D}_{,\mathbf{U}}\left(\dot{\mathbf{\Phi}}, \mathbf{U}\right) = \dot{\mathbf{U}} \cdot \mathbf{D}_{,\mathbf{U}}\left(\delta\mathbf{\Phi}, \mathbf{U}\right) \tag{3.51}$$

is satisfied. In this case, it is also equivalent to an extremum principle since the following statement holds:

Proposition 5 *Under the assumption of symmetry, the rate* $\dot{\mathbf{U}} = (\dot{\mathbf{u}}, \dot{\mathbf{\Phi}})$ *minimizes the rate-functional* $\mathbf{H}(\delta\mathbf{U})$ *among the admissible rates (*cf. *[116])*

$$\mathbf{H}(\delta\mathbf{U}) = \frac{1}{2}\mathbf{W}_{,\mathbf{UU}}\left[\delta\mathbf{U}, \delta\mathbf{U}\right] + \delta\mathbf{U} \cdot \mathbf{D}_{,\mathbf{U}}\left(\delta\mathbf{U}, \mathbf{U}\right) - \dot{\mathbf{F}} \cdot \delta\mathbf{U} \tag{3.52}$$

when the following condition of positivity holds

$$\mathbf{W}_{,\mathbf{UU}}\left[\delta\mathbf{U}, \delta\mathbf{U}\right] + \delta\mathbf{U} \cdot \mathbf{D}_{,\mathbf{U}}\left(\delta\mathbf{U}, \mathbf{U}\right) > 0 \quad \forall \quad \delta\mathbf{U} \quad \text{admissible} \tag{3.53}$$

Indeed, for any admissible field $\delta\mathbf{U}$,

$$\begin{cases} \mathbf{H}(\delta\mathbf{U}) - \mathbf{H}(\dot{\mathbf{U}}) = \mathbf{W}_{,\mathbf{UU}}\left[\delta\mathbf{U} - \dot{\mathbf{U}}, \delta\mathbf{U} - \dot{\mathbf{U}}\right] + (\delta\mathbf{U} - \dot{\mathbf{U}}) \cdot \mathbf{D}_{,\mathbf{U}}\left(\delta\mathbf{U} - \dot{\mathbf{U}}, \mathbf{U}\right) \\ + \mathbf{W}_{,\mathbf{U}} \cdot (\delta\mathbf{U} - \dot{\mathbf{U}}) + \mathbf{D}(\delta\mathbf{U}, \mathbf{U}) - \mathbf{D}(\dot{\mathbf{U}}, \mathbf{U}) - \mathbf{F} \cdot (\delta\mathbf{U} - \dot{\mathbf{U}}) \geq 0 \end{cases}$$

The rate $\dot{\mathbf{U}}$ is also unique if the quadratic form (3.53) is strictly positive on the linear space generated by the admissible rates.

In particular, when the dissipation potential is state-independent, the strict convexity of the energy potential ensures the uniqueness of the rate response.

In the same spirit as in Classical Plasticity, the description of the rate problem leads naturally to the study of the stability of an equilibrium position and the bifurcation of a quasi-static response, [87]. For example, the same strictly positive condition on the set of admissible rates is a criterion of stability of the present equilibrium, *cf.* [87], [117].

From a criterion of plasticity $f(X_d, \boldsymbol{Y}_d, \phi) \leq 0$, with the notation $\alpha = (\dot{\phi}, \nabla\dot{\phi})$ and $A = (X_d, \boldsymbol{Y}_d)$, the expression

$$D(\alpha, \phi) = \max_{f(A^*, \phi) \leq 0} \left(A^* \cdot \alpha = A \cdot \alpha - \lambda f(A, \phi)\right)$$

gives

$$\begin{cases} \delta\phi \cdot D_{,\phi}\,(\alpha,\phi) = \delta A \cdot (\alpha - \lambda f_{,A}\,) - \lambda f_{,\phi}\,\delta\phi - \delta\lambda\; f \\ = \mu f_{,X_d} \cdot f_{,\phi}\,\lambda \quad \text{with} \quad \delta\phi = \mu f_{,X_d} \end{cases}$$

Thus the symmetry is ensured and the rate $\dot{\mathbf{U}}$ satisfies

$$\begin{cases} \int_V \nabla\delta u \cdot (w_{,\nabla u\,\nabla u} \cdot \nabla\dot{u} + w_{,\nabla u\phi} \cdot \dot{\phi})\; dV - \dot{\mathbf{F}} \cdot \delta\mathbf{u} = 0 \\ \int_V (\delta\phi - \dot{\phi}) \cdot (w_{,\nabla u\phi} \cdot \nabla u + w_{,\phi\phi} \cdot \dot{\phi}) + (\mu - \lambda) f_{,X_d} \cdot f_{,\phi}\,\lambda \geq 0 \\ \quad \forall\ \ \delta\mathbf{u}\ ,\ \delta\mathbf{\Phi} \quad \text{admissible}\ \ ,\ \ \delta\phi = \mu f_{,X_d} \end{cases}$$

The rate $\dot{\mathbf{U}}$ minimizes the functional $\mathbf{H}(\delta\mathbf{U})$ in $\mathcal{R}$:

$$\begin{cases} \mathbf{H}(\delta\mathbf{U}) \;=\; \int_V \tfrac{1}{2}(\nabla\delta u \cdot w_{,\nabla u\,\nabla u} \cdot \nabla\delta u + 2\;\delta\phi \cdot w_{,\nabla u\phi} \cdot \nabla\delta u + \delta\phi \cdot w_{,\phi\phi} \cdot \delta\phi \\ + f_{,X_d} \cdot f_{,\phi}\,\mu^2)\; dV \;-\; \dot{\mathbf{F}} \cdot \delta\mathbf{u} \end{cases}$$

More generally, the considered symmetry is equivalent to the symmetry of the interaction matrix $h_{ij} = f^i{}_{,X_d} \cdot f^j{}_{,\phi}$ in the case of multiple plastic criterion $f^i(X_d, \boldsymbol{Y}_d, \phi) \leq 0\ ,\ \ i = 1, n$

c) Example of Gradient Model of Plasticity with Isotropic-Kinematic Hardening

In small transformation, an interesting model of plasticity with isotropic-kinematic hardening consists of internal variable $\phi = (\boldsymbol{\varepsilon}^p, \gamma)$ with $\gamma = \int_0^t \sqrt{\tfrac{2}{3}\boldsymbol{\varepsilon}^p : \boldsymbol{\varepsilon}^p}\; \mathrm{d}\tau$ being accumulated plastic strain, of energy

$$W = W_e(\boldsymbol{\varepsilon} - \boldsymbol{\varepsilon}^p) + W_c(\boldsymbol{\varepsilon}^p) + W_i(\gamma) + W_g(\nabla\gamma) \tag{3.54}$$

and a Mises-like criterion of plasticity of the form

$$f(\boldsymbol{X}_d^p, X_d^\gamma, \boldsymbol{Y}_d^\gamma) = \|\boldsymbol{X}_d^p\| + \frac{1}{\ell}\|\boldsymbol{Y}_d^\gamma\| + X_d^\gamma - k \leq 0 \tag{3.55}$$

where k is a positive constant. The dissipation potential and the normality law are

$$D(\dot{\varepsilon}^p, \dot{\gamma}, \nabla\dot{\gamma}) = \max_{f(\boldsymbol{X}_d^{p*}, X_d^{\gamma*}, \boldsymbol{Y}_d^{\gamma*}) \leq 0} \{\boldsymbol{X}_d^{p*} \cdot \dot{\varepsilon}^p + \boldsymbol{Y}_d^{\gamma*} \cdot \nabla\dot{\gamma} + X_d^{\gamma*}\;\dot{\gamma}\}$$

$$\begin{cases} \dot{\varepsilon}^p = \lambda \frac{\partial f}{\partial \boldsymbol{X}_d^p} = \lambda \frac{\boldsymbol{X}_d^p}{\|\boldsymbol{X}_d^p\|} \\ \dot{\gamma} = \lambda \frac{\partial f}{\partial X_d^\gamma} = \lambda \qquad\qquad f \leq 0 \quad ,\quad \lambda \geq 0 \quad ,\quad f\,\lambda = 0 \\ \nabla\dot{\gamma} = \lambda \frac{\partial f}{\partial \boldsymbol{Y}_d^\gamma} = \frac{1}{\ell}\lambda \frac{\boldsymbol{Y}_d^\gamma}{\|\boldsymbol{Y}_d^\gamma\|} \end{cases} \tag{3.56}$$

γ is thus the equivalent plastic strain and the dissipation is $\;d = \boldsymbol{X}_d^p \cdot \dot{\varepsilon}^p + \boldsymbol{Y}_d^\gamma \cdot \nabla\dot{\gamma} + X_d^\gamma\;\dot{\gamma} = k\,\lambda$

d) Example of Uniqueness of the Response

The response of a solid of governing equation (3.36) under a given loading path and insulation condition is considered from a given initial state in isothermal transformation. Let $\mathbf{U_i},\ i = 1, 2$ denote two

possible solutions, if the dissipation potential is state-independent, then the combination of the governing equations associated with these solutions gives

$$(\mathbf{W}_{,\mathbf{U_2}} - \mathbf{W}_{,\mathbf{U_1}}) \cdot (\dot{\mathbf{U}}_\mathbf{2} - \dot{\mathbf{U}}_\mathbf{1}) \leq 0$$

If the energy $\mathbf{W}(\mathbf{U})$ is a quadratic functional, since

$$\frac{d}{dt}\big(\mathbf{W}(\mathbf{U_2} - \mathbf{U_1})\big) = 2(\mathbf{W}_{,\mathbf{U_2}} - \mathbf{W}_{,\mathbf{U_1}}) \cdot (\dot{\mathbf{U}}_\mathbf{2} - \dot{\mathbf{U}}_\mathbf{1}) \leq 0$$

there is *a contraction of the energy distance between two responses*. It follows that

$$\mathbf{W}\big(\mathbf{U_2(t)} - \mathbf{U_1(t)}\big) \leq \mathbf{W}\big(\mathbf{U_2(0)} - \mathbf{U_1(0)}\big) = 0$$

The positivity condition

$$\mathbf{W}(\mathbf{U}) \geq \mathbf{a}\|\mathbf{U}\|^\mathbf{2}$$

ensures then $U_2(t) = U_1(t)$ for all $t \geq 0$. Thus, the following statement holds:

Proposition 6 *The uniqueness of the response is ensured if the energy potential is quadratic and strictly positive and if the dissipation pseudo-potential is state-independent* (cf. *[116]).*

For example, in linear isotropic-kinematic hardening with

$$\begin{cases} W = W_e + W_c + W_i + W_g; \\ W_e = \frac{1}{2}\,(\boldsymbol{\varepsilon} - \boldsymbol{\varepsilon}^p) : \mathbb{L} : (\boldsymbol{\varepsilon} - \boldsymbol{\varepsilon}^p) \quad , \quad W_c = \frac{1}{2}\mathrm{H}\,\boldsymbol{\varepsilon}^p : \boldsymbol{\varepsilon}^p \quad , \\ W_i = \frac{1}{2}\mathrm{J}\,\gamma^2 \quad , \quad W_g = \frac{1}{2}\mathrm{G}\,\nabla\boldsymbol{\varepsilon}^p \vdots \nabla\boldsymbol{\varepsilon}^p \\ f = (\|\boldsymbol{X}_d^p\|^2 + \frac{1}{\ell^2}\|\boldsymbol{Y}_d^p\|^2)^{1/2} + X_d^\gamma - k \leq 0 \end{cases} \tag{3.57}$$

the response in stress and strain of a solid from a given initial state under a given loading path is unique when $G > 0$ even when $H = J = 0$, in contrast with the well known phenomenon of localization obtained in perfect plasticity (where $G = H = J = 0$). A discussion on existence and uniqueness of a solution has been recently given by Giacomini & Musesti [71] in linear isotropic hardening ($H = 0, G = 0, J > 0$).

At finite strain, several models of gradient plasticity have been proposed *cf.* Gurtin [80], using the classical multiplicative decomposition $\nabla u = F_e F_p$ where F_e and F_p are the elastic and plastic transformation gradients, the internal parameter is F_p:

$$W(\nabla u, F_p, \nabla F_p) = W_e(\nabla u, F_p) + W_c(F_p) + W_g(F_p, Curl F_p)$$

Some mathematical results on the question of existence and uniqueness of a solution have also been given for the models I, *cf.* Mainik & Mielke [99].

e) Energy Regularization

The following approach is proposed to avoid the indetermination difficulty aforementioned in section 3.1.5. The idea is to recover the model I case by *energy regularization*, thanks to the introduction of an additional internal parameter $\boldsymbol{\beta}$ and of an additional energy. For example, an additional term of the form $1/2\ \mathrm{r}\|\boldsymbol{\beta}-\nabla\phi\|^2$ can be included in the energy while $\nabla\dot{\phi}$ is replaced by $\dot{\boldsymbol{\beta}}$ in the dissipation potential. The coefficient of rigidity r is positive. This leads to a model I of potentials W^* and D^* with internal parameters $\phi,\ \boldsymbol{\beta}$:

$$\begin{cases} W^*(\nabla u,\phi,\nabla\phi,\boldsymbol{\beta}) = W(\nabla u,\phi,\nabla\phi) + \frac{1}{2}\mathrm{r}\|\boldsymbol{\beta}-\nabla\phi\|^2 \\ D^*(\dot{\phi},\dot{\boldsymbol{\beta}},\phi) = D(\dot{\phi},\nabla\dot{\phi},\phi) \end{cases} \tag{3.58}$$

For the regularized model, the governing equations (3.35) lead to the same elastic domain C in the force space $(X_d^\phi, \boldsymbol{X}_d^\beta)$ and the normality law for $(\dot{\phi},\dot{\boldsymbol{\beta}})$.

For example, the model described with (3.32) and (3.33), using the transformation (3.58), leads to:

$$\begin{cases} f^* = (\|X_d^\phi\|^2 + \frac{1}{\ell^2}\|\boldsymbol{X}_d^\beta\|^2)^{1/2} - k(\phi) \\ \dot{\phi} = \lambda\frac{\partial f}{\partial X_d^\phi} \quad , \quad \dot{\boldsymbol{\beta}} = \lambda\frac{\partial f}{\partial \boldsymbol{X}_d^\beta} \quad , \quad f\le 0 \quad , \quad \lambda\ge 0 \quad , \quad f\lambda = 0 \\ X_d^\phi = -X_e^\phi + \nabla\cdot\boldsymbol{Y}_e^\phi + \mathrm{r}\,\Delta\phi - \mathrm{r}\,\nabla\cdot\boldsymbol{\beta} \quad , \quad \boldsymbol{X}_d^\beta = \mathrm{r}\,(\nabla\phi-\boldsymbol{\beta}) \end{cases} \tag{3.59}$$

Thus $\boldsymbol{\beta}$ approaches $\nabla\phi$ and $\boldsymbol{X}_d^\beta$ plays the role of $\boldsymbol{Y}_d^\phi$ when the coefficient of rigidity r is high enough.

In the same spirit, the Gradient Model of isotropic and kinematic hardening described with a Mises-like plastic criterion of the forms (3.54) and (3.55), respectively, leads to a regularized model defined by:

$$\begin{cases} f^* = \|\boldsymbol{X}_d^p\| + X_d^\gamma + \frac{1}{\ell}\,\|\boldsymbol{X}_d^\beta\| - k \le 0 \\ \dot{\varepsilon}^p = \lambda\frac{\partial f}{\partial \boldsymbol{X}_d^p} \quad , \quad \dot{\gamma} = \lambda\frac{\partial f}{\partial X_d^\gamma} = \lambda \quad , \quad \dot{\boldsymbol{\beta}} = \lambda\frac{\partial f}{\partial \boldsymbol{X}_d^\beta} \\ f\le 0 \quad , \quad \lambda\ge 0 \quad , \quad f\lambda = 0 \\ \boldsymbol{X}_d^p = \boldsymbol{\sigma} - \mathrm{H}\boldsymbol{\varepsilon}^p \ , \ X_d^\gamma = -W_i' + \mathrm{G}\,\Delta\gamma + \nabla\cdot\mathrm{r}\,(\nabla\gamma-\boldsymbol{\beta}) \ , \ \boldsymbol{X}_d^\beta = \mathrm{r}\,(\nabla\gamma-\boldsymbol{\beta}) \end{cases} \tag{3.60}$$

3.1.7 Gradient Model of accumulated plasticity γ with isotropic-kinematic hardening

a) State and complementary laws

In small transformation, a Gradient Model of accumulated plasticity γ with isotropic-kinematic hardening consists of the internal variable $\phi = (\boldsymbol{\varepsilon}^p,\gamma)$, which represents the plastic strain and the equivalent plastic strain, such that $\boldsymbol{\varepsilon}_{kk}^p = 0$ (plastic incompressibility) and $\gamma \ge 0$ (accumulated plastic strain), and of the following energy and dissipation potentials (started with the case of linear hardening)

$$\begin{cases} W &= W(\boldsymbol{\varepsilon},\boldsymbol{\varepsilon}^p,\gamma,\nabla\gamma) = W_e + W_c + W_i + W_g \\ &= \frac{1}{2}(\boldsymbol{\varepsilon}-\boldsymbol{\varepsilon}^p) : \mathbb{L} : (\boldsymbol{\varepsilon}-\boldsymbol{\varepsilon}^p) + \frac{1}{2}\boldsymbol{\varepsilon}^p : \mathbb{H} : \boldsymbol{\varepsilon}^p + \frac{1}{2}\mathrm{J}\gamma^2 + \frac{1}{2}\mathrm{G}\nabla\gamma\cdot\nabla\gamma & \text{(3.61a)} \\ D &= D(\dot{\boldsymbol{\varepsilon}^p},\dot{\gamma},\nabla\dot{\gamma},\boldsymbol{\varepsilon}^p,\gamma) \Longleftrightarrow \text{gradient-dependent (model II)} & \text{(3.61b)} \end{cases}$$

and under the regularized form:

$$\begin{cases} W^* &= W^*(\boldsymbol{\varepsilon}, \boldsymbol{\varepsilon}^p, \gamma, \boldsymbol{\beta}) = W(\boldsymbol{\varepsilon}, \boldsymbol{\varepsilon}^p, \gamma, \nabla\gamma) \ + \ \frac{1}{2}\mathrm{r}\,(\boldsymbol{\beta} - \nabla\gamma)^2 \\ &= \frac{1}{2}(\boldsymbol{\varepsilon}-\boldsymbol{\varepsilon}^p) : \mathbb{L} : (\boldsymbol{\varepsilon}-\boldsymbol{\varepsilon}^p) + \frac{1}{2}\boldsymbol{\varepsilon}^p : \mathbb{H} : \boldsymbol{\varepsilon}^p + \frac{1}{2}\mathrm{J}\gamma^2 + \frac{1}{2}\mathrm{G}\nabla\gamma\cdot\nabla\gamma \ + \ \frac{1}{2}\mathrm{r}\,(\boldsymbol{\beta}-\nabla\gamma)^2 \quad (3.62a) \\ \\ D^* &= D^*(\dot{\boldsymbol{\varepsilon}^p}, \dot{\gamma}, \dot{\boldsymbol{\beta}}, \boldsymbol{\varepsilon}^p, \gamma) \Longleftrightarrow \text{gradient-independent (model I)} \quad (3.62b) \end{cases}$$

State and complementary laws after (3.5) offer the non-dissipative forces in this case:

$$\begin{cases} \boldsymbol{X}_e^p = W^*_{,\boldsymbol{\varepsilon}^p} = -\boldsymbol{\sigma} + \mathbb{H} : \boldsymbol{\varepsilon}^p & \boldsymbol{Y}_e^p = W^*_{,\nabla\boldsymbol{\varepsilon}^p} = 0 \\ X_e^\gamma = W^*_{,\gamma} = \mathrm{J}\gamma & \boldsymbol{Y}_e^\gamma = W^*_{,\nabla\gamma} = \mathrm{G}\nabla\gamma - \mathrm{r}\,(\boldsymbol{\beta} - \nabla\gamma) \\ \boldsymbol{X}_e^\beta = W^*_{,\boldsymbol{\beta}} = \mathrm{r}\,(\boldsymbol{\beta} - \nabla\gamma) & \boldsymbol{Y}_e^\beta = W^*_{,\nabla\boldsymbol{\beta}} = 0 \end{cases} \quad (3.63)$$

and the dissipative forces:

$$\begin{cases} \boldsymbol{X}_d^p = \partial D^*_{\dot{\boldsymbol{\varepsilon}^p}} \neq 0 & \boldsymbol{Y}_d^p = \partial D^*_{\nabla\dot{\boldsymbol{\varepsilon}^p}} = 0 \\ X_d^\gamma = \partial D^*_{\dot{\gamma}} \neq 0 & \boldsymbol{Y}_d^\gamma = \partial D^*_{\nabla\dot{\gamma}} = 0 \ \text{(actually substituted with } \boldsymbol{X}_d^\beta) \\ \boldsymbol{X}_d^\beta = \partial D^*_{\dot{\boldsymbol{\beta}}} \neq 0 & \boldsymbol{Y}_d^\beta = \partial D^*_{\nabla\dot{\boldsymbol{\beta}}} = 0 \end{cases} \quad (3.64)$$

Applying generalized local equilibrium equation after (3.18) for extended forces associated with ε_p, γ and $\boldsymbol{\beta}$ yields:

$$\begin{cases} (\boldsymbol{X}_e^{\boldsymbol{p}} - \nabla\cdot\boldsymbol{Y}_e^p) + (\boldsymbol{X}_d^p - \nabla\cdot\boldsymbol{Y}_d^p) = 0 \Longrightarrow \boldsymbol{X}_e^{\boldsymbol{p}} + \boldsymbol{X}_d^p = 0 & (3.65a) \\ (X_e^\gamma - \nabla\cdot\boldsymbol{Y}_e^\gamma) + X_d^\gamma = 0 \quad \text{(i.e, it comes back model I)} & (3.65b) \\ (\boldsymbol{X}_e^\beta - \nabla\cdot\boldsymbol{Y}_e^\beta) + (\boldsymbol{X}_d^\beta - \nabla\cdot\boldsymbol{Y}_d^\beta) = 0 \Longrightarrow \boldsymbol{X}_e^\beta + \boldsymbol{X}_d^\beta = 0 & (3.65c) \end{cases}$$

and then to express the dissipative forces as:

$$\begin{cases} \boldsymbol{X}_d^p = -\boldsymbol{X}_e^{\boldsymbol{p}} = \boldsymbol{\sigma} - \mathbb{H} : \boldsymbol{\varepsilon}^p & (3.66a) \\ X_d^\gamma = -X_e^\gamma + \nabla\cdot\boldsymbol{Y}_e^\gamma = -\mathrm{J}\gamma + \mathrm{G}\nabla^2\gamma - \mathrm{r}\,(\nabla\cdot\boldsymbol{\beta} - \nabla^2\gamma) & \\ \qquad = -\mathrm{J}\gamma + (\mathrm{G}+\mathrm{r})\nabla^2\gamma - \mathrm{r}\,\nabla\cdot\boldsymbol{\beta} & (3.66b) \\ \boldsymbol{X}_d^\beta = -\boldsymbol{X}_e^\beta = \mathrm{r}\,(\nabla\gamma - \boldsymbol{\beta}) & (3.66c) \end{cases}$$

b) Plastic criterion

Mises-like plastic criterion (by means of loading functions) of the form, as (3.60.a)

$$f = f(\boldsymbol{X}_d^p, X_d^\gamma, \boldsymbol{X}_d^\beta) = \|\boldsymbol{X}_d^p\| + X_d^\gamma + \frac{1}{\ell}\,\|\boldsymbol{X}_d^\beta\| - k \leq 0 \quad (3.67)$$

is considered.

where ℓ is defined here as a *material characteristic length parameter*. The micro-experiments are used to identify ℓ. According to the literature, ℓ is roughly of micrometer or sub-micrometer order, and actually reflects mechanical behavior at micro scale.

c) Evolution laws (normality laws)

$$\begin{cases} \dot{\boldsymbol{\varepsilon}}^p = \lambda \frac{\partial f(\boldsymbol{X}_d^p, X_d^\gamma, \boldsymbol{X}_d^\beta)}{\partial \boldsymbol{X}_d^p} = \lambda \frac{\boldsymbol{X}_d^p}{\|\boldsymbol{X}_d^p\|} \\ \dot{\gamma} = \lambda \frac{\partial f(\boldsymbol{X}_d^p, X_d^\gamma, \boldsymbol{X}_d^\beta)}{\partial X_d^\gamma} = \lambda \\ \dot{\boldsymbol{\beta}} = \lambda \frac{\partial f(\boldsymbol{X}_d^p, X_d^\gamma, \boldsymbol{X}_d^\beta)}{\partial \boldsymbol{X}_d^\beta} = \frac{1}{\ell}\, \lambda \frac{\boldsymbol{X}_d^\beta}{|\boldsymbol{X}_d^\beta|} \end{cases} \quad \text{where: } \lambda \geq 0;\ \ f \leq 0;\ \ \lambda f = 0 \tag{3.68}$$

The additional boundary condition (3.14.d) in this case is:

$$\begin{aligned} &\boldsymbol{Y}^\gamma \cdot \boldsymbol{n} = 0, \quad (3.63)\ \&\ (3.64) \implies \boldsymbol{Y}^\gamma = \boldsymbol{Y}_e^\gamma + \boldsymbol{Y}_d^\gamma = \boldsymbol{Y}_e^\gamma = \big(\mathrm{G}\,\nabla\gamma - \mathrm{r}\,(\boldsymbol{\beta} - \nabla\gamma)\big) \\ &\text{thus} \quad \big(\mathrm{G}\,\nabla\gamma - \mathrm{r}\,(\boldsymbol{\beta} - \nabla\gamma)\big) \cdot \boldsymbol{n} = \big((\mathrm{G}+\mathrm{r})\nabla\gamma - \mathrm{r}\,\boldsymbol{\beta}\big) \cdot \boldsymbol{n} = 0 \end{aligned} \tag{3.69}$$

Finally, for a solid V subjected to a classical loading path and a controlled displacement on a portion of its boundary, in small and quasi-static transformation from a given initial state u_o, f_o, under the constitutive insulation condition following Polizzotto, the governing equations are:

• $\forall x \in V$

$$\begin{aligned} \boldsymbol{X}_e^p &= -\boldsymbol{\sigma} + \mathbb{H} : \boldsymbol{\varepsilon}^p & \boldsymbol{Y}_e^p &= 0 \\ X_e^\gamma &= \mathrm{J}\gamma & \boldsymbol{Y}_e^\gamma &= \mathrm{G}\nabla\gamma - \mathrm{r}\,(\boldsymbol{\beta} - \nabla\gamma) \\ \boldsymbol{X}_e^\beta &= \mathrm{r}\,(\boldsymbol{\beta} - \nabla\gamma) & \boldsymbol{Y}_e^\beta &= 0 \\ \boldsymbol{X}_d^p &= \boldsymbol{\sigma} - \mathbb{H} : \boldsymbol{\varepsilon}^p & \boldsymbol{Y}_d^\gamma &= 0 \\ X_d^\gamma &= -\mathrm{J}\gamma + (\mathrm{G}+\mathrm{r})\nabla^2\gamma - \mathrm{r}\nabla\cdot\boldsymbol{\beta} & \boldsymbol{Y}_d^\gamma &= 0 \\ \boldsymbol{X}_d^\beta &= \mathrm{r}(\nabla\gamma - \boldsymbol{\beta}) & \boldsymbol{Y}_d^\beta &= 0 \end{aligned}$$

$\boldsymbol{X}_d^\beta$ used to replace the role of $\boldsymbol{Y}_d^\gamma$ in loading functions as well as flow laws of model II, thus leading to model I problem.

$$\begin{aligned} f &= f(\boldsymbol{X}_d^p, X_d^\gamma, \boldsymbol{X}_d^\beta) = \|\boldsymbol{X}_d^p\| + X_d^\gamma + \frac{1}{\ell}\,\|\boldsymbol{X}_d^\beta\| - k \leq 0; \\ \dot{\boldsymbol{\varepsilon}}^p &= \lambda \frac{\partial f(\boldsymbol{X}_d^p, X_d^\gamma, \boldsymbol{X}_d^\beta)}{\partial \boldsymbol{X}_d^p} = \lambda \frac{\boldsymbol{X}_d^p}{\|\boldsymbol{X}_d^p\|} \\ \dot{\gamma} &= \lambda \frac{\partial f(\boldsymbol{X}_d^p, X_d^\gamma, \boldsymbol{X}_d^\beta)}{\partial X_d^\gamma} = \lambda \qquad \text{where} \quad \lambda \geq 0; f \leq 0; \lambda f = 0 \\ \dot{\boldsymbol{\beta}} &= \lambda \frac{\partial f(\boldsymbol{X}_d^p, X_d^\gamma, \boldsymbol{X}_d^\beta)}{\partial \boldsymbol{X}_d^\beta} = \frac{1}{\ell}\,\lambda \frac{\boldsymbol{X}_d^\beta}{|\boldsymbol{X}_d^\beta|} \\ &\nabla\cdot\boldsymbol{\sigma} + f_{vu} = 0 \end{aligned}$$

• $\forall x \in \partial V$

$$\begin{aligned} &\boldsymbol{\sigma}\cdot n = f_{su} \quad \text{on } \partial V_{fu}, \quad u = u_d \quad \text{on } \partial V_u, \quad \partial V_{fu} \cap \partial V_u = \partial V \\ &\big((\mathrm{G}+\mathrm{r})\,\nabla\gamma - \mathrm{r}\,\boldsymbol{\beta}\big)\cdot\boldsymbol{n} = 0 \quad \text{on } \partial V \end{aligned}$$

3.1.8 Gradient Model of plasticity ε^p with isotropic and kinematic hardening

a) State and complementary laws

Similarly, in small transformation, a Gradient Model of the total plasticity $\boldsymbol{\varepsilon}^p$ with isotropic-kinematic hardening is now considered in the context of the linear hardening and model I, for the sake of simplicity:

$$\begin{cases} W & = W(\boldsymbol{\varepsilon}, \boldsymbol{\varepsilon}^p, \nabla\boldsymbol{\varepsilon}^p, \gamma) = W_e + W_c + W_i + W_g \\ & = \frac{1}{2}(\boldsymbol{\varepsilon}-\boldsymbol{\varepsilon}^p) : \mathbb{L} : (\boldsymbol{\varepsilon}-\boldsymbol{\varepsilon}^p) + \frac{1}{2}\boldsymbol{\varepsilon}^p : \mathbb{H} : \boldsymbol{\varepsilon}^p + \frac{1}{2}\mathrm{J}\gamma^2 + \frac{1}{2}\,\mathrm{G}\,\nabla\boldsymbol{\varepsilon}^p \vdots \nabla\boldsymbol{\varepsilon}^p \quad (3.71a) \\ D & = D(\dot{\boldsymbol{\varepsilon}^p}, \dot{\gamma}) \Longleftrightarrow \text{gradient-independent function (model I)} \quad (3.71b) \end{cases}$$

For example, a dissipation potential of the form $D = k(\gamma)\left\|\dot{\phi}\right\|$ can be assumed.

Using (3.5) with $\phi = (\boldsymbol{\varepsilon}^p, \gamma)$ and (3.17), the state and complementary laws and extended forces expressions yield:

$$\begin{cases} \boldsymbol{\sigma}_e = W_{,\varepsilon} = \mathbb{L} : (\boldsymbol{\varepsilon} - \boldsymbol{\varepsilon}^p) = \boldsymbol{\sigma} - \boldsymbol{\sigma}_d = \boldsymbol{\sigma}, & \boldsymbol{\sigma}_d = \partial D_{\dot{\varepsilon}} = 0 \\ \boldsymbol{X}_e^{\varepsilon^p} = W_{,\boldsymbol{\varepsilon}^p} = -\mathbb{L}:(\boldsymbol{\varepsilon}-\boldsymbol{\varepsilon}^p) + \mathbb{H}:\boldsymbol{\varepsilon}^p = -\boldsymbol{\sigma}+\mathbb{H}:\boldsymbol{\varepsilon}^p & \boldsymbol{X}_d^{\varepsilon^p} = \partial D_{\dot{\boldsymbol{\varepsilon}}^p} \neq 0 \\ \boldsymbol{Y}_e^{\varepsilon^p} = W_{,\nabla\boldsymbol{\varepsilon}^p} = \mathrm{G}\nabla\boldsymbol{\varepsilon}^p & \boldsymbol{Y}_d^{\varepsilon^p} = \partial D_{\nabla\dot{\boldsymbol{\varepsilon}}^p} = 0 \\ \boldsymbol{A}_e^{\varepsilon^p} = W_{,\boldsymbol{\varepsilon}^p} - \nabla\cdot W_{,\nabla\boldsymbol{\varepsilon}^p} = -\boldsymbol{\sigma} + \mathbb{H} : \boldsymbol{\varepsilon}^p - \mathrm{G}\,\nabla^2\boldsymbol{\varepsilon}^p, & \boldsymbol{A}_d^{\varepsilon^p} = -\boldsymbol{A}_e^{\varepsilon^p} \\ A_e^{\gamma} = W_{,\gamma} = \mathrm{J}\gamma, & A_d^{\gamma} = -A_e^{\gamma} \end{cases} \quad (3.72)$$

in which $\boldsymbol{A}_d^{\varepsilon^p}$ and A_d^{γ} are the dissipative forces associated with $\boldsymbol{\varepsilon}^p$ and γ respectively. The constitutive equations under insulation condition leads to a Mises-like plastic criterion for the force $(\boldsymbol{A}_d^{\varepsilon^p}, A_d^{\gamma})$ as follows:

b) Plastic criterion

A Mises-like plastic criterion (loading functions) is of the form:

$$f(\boldsymbol{A}_d^{\varepsilon^p}, A_d^{\gamma}) = \left\|\boldsymbol{A}_d^{\varepsilon^p}\right\|_{eq} + A_d^{\gamma} - k(\gamma) \leq 0 \quad (3.73)$$

$$\left\|\boldsymbol{A}_d^{\varepsilon^p}\right\|_{eq} = \sqrt{\frac{3}{2}\mathrm{dev}(\boldsymbol{A}_d^{\varepsilon^p}) : \mathrm{dev}(\boldsymbol{A}_d^{\varepsilon^p})}, \quad \mathrm{dev}(\boldsymbol{A}_d^{\varepsilon^p}) = \boldsymbol{s} - \mathbb{H} : \boldsymbol{\varepsilon}^p + \mathrm{G}\,\nabla^2\boldsymbol{\varepsilon}^p$$

The condition $f(\boldsymbol{A}_d^{\varepsilon^p}, A_d^{\gamma}) \leq 0$ defines the convex domain C of admissible forces $\boldsymbol{A}_d^{\varepsilon^p}$ and A_d^{γ}.

c) Evolution laws (normality laws)

• Dual dissipation potential D^* with the help of the indicator function **I**:

$$D^* = D^*(\boldsymbol{A}_d^{\varepsilon^p}, A_d^{\gamma}) = \mathbf{I}\left(\left\|\boldsymbol{A}_d^{\varepsilon^p}\right\| + A_d^{\gamma} - k(\gamma) \leq 0\right)$$

• Plastic strain and equivalent plastic strain rates:

$$\begin{cases} \dot{\boldsymbol{\varepsilon}^p} = N_C(\boldsymbol{A}_d^{\varepsilon^p}) = \lambda\frac{\partial f(\boldsymbol{A}_d^{\varepsilon^p}, A_d^{\gamma})}{\partial \boldsymbol{A}_d^{\varepsilon^p}} \\ \dot{\gamma} = N_C(A_d^{\gamma}) = \lambda\frac{\partial f(\boldsymbol{A}_d^{\varepsilon^p}, A_d^{\gamma})}{\partial A_d^{\gamma}} \end{cases} \quad f \leq 0,\ \ \lambda \geq 0,\ \ f\,\lambda = 0 \quad (3.74)$$

The additional boundary condition from (3.14.d), using (3.72), gives:

$$\boldsymbol{Y}\cdot\boldsymbol{n}=\boldsymbol{Y}_e\cdot\boldsymbol{n}=\mathrm{G}\,\nabla\varepsilon^p\cdot\boldsymbol{n},\quad\Longleftrightarrow\quad\varepsilon^p_{,n}=0 \tag{3.75}$$

Finally, for a solid V subjected to a classical loading path and a controlled displacement on a portion of its boundary, in small and quasi-static transformation from a given initial state u_o, f_o, under the constitutive insulation condition after Polizzotto, the governing equations are here reported:

- $\forall x\in V$

$$\begin{aligned}
\boldsymbol{\sigma}=\boldsymbol{\sigma}_e=W_{,\varepsilon}=\mathbb{L}:(\boldsymbol{\varepsilon}-\boldsymbol{\varepsilon}^p) &\qquad \boldsymbol{\sigma}_d=0\\
\boldsymbol{X}_e^{\varepsilon^p}=-\boldsymbol{\sigma}+\mathbb{H}:\boldsymbol{\varepsilon}^p &\qquad \boldsymbol{X}_d^{\varepsilon^p}\neq 0\\
\boldsymbol{Y}_e^{\varepsilon^p}=\mathrm{G}\nabla\boldsymbol{\varepsilon}^p &\qquad \boldsymbol{Y}_d^{\varepsilon^p}=0\\
\boldsymbol{A}_e^{\varepsilon^p}=-\boldsymbol{\sigma}+\mathbb{H}:\boldsymbol{\varepsilon}^p-\mathrm{G}\,\nabla^2\boldsymbol{\varepsilon}^p &\qquad \boldsymbol{A}_d^{\varepsilon^p}=-\boldsymbol{A}_e^{\varepsilon^p}\\
A_e^{\gamma}=\mathrm{J}\gamma &\qquad A_d^{\gamma}=-A_e^{\gamma}
\end{aligned}$$

$$\left\|\boldsymbol{A}_d^{\varepsilon^p}\right\|_{eq}=\sqrt{\frac{3}{2}\mathrm{dev}\,(\boldsymbol{A}_d^{\varepsilon^p}):\mathrm{dev}\,(\boldsymbol{A}_d^{\varepsilon^p})}$$

$$f(\boldsymbol{A}_d^{\varepsilon^p},A_d^{\gamma})=\left\|\boldsymbol{A}_d^{\varepsilon^p}\right\|_{eq}+A_d^{\gamma}-k(\gamma);\quad f\leq 0,\quad\lambda\geq 0,\quad f\,\lambda=0$$

$$\dot{\boldsymbol{\varepsilon}}^p=\lambda\frac{\partial f(\boldsymbol{A}_d^{\varepsilon^p},A_d^{\gamma})}{\partial\boldsymbol{A}_d^{\varepsilon^p}}=\lambda\sqrt{\frac{3}{2}}\frac{\boldsymbol{A}_d^{\varepsilon^p}}{\left\|\boldsymbol{A}_d^{\varepsilon^p}\right\|}$$

$$\dot{\gamma}=\lambda\frac{\partial f(\boldsymbol{A}_d^{\varepsilon^p},A_d^{\gamma})}{\partial A_d^{\gamma}}=\lambda=\sqrt{\frac{2}{3}}\left\|\dot{\boldsymbol{\varepsilon}}^p\right\|$$

$$\nabla\cdot\boldsymbol{\sigma}+f_{vu}=0$$

- $\forall x\in\partial V$

$$\boldsymbol{\sigma}\cdot\boldsymbol{n}=f_{su}\quad\text{on}\ \partial V_{fu},\qquad u=u_d\quad\text{on}\ \partial V_u,\quad\partial V_{fu}\cap\partial V_u=\partial V$$

$$\varepsilon^p_{,n}=0\quad\text{on}\ \partial V$$

3.1.9 Discussion

In this section, the constitutive equations of Standard Gradient Models are conveniently described from the expressions of the energy and dissipation potentials. Our attention is focussed on the derivation of the governing equations as a generalized Biot equation, on the formalism of generalized standard materials and on time-independent processes such as incremental plasticity and brittle damage. In particular, the theoretical difficulty concerning the case of gradient-dependent dissipation (Models II) is underlined. In the next section, as example, illustrations for several common cases are shown, and one of them, a Gradient Model of accumulated plasticity with linear or nonlinear isotropic-kinematic hardening, is

also detailed in the computational aspect. And finally this will be applied to represent, via some typical problems, the well-known micro-mechanical phenomenon called the effect ***"smaller is stronger"***.

3.2 Numerical implementation

3.2.1 Gradient Model of accumulated plasticity γ with isotropic and kinematic hardening

This section is devoted to the numerical implementation of the proposed Gradient Model, in which the ***deformation plasticity method (deformation theory)*** is used. The model II is considered for the sake of generality as the model I can be easily obtained from that by just imposing $\mathrm{r}=0$. On the other hand, in the present work, only materials with spatially isotropic behavior are considered. First, a linear hardening is examined and then the generalization for nonlinear hardening is treated.

a) Governing equations

1. von Mises-like plastic criteria (3.67):

$$\begin{cases} f = f(\boldsymbol{X}_d^p, X_d^\gamma, \boldsymbol{X}_d^\beta) = \|\boldsymbol{X}_d^p\| + X_d^\gamma + \dfrac{1}{\ell}\,\|\boldsymbol{X}_d^\beta\| - k \le 0 & \text{(3.77a)} \\ \text{with:} \quad \|\boldsymbol{X}_d^p\| = \sqrt{\dfrac{3}{2}(\boldsymbol{\xi}:\boldsymbol{\xi})} = \sqrt{\dfrac{3}{2}}\,\|\boldsymbol{\xi}\| & \\ \qquad \boldsymbol{\xi} = \mathrm{dev}(\boldsymbol{X}_d^p) = \mathrm{dev}(\boldsymbol{\sigma} - \mathbb{H}\boldsymbol{\varepsilon}^p) = \boldsymbol{s} - \mathbb{H}\boldsymbol{\varepsilon}^p \ \ (\mathbb{H}\text{: 4-order tensor}) & \\ \qquad X_d^\gamma = -\mathrm{J}\gamma + (\mathrm{G}+\mathrm{r})\nabla^2\gamma - \mathrm{r}\,\nabla\cdot\boldsymbol{\beta} & \text{(3.77b)} \\ \qquad \boldsymbol{X}_d^\beta = \mathrm{r}(\nabla\gamma - \boldsymbol{\beta}) & \text{(3.77c)} \\ \text{thus} \quad f = \sqrt{\dfrac{3}{2}}\|\boldsymbol{\xi}\| - \mathrm{J}\gamma + (\mathrm{G}+\mathrm{r})\nabla^2\gamma - \mathrm{r}\,\nabla\cdot\boldsymbol{\beta} + \dfrac{1}{\ell}\big|\mathrm{r}(\nabla\gamma - \boldsymbol{\beta})\big| - k \le 0 & \text{(3.77d)} \end{cases}$$

2. Evolution laws (3.68), with the boundary conditions as in (3.70):

$$\begin{cases} \bullet\ \dot{\boldsymbol{\varepsilon}}^p = \lambda\dfrac{\partial f(\boldsymbol{X}_d^p, X_d^\gamma, \boldsymbol{X}_d^\beta)}{\partial \boldsymbol{X}_d^p} = \lambda\sqrt{\dfrac{3}{2}}\,\dfrac{\boldsymbol{\xi}}{\|\boldsymbol{\xi}\|} \\ \bullet\ \dot{\gamma} = \lambda\dfrac{\partial f(\boldsymbol{X}_d^p, X_d^\gamma, \boldsymbol{X}_d^\beta)}{\partial X_d^\gamma} = \lambda \\ \bullet\ \dot{\boldsymbol{\beta}} = \lambda\dfrac{\partial f(\boldsymbol{X}_d^p, X_d^\gamma, \boldsymbol{X}_d^\beta)}{\partial \boldsymbol{X}_d^\beta} = \dfrac{1}{\ell}\,\lambda\dfrac{\boldsymbol{X}_d^\beta}{|\boldsymbol{X}_d^\beta|} \\ \bullet\ \text{Boundary conditions as in (3.70)} \end{cases} \qquad \text{where: } \lambda \ge 0;\ f \le 0;\ \lambda f = 0 \qquad \text{(3.78)}$$

From the last incremental equations, an associated model of deformation plasticity (Hencky) can be defined by replacing $\dot{\boldsymbol{\varepsilon}}^p$, $\dot{\gamma}$ and $\dot{\boldsymbol{\beta}}$ by $\boldsymbol{\varepsilon}^p$, γ and $\boldsymbol{\beta}$. Thus, the associated Hencky model equations are:

$$\begin{cases} \bullet\ \boldsymbol{\varepsilon}^p = \lambda\sqrt{\dfrac{3}{2}}\,\dfrac{\boldsymbol{\xi}}{\|\boldsymbol{\xi}\|} & \text{(3.79a)} \\ \bullet\ \gamma = \lambda \qquad \text{where: } \lambda \geq 0; f \leq 0; \lambda f = 0 & \text{(3.79b)} \\ \bullet\ \boldsymbol{\beta} = \dfrac{1}{\ell}\,\lambda\dfrac{\boldsymbol{X}_d^\beta}{|\boldsymbol{X}_d^\beta|} & \text{(3.79c)} \\ \bullet\ \text{Boundary conditions as in (3.70)} & \text{(3.79d)} \end{cases}$$

The next item is devoted to numerical integration of the deformation theory in which an 1-step schema is used (Hencky algorithm). The inherent nature of this method, by means of the passage from (3.78) to (3.79), makes it an implicit algorithm.

b) Algorithm (implicit schema)

The case of deformation plasticity is thus obtained from the incremental description by a 1-step increment from the initial state. However, the problem is solved by iterations in which the total forces are updated as $F^{tot} = F_d^{ext} + F^p(\boldsymbol{\varepsilon}^p)$ after the value of $\boldsymbol{\varepsilon}^p$ of the previous iteration; F_d^{ext} are the external forces and $F^p(\boldsymbol{\varepsilon}^p)$ the plastic forces associated with $\boldsymbol{\varepsilon}^p$.

For each iteration, all quantities $u, \varepsilon, \gamma, \boldsymbol{\varepsilon}^p, \boldsymbol{\sigma}, etc$, are re-calculated from the initial state 0, using the updated total forces F^{tot}.

All the following quantities are understood corresponding to the last increment with regard to the considered problem, therefore accompanied without any iteration index.

For each iteration, one has to:

1. Calculate u, ε as elastic solution

2. Compute γ and $\boldsymbol{\beta}$ by solving a Laplacian equation of unknown γ after an explicit schema with internal iterations between γ and $\boldsymbol{\beta}$:

   - Calculate $\boldsymbol{\beta}$:
     From (3.79c), $\boldsymbol{\beta}$ is collinear with $\boldsymbol{X}_d^\beta$; combining with (3.77c) and noting the positivity of r, $\boldsymbol{\beta}$ is also collinear with $\nabla\gamma$. Finally one gets:

     $$\boldsymbol{\beta} = \frac{\gamma\,\nabla\gamma}{\ell\,|\nabla\gamma|} = \boldsymbol{\beta}(\gamma) \tag{3.80}$$

   - Calculate γ:

     $$\boldsymbol{\xi} = \boldsymbol{s} - \mathbb{H}\boldsymbol{\varepsilon}^p = 2\mu\,\boldsymbol{e} - (\mathbb{H} + 2\mu)\boldsymbol{\varepsilon}^p \tag{3.81}$$

     where $\boldsymbol{s} = \text{dev}(\boldsymbol{\sigma})$; $\boldsymbol{\sigma} = \lambda_L\, tr(\boldsymbol{\varepsilon} - \boldsymbol{\varepsilon}^p)\underline{\underline{\mathbf{1}}} + 2\mu(\boldsymbol{\varepsilon} - \boldsymbol{\varepsilon}^p)$; and $\boldsymbol{e} = \text{dev}(\boldsymbol{\varepsilon})$. Here λ_L and μ are Lamé coefficients.
     $\mathbb{H}\boldsymbol{\varepsilon}^p = \text{H}\boldsymbol{\varepsilon}^p$ for a spatially isotropic material (H: hardening modulus).

From (3.79a), $\boldsymbol{\xi}$ and $\boldsymbol{\varepsilon}^p$ are collinear. Combining with (3.81), $\boldsymbol{\xi}$ and $\boldsymbol{e}$ are collinear too. Therefore the last allows to write:

$$\|\boldsymbol{\xi}\| = 2\mu\,\|\boldsymbol{e}\| - (\mathrm{H}+2\mu)\|\boldsymbol{\varepsilon}^p\| = 2\mu\,\|\boldsymbol{e}\| - (\mathrm{H}+2\mu)\lambda\sqrt{\frac{3}{2}} \tag{3.82}$$

Thus (3.77d) follows, with the mind that $\gamma = \lambda$:

$$-\ell^2 f_1(1+f_2)\nabla^2\gamma + \left(\frac{\mathrm{J}+1.5\mathrm{H}+\mathrm{r}/\ell^2}{2\mu}+\frac{3}{2}\right)\gamma = \sqrt{\frac{3}{2}}\,\|\boldsymbol{e}\| - \frac{k+\mathrm{r}\left(\nabla\cdot\boldsymbol{\beta}+|\nabla\gamma|/\ell\right)}{2\mu} \tag{3.83}$$

Two coefficients f_1 and f_2, defined by $\mathrm{G}=2\mu\ell^2 f_1$ and $\mathrm{r}=f_2\mathrm{G}$ are used instead of G and r to make more flexible for the modules' magnitude.

For example, a particular case, the non-Gradient Model ($\mathrm{r}=0$) with linear isotropic hardening, i.e. $J(\gamma)=J\gamma$, gives:

$$\gamma = \frac{2\mu}{\mathrm{J}+3\mu}\left\langle\sqrt{\frac{3}{2}}\,\|\boldsymbol{e}\| - \frac{k}{2\mu}\right\rangle_+ \tag{3.84}$$

$\left\langle\ \cdot\ \right\rangle_+$ denotes the positive part.

Consequently, (3.83) in a more familiar form, is:

$$\begin{cases} -\mathrm{K}\nabla^2\gamma + \mathrm{c}\gamma = \mathrm{f}_{imp} \\ \mathrm{K} = \ell^2 f_1(1+f_2) \quad \text{and} \quad \mathrm{c} = \left(\dfrac{\mathrm{J}+1.5\mathrm{H}}{2\mu}+\dfrac{3}{2}\right) \\ \mathrm{f}_{imp} = \left\langle\sqrt{\dfrac{3}{2}}\,\|\boldsymbol{e}\| - \dfrac{k}{2\mu}\right\rangle_+ - \dfrac{\mathrm{r}\left(\nabla\cdot\boldsymbol{\beta}+|\nabla\gamma|/\ell\right)}{2\mu} \\ \text{Boundary conditions as in (3.70)} \end{cases} \tag{3.85}$$

With a **given deformation field**, $\mathrm{f}_{imp} = f(\gamma)$ is a function of γ as it includes $\boldsymbol{\beta}$ which is a nonlinear function with respect to γ due to the expression (3.80).

The second of the boundary conditions in (3.70) in this case, is:

$$\begin{aligned} &[(\mathrm{G}+\mathrm{r})\nabla\gamma - \mathrm{r}\boldsymbol{\beta}\,]\cdot\boldsymbol{n} = 0 \iff \left[\ell^2 f_1(1+f_2)\nabla\gamma - \ell^2 f_1 f_2\boldsymbol{\beta}\,\right]\cdot\boldsymbol{n} = 0 \\ &\implies \mathrm{K}\nabla\gamma\cdot\boldsymbol{n} = \frac{\mathrm{r}\boldsymbol{\beta}}{2\mu}\cdot\boldsymbol{n} = \Phi_d; \quad \Phi_d \text{ defined for use later in (3.91)} \end{aligned} \tag{3.86}$$

In the more general case, a Gradient Model with nonlinear isotropic and kinematic hardening, the corresponding energy potential parts W_i and W_c in (3.61a) are no longer so simple, they are only known under their derivative forms $W_i' = \mathrm{J}(\gamma)$ and $W_c' = \mathrm{H}(\boldsymbol{\varepsilon}^p)$ (instead of $\mathrm{J}\gamma$ and $\mathrm{H}\boldsymbol{\varepsilon}^p$ as before). $\mathrm{J}(\gamma)$ and $\mathrm{H}(\boldsymbol{\varepsilon}^p)$ are nonlinear functions with respect to their arguments.

For example, a function of isotropic hardening $\mathrm{J}(\gamma)$ can be deduced from a given Ramberg-Osgood uniaxial tensile stress-strain curve whose form, denoting E as Young modulus, is:

$$\frac{\varepsilon}{\varepsilon_0} = \frac{\sigma}{\sigma_0} + \left(\frac{\sigma}{\sigma_0}\right)^n,\ n = 5 \div 10,\ \ \varepsilon_0, \sigma_0 \text{ are material parameters, } \varepsilon_0 = \frac{\sigma_0}{E} \tag{3.87}$$

Or, a more simple and popular form of isotropic hardening $\mathrm{J}(\gamma)$ is an exponential function with two material parameters J_∞ and b:

$$\mathrm{J}(\gamma) = J_\infty(1 - e^{-b\gamma}) \tag{3.88}$$

In this work, the second form of $\mathrm{J}(\gamma)$ is used because it offers an easy and rapid numerical convergence. The first one even causes divergence in some cases (see details in the next section).

Then (3.83) becomes:

$$-\ell^2 f_1(1+f_2)\nabla^2\gamma + (\frac{\mathrm{r}}{2\mu\ell^2} + \frac{3}{2})\gamma = \sqrt{\frac{3}{2}}\,\|\boldsymbol{e}\| - \frac{k+\mathrm{J}(\gamma)+1.5\mathrm{H}(\boldsymbol{\varepsilon}^p)+\mathrm{r}\left(\nabla\cdot\boldsymbol{\beta}+|\nabla\gamma|/\ell\right)}{2\mu}$$

And (3.85) becomes:

$$\begin{cases} -\mathrm{K}\nabla^2\gamma + \mathrm{c}\gamma = \mathrm{f}_{imp} \\ \mathrm{K} = \ell^2 f_1(1+f_2) \quad \text{and} \quad \mathrm{c} = \dfrac{3}{2} \\ \mathrm{f}_{imp} = \left\langle \sqrt{\dfrac{3}{2}}\,\|\boldsymbol{e}\| - \dfrac{k}{2\mu} \right\rangle_+ - \dfrac{\mathrm{J}(\gamma)+1.5\mathrm{H}(\boldsymbol{\varepsilon}^p)+\mathrm{r}\left(\nabla\cdot\boldsymbol{\beta}+|\nabla\gamma|/\ell\right)}{2\mu} \\ \text{Boundary conditions still as in (3.70) which second one is (3.86) too} \end{cases} \tag{3.89}$$

Note that $\boldsymbol{\xi}$ and $\boldsymbol{e}$ are collinear and that $\boldsymbol{e}$ is known, (3.79a) allows to express:

$$\boldsymbol{\varepsilon}^p = \lambda\sqrt{\frac{3}{2}}\,\frac{\boldsymbol{\xi}}{\|\boldsymbol{\xi}\|} = \gamma\sqrt{\frac{3}{2}}\,\frac{\boldsymbol{e}}{\|\boldsymbol{e}\|} = \boldsymbol{\varepsilon}^p(\gamma) \tag{3.90}$$

Then $\mathrm{H}(\boldsymbol{\varepsilon}^p) = \mathrm{H}\big(\boldsymbol{\varepsilon}^p(\gamma)\big)$, a nonlinear function with respect to γ.

Thus f_{imp} is a nonlinear function of γ, including the nonlinear terms $\nabla\cdot\boldsymbol{\beta}(\gamma)$, $\mathrm{J}(\gamma)$, $\mathrm{H}\big(\boldsymbol{\varepsilon}^p(\gamma)\big)$, $|\nabla\gamma|$, not only $\nabla\cdot\boldsymbol{\beta}(\gamma)$ as before. Once f_{imp} is known (via the value of γ know from the previous iteration), a familiar diffusion-like equation is found which can be classically solved in global way. Eq. 3.89 is thus solved by a Newton method, using *internal iterations*. See details in the appendix .1.

Finally, (3.85) or (3.89) are the constitutive equations which give γ and $\boldsymbol{\varepsilon}^p$ in terms of $\boldsymbol{\varepsilon}$ (or $\boldsymbol{e}$ rather) as the solution of a diffusion problem in which the right member f_{imp} is assumed known.

Hence, an *explicit schema* is needed where $\mathrm{f}_{imp} = f(\gamma)$ of the current iteration is known via the value γ from the previous internal iteration; and then the Laplacian equation (3.85) or (3.89) are solved as in diffusion problem.

The principal steps for the internal iterations (index "i" is assigned to the i^{th} iteration) are:

- Initializing $\gamma_1 = 0$ for the 1^{st} internal iteration.

- Calculating for the i^{th} internal iteration the value of $\mathrm{f}^i_{imp} = f(\gamma_{i-1})$.

- Calculating γ^i by solving the laplacian equation (as thermal problem) with f^i_{imp} known.

- Repeating the above steps (steps $2^{nd}, 3^{rd}$) until the convergence of γ.

Finally after calculating γ and then the other quantities such as $\boldsymbol{\beta}$ (with the help of (3.80)), $\boldsymbol{\varepsilon}^p, \boldsymbol{\sigma}$, ..., and $F^{tot} = F^{ext}_d + F^p(\boldsymbol{\varepsilon}^p)$ is updated for the next global iteration.

3. Restart a new global iteration until the convergence.

c) Numerical implementation

By finite elements (FE), the following Galerkin representation is considered:

$$u(x) = u^m U_m(x); \gamma(x) = \gamma^n N_n(x)$$

The nodal values u^m and γ^n lead to column matrices $[u]$ and $[\gamma]$ while $\boldsymbol{\varepsilon}$, $\boldsymbol{\varepsilon}^p$ and $\boldsymbol{\sigma}$ are fields defined numerically at Gauss points.

For a given field of plastic strain $\boldsymbol{\varepsilon}^p$, the equilibrium equations under a given loading and plastic strain lead to a global matrix equation for the displacement u.

$$\big[\mathcal{K}\big]\{\mathbb{U}\} = F^{ext}_d + F^p(\boldsymbol{\varepsilon}^p)$$

where $\big[\mathcal{K}\big]$ denotes the elastic stiffness matrix.

For a given displacement $[u]$, the associated fields of $\boldsymbol{\varepsilon}^p$ and $\boldsymbol{\sigma}$ and the equivalent plastic $[\gamma]$ are determined by a diffusion-like problem since (3.85) or (3.89) depending on the case of linear or nonlinear hardening, respectively.

As in diffusion problem, matrix equations are:

$$\begin{cases} \big[\,[\mathbb{K}] + [\mathbb{C}]\,\big]\{\gamma\} = \{\mathbb{F}\} \\ [\mathbb{K}] = \displaystyle\int_V \{\nabla \mathrm{N}_i\}^T \mathrm{K}\, \{\nabla \mathrm{N}_j\}\, dV \quad \text{and} \quad [\mathbb{C}] = \int_V \{\mathrm{N}_i\}^T \rho \mathrm{c}\, \{\mathrm{N}_j\}\, dV \\ \{\mathbb{F}\} = \displaystyle\int_V \{\mathrm{N}_j\}\, \mathrm{f}_{imp}\, dV \quad + \quad \int_{\partial V_q} \{\mathrm{N}_j\}\, \Phi_d\, d\Gamma \end{cases} \tag{3.91}$$

where K, c and f_{imp} can be directly found at (3.85) or (3.89), Φ_d as roughly mentioned in (3.86) or more detailed in Appendix (10). A clear distinction with the non-gradient model can be seen by means of the expression of $\{\mathbb{F}\}$. The presence of the second term here corresponding to the additional boundary condition (insulation condition by Polizzotto) which only exists in the gradient model.

This equation is similar to classical diffusion equation found in computer FE codes, *cf.* CAST3M for example. The presence of nonlinear term $\mathrm{H}\big(\boldsymbol{\varepsilon}^p(\gamma)\big), \mathrm{J}(\gamma), \boldsymbol{\beta}(\gamma), |\nabla\gamma|$ in the expression of f_{imp} and Φ_d is dealt by Newton method. The positive condition $\gamma \geq 0$ leads finally to the following algorithm, in the

general case of nonlinear hardening:

$$\begin{cases} \big[\,[\mathbb{K}]+[\mathbb{C}]\,\big]\{\gamma^*\}=\{\mathbb{F}\} \\ \gamma=0 \;\text{ if }\; \|\boldsymbol{e}\|<\sqrt{\dfrac{2}{3}}\dfrac{k}{2\mu} \;\text{ or }\; \gamma^*<0, \quad \text{after (3.89)} \\ \gamma=\gamma^* \quad \text{otherwise} \end{cases}$$

Details of the numerical implementation are given in Appendix (.1).

3.2.2 Applications

Here are some most typical examples in applying SSGP models for mechanical problems at micro scale. The gradient plasticity model with isotropic-kinematic hardening is used.

All the following results are numerical simulations of the reference counterparts in [53; 54]. The numerical results of Fleck and Hutchinson in [54] are obtained from flow and deformation theories. All quantities (stress, strain, torque, twist, displacement, volume change, film thickness, radius of wire, of void...) are plotted in diagrams with their *respective normalized values* concerning the well-known parameters $(\sigma_0, \varepsilon_0)$ of the Ramberg-Osgood uniaxial tensile stress-strain curve in (3.87).

Three problems are computationally solved in this section: *(1)* shearing of a thin film layer sandwiched between two substrates, *(2)* thin wire torsion, and *(3)* expansion of a spherical micro void (similar to the role of indenter size in micro-indentation). These typical problems permit to draw conclusions about the effective of Gradient Model as well as the role the material length parameter ℓ plays. In each study, a Ramberg-Osgood curve characterizing the uniaxial tensile stress-strain relation of the solid, is replaced by an equivalent exponential curve.

Every numerical result shows a rather good accordance with the reference counterparts in which the effect *"Smaller is Stronger"* at sufficiently small scale is found. Moreover, apart from the numerical curves of the proposed model corresponding to different specimen size, the **upper and lower saturation bounds** about the specimen size are also found and presented. They define the range of validity of the model.

a) Thin film shearing: the role of film thickness

Consider the typical shearing problem of a thin film layer. An infinite elastic plastic film layer is sandwiched between two substrates rigid enough, $-\infty \leq x_1 \leq \infty$, of height $2L$, $-L \leq x_2 \leq L$, where each face is bonded to a rigid substrate. The substrates are displaced such that top and bottom of the layer undergo relative shearing displacements, $u_1 = U$ and $u_1 = -U$ at $x_2 = \pm L$, respectively. The only non-zero displacement is $u_1(x_2)$, which is assumed to be independent of x_1.

The "size effect" is here taken into account by the help of two factors. The first, as the inherent nature of Gradient Model adopted, is the presence of the *"gradient term"* in governing equations; and the second, just appearing in the *"inclusion/interface problems"* because of a supplementary boundary condition called **(nonstandard boundary or interface conditions)**, is the presence of the constrained

plastic flow within the *"inclusion/interface layer"*. In this specific case, the shearing of a thin film blocked between two substrates rigid enough, such an additional condition is to ensure the vanishing of plastic strain, i.e. $\varepsilon^p = 0, \gamma = 0$, at the boundary of thin film. These conditions using classical models without SSGP term are not enough to offer a good numerical result especially in the case the "inclusion" scale is more and more smaller. Thus, a model with both factors included (the presence of SSGP term and the complementary boundary condition concerning the constrained plastic flow within "inclusion/interface") is necessary in this case.

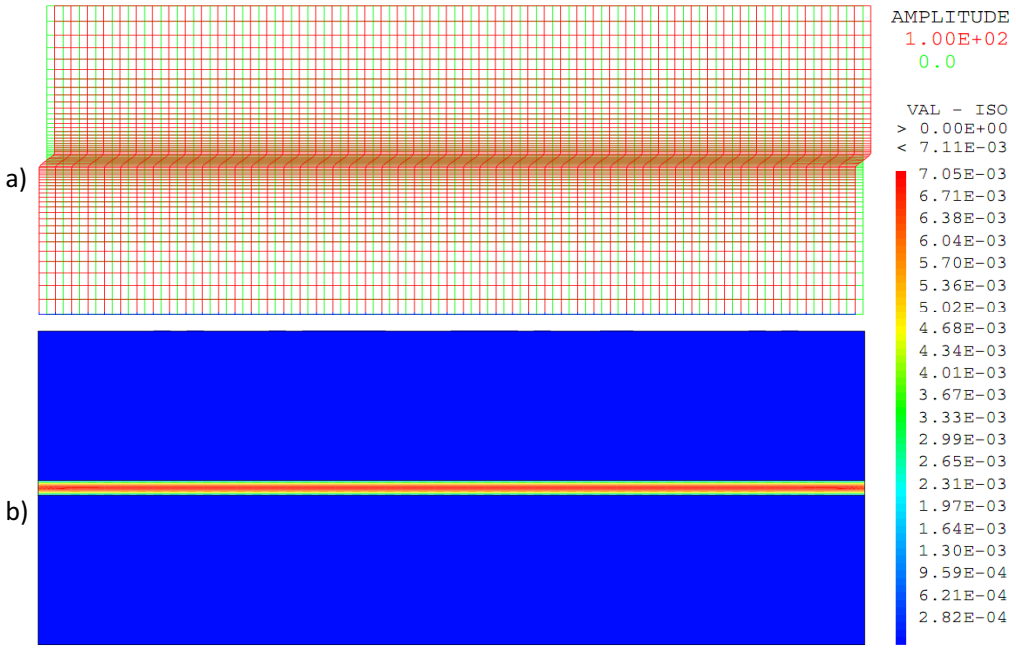

Figure 3.1 : *Thin film shearing simulation: (a) deformation; (b) accumulated plasticity* (*cf.* Fleck and Hutchinson [54])

Numerical results are plotted on diagrams as in Fig.3.2 and Fig.3.3. The role of passivated film thickness is: the smaller the film thickness, the higher the material resistance.

A procedure to validate the reference numerical results of Fleck & Hutchinson 2001 is given in Appendix (.2). A very brief procedure is summarized here by means of the thin film case as illustration. The set of parameters to identify is $\varepsilon_0, \sigma_0, \ell$. Their calibration is performed using the following procedure: for a given film thickness, we seek for the parameters giving the same curves as the ones of FH (Fleck and Hutchinson). The length scale ℓ obtained here is a half the FH's one. Then, shearing of thin films of various thicknesses continues to be simulated. A rather good agreement between numerical results and counterparts is shown. The same procedure is applied for the following other tests.

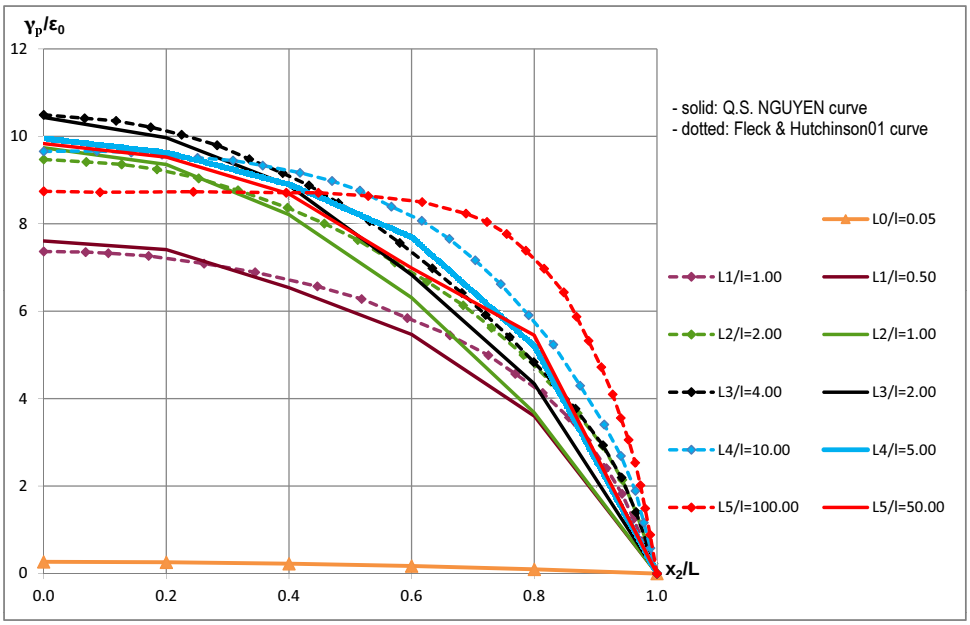

Figure 3.2 : *Thin film shearing simulation: distribution of plastic shear strain across the upper half of the sheared layer at* $U/(\varepsilon_0 L)=10$ *for various values of* ℓ/L (*cf.* Fleck and Hutchinson [54])

b) Thin wire torsion: the role of wire size

A solid cylindrical wire of radius R is subjected to torsion. A cylindrical coordinate system (r,θ,z) is employed. When the wire of isotropic material is twisted monotonically, the total shear strain is $\varepsilon_s=\alpha r$ where α is the twist per unit length. The case-study is without constraint to the plastic flow at the surface of the wire (constraint-free surface). [3] Simulation results are presented in Fig.3.4. A very close accordance between numerical results and counterparts is shown. The role of wire size is: the smaller the radius of the wire, the higher the material resistance.

c) Micro-void growth: the role of void size

Micro-void growth problem has been intensively studied in damage mechanics to interpret a common fracture mechanism of ductile metals which is nucleation, growth, and coalescence of voids (e.g. Rice and Tracey 1969 [147]; Gurson 1977 [75]; Needleman et all. 1992 [114]; Tvergaard 1990 [168]). However, none of those widely used for void growth problems from the literature involve any dependence on void size, even though they are sometimes applied to voids of micron or even sub-micron size. There is some indirect evidence that voids in the micron to sub-micron size range are less susceptible to growth at a given stress state than larger voids. Nowadays more and more experimental examinations of this issue were carried out. Theoretically, N.A. Fleck and J.W. Hutchinson (*cf.* Fleck 1997 [53], Fleck

[3] If the surface of the wire is covered by a very thin elastic coating that blocked dislocations, a supplementary boundary condition must be $\dot{\varepsilon_p}=0$.

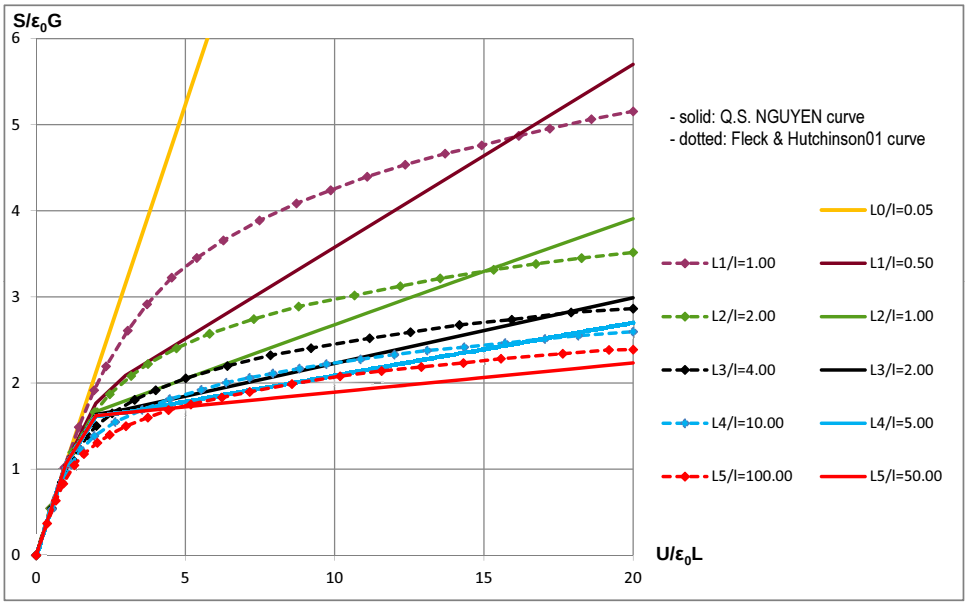

Figure 3.3 : *Thin film shearing simulation: effect of the material length parameter ℓ on the overall relation between the shear traction and the shearing displacement for the elastic-plastic layer* (*cf.* Fleck and Hutchinson [54])

01 [54]) are ones of the pioneers with their first work presented in [53] and a reformulation later in [54]. It is interesting to study theoretically the effect of void size upon void growth and within the context of the present class of SSGP theory. Moreover, as often discussed in the literature, void growth phenomena may provide a robust means for confronting strain gradient plasticity predictions with experiment. Void growth mechanism is of the same nature as that of micro-indentation and the results of one of both can be used for the other.

Let us consider a sphere of initial radius R in an infinite solid subject to a remote spherically symmetric tension $\boldsymbol{\sigma}^{\infty}$. Numerical results obtained with the model proposed show a very good agreement with the corresponding counterparts from Fleck and Hutchinson [54] as in Fig.3.5. The role of void size is: the smaller the radius of void, the harder the stretch.

d) Micro-indentation: the role of indenter size

Indentation tests are a common means of assessing the hardness of material. The indenter is either a rigid cone with angle $\boldsymbol{\beta}$ or a rigid sphere of radius R, and is loaded with a normal force P. The hardness is defined as $H = \dfrac{P}{\pi a^2}$, where a is the radius of contact of the indenter (*cf.* Wei 2003 [180], Fleck 1997 [53]). The "size effect" has been found in indentation hardness testing for long time, similarly to the void growth problem. A lot of factors can give rise to a hardness measurement such as the indentation shape and size, surface effects, and the absence of nearby dislocation sources for micro/nano-scale indents, etc. However, it seems clear about a strong dependence on indentation size in the range of micron to sub-

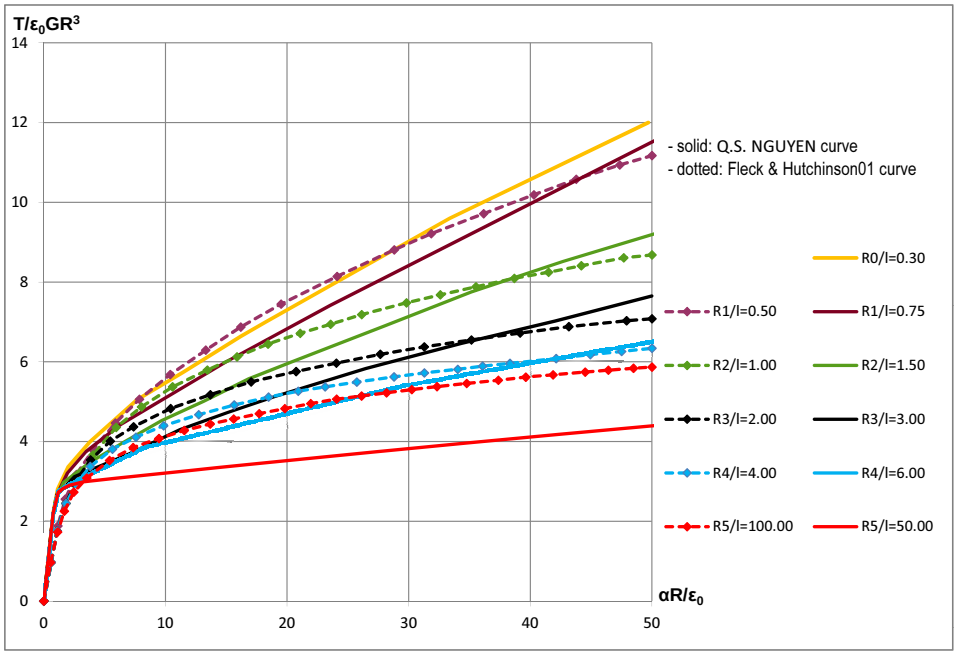

Figure 3.4 : *Thin wire torsion simulation: torque versus twist for a solid wire of radius* R (*cf.* Fleck and Hutchinson [54])

micron indents. That dependence is attributed to the increasing dominance of Geometrically Necessary Dislocations compared to Statistically Stored Dislocations when indents become smaller (Poole *et al.* 1996 [145]; Stelmashenko *et al.* 1993 [158]; Ma and Clarke 1995 [98]; Nix 1988 [123]). The indentation test is a good manner for measuring the material length scale ℓ in the strain gradient constitutive model. Further, this problem is actually very related to the micro-void growth problem because of the same mechanism for both. In the literature, one even uses micro-indentation problem result as approximate result for the micro-void growth problem, or vice versa. For this reason, this work does not dedicate longer to that case-study.

3.2.3 Discussion

a) Procedure to calibrate the experimental results

Detail of procedure to validate the reference numerical results of Fleck & Hutchinson 2001 can be found in Appendix (.2). In the same spirit with a bit change, a method to calibrate the adopted model via the experimental results requires to:

- carry out experiments to draw the uniaxial tensile stress-strain curve of the considered material.
- carry out experiments to draw the experimental curves similar to those in [54], such as curves "Normalized remote stress against normalized volume expansion of micro-void" for example. They are corresponding to various radii in a certain consistent ration between each other, for example, by

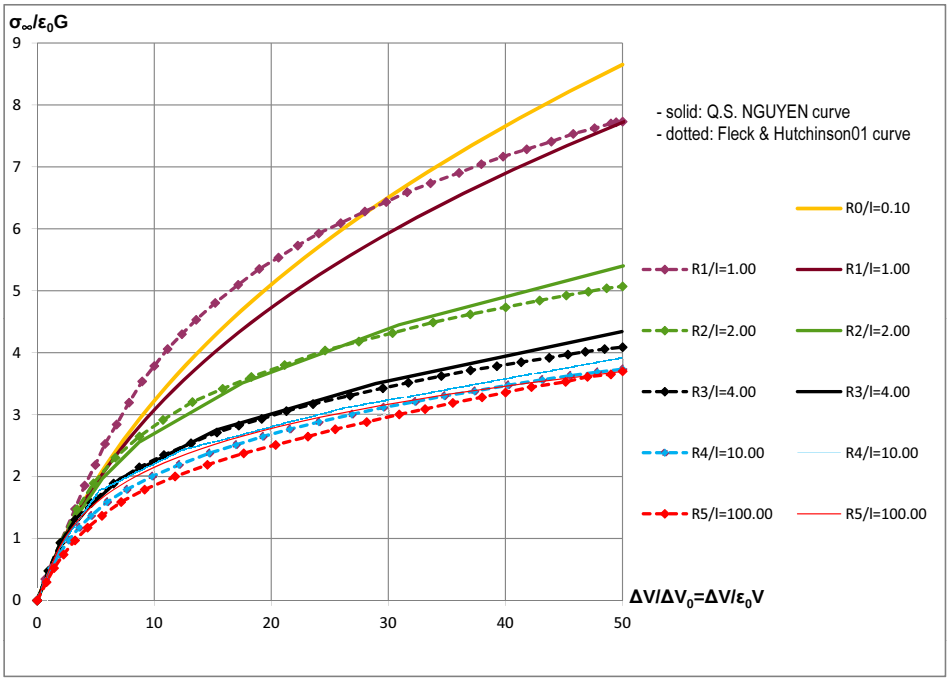

Figure 3.5 : *Micro-void growth simulation: remote stress as a function of normalized volume expansion for a spherical void subject to hydrostatic tension* $\boldsymbol{\sigma}_\infty$ *at infinity* (*cf.* Fleck and Hutchinson [54])

always keeping $R_{i+1}^{exp}/R_i^{exp} = 2,\ i = 1 \div 4$. These radii are real values of specimen tests. Hence that is not the same situation as the validation of the reference numerical results in ([54]) where the radii just play "symbolic" role (see Appendix).

- identify a set of parameters (J_∞, b) of the exponential uniaxial tensile stress-strain curve after the experimental data.

- identify a set of parameters (G or f_1, r or f_2,...), and ℓ in order that simulated curves fit as well as possible experimental ones, provided that the radii used in simulation are the same as experimental ones. To do so, the following process is performed:

  - For each set of parameters of the model adopted excluding ℓ, try to find ℓ in order that the first simulated curve (curve 1) fits well the experimental curve 1.

  - With that value of ℓ then R_i/ℓ already known at the moment for any of i, other parameters also known, thereby remaining simulated curves ($i = 2, 3...$) are easily drawn on the same plot.

  - Try these steps a number of times with various sets of parameters. Among them, find out an optimal set of parameters including ℓ which is the one giving a good agreement not only for the curve 1 as first supposed, but also for the other curves 2, 3,...

Remark: The length ℓ is in principle a *material intrinsic quantity*, so independent from the load level and geometry dimension. That means, that value of ℓ experimentally determined can be re-used to

predict mechanical behavior for any load level of the same loading mode, and for any dimension of the same material (any radius R of micro-void, for example).

b) Comments

(i) Comparison between Model-I or Model-II

Numerical results of the cases considered show that there is no too much difference between simulations by Model I and Model II. An preliminary conclusion is that, at least for the problems related to microsystems (thin film, micro-void, micro wire, etc.), the Model I is favored thanks to its simplicity as compared to the Model II, and enough to predict mechanical behaviors in micro-mechanics.

For the problems concerning material microstructure (grain size, reinforcement size), such a conclusion is left out due to the lack of experimental data.

(ii) Advantage of the model adopted

The model proposed is rather simple, but rather well reproduces the "size effect" in microsystems problems, at least for some typical case-studies in [54] which are well-known and acknowledged by many other authors as reference data.

Numerical calculation also shows the meshing-independent property as expected.

(iii) Limit of the model: order of the material intrinsic length ℓ

Computation shows that the "size effect" is captured only within a certain range of the ratio R/ℓ, out of which the numerical results tend to be unchanged. More concretely, the simulation for some typical case-studies displays the ratio R/ℓ lies within roughly 0.01 up to 100 (most frequently $0.1 \div 10$). On the other hand, the magnitude order of the "basic dimension" of this kind of micromechanical problems (radii R of micro-void or thin wire, thickness L of thin film, for example), from the literature, is only about micron or sub-micron ([53; 54]). Consequently the value of ℓ here, which needs to be experimentally determined, is theoretically estimated about $(0.1 \div 10)\ \mu m$, that means in micron also.
Using the Gradient Models adopted, both lower and upper saturation bounds about specimen size are observed. Using the models for specimen size out of the interval delimited by the two thresholds, the numerical results seems not to be changed. The results corresponding to specimen size as from the upper threshold are similar to those by classical models.

To sum up, the preliminary conclusion is that: the scope of the model adopted lies within **micron or sub-micron scale, i.e, micro-mechanics**, not smaller. A nano-scale, for example, it requires other approaches.

3.3 Conclusion

The present work presents a simple formulation of gradient plasticity model extending the classical standard plasticity model. The objective is to predict both "size" and gradient effects, not included yet in the classical mechanics but become important in micro-mechanics, by taking into account just the

gradient effect[4]. A new class of SSGP [5] Constitutive Models in the context of the **micro-mechanics, continuum thermodynamics and generalized standard materials**, are proposed. Both formulation and numerical implementation are addressed. The constitutive equations are conveniently described from the expressions of the energy and the dissipation potentials, or from a generalized Biot equation using an extended version of virtual work principle. The attention is focussed on time-independent processes such as incremental plasticity and brittle damage. In particular, the theoretical difficulty concerning the case of gradient-dependent dissipation is underlined.

The presence of strain gradient in the local formulation leads to a **Laplacian equation needing to be solved at global level**, and insulation boundary condition to **non-standard boundary value problem**. A computational method based on diffusion-like problem is used. Some illustrations are given, including SSGP Model of accumulated plasticity with linear or nonlinear isotropic and kinematic hardening. The model well reproduces both phenomena **"Smaller is Stronger" and "Higher Gradient is Stronger"** concerning the microsystems' geometry size for some available reference data. In this work, the nature of these two phenomena is also clarified. "Higher Gradient is Stronger" is only related to the gradient effect, while "Smaller is Stronger" is related to both the pure size and gradient effects where the latter is dominant - rather than totally to the pure size effect as usually believed. Finally consulting the value of the material length scale ℓ from literature and basing on the simulation for some typical problems, a conclusion drawn is that, the scope of the model proposed with respect to specimen size is about **micron or sub-micron**.

The formulation simplicity and distinct computational advantages of the class of models adopted make it convenient for applications in micro-mechanical problems.

In this study, apart from microsystems problems well treated, microstructure problems (concerning the material grain size) are expected to be also done with the model adopted due to the *material characteristic length* related to the grain size. Because of lack of experimental data, validation for this case is left for a further work.

[4] Let us recall that in this study, the gradient effect has to be present as prerequisite, whereas the pure size effect is proved unimportant, and the size effect by Dislocation Starvation is left out at micron scale; then taking into account the gradient effect is enough to model both gradient effect and "size effect" which actually is rather the gradient effect related to the size.

[5] Strain Standard Gradient Plasticity

PART B: Gradient Fatigue Criteria

CHAPTER 4

Literature review

The synthesis and analysis of [131; 17; 132; 179; 112] together with some comments is represented in this chapter. The specific citations will be detailed later.

4.1 Problematic introduction: fatigue at small scale

Fatigue criteria for metals under multiaxial cyclic loadings at small scales have taken interest more and more in mechanics communities. The need derives from the appearance of small components in the industrial domain such as electronic components, electro-mechanical devices, etc. In addition, a reliable design of industrial parts against high-cycle multiaxial fatigue requires fatigue criteria capable of predicting as much as possible important effects at small scale such as the size, gradient (volumetric distribution of stresses), load type (loading mode), machining (residual stress state, defect distribution) effects, etc. These effects are very important in the transfer of fatigue data from laboratory specimen to component, or from one components to an other. Indeed, the fatigue data transferability is often very difficult due to the previous effects which are not considered in the conventional fatigue criteria. In literature, experimental evidences show the influence of these factors on the fatigue strength via a typical example of round specimens with different diameters resulting in difference fatigue limits. In addition, the same phenomenon can be seen with the material specimens including notches with different sizes and geometries, or those possessing different residual stress states. All these are useful for demonstrating tendencies; but in most cases, components have much more complex shape, notches, and residual stress state, etc, so that the data transfer seems to be impossible. Furthermore, for the same size and geometry of a specimen or a component it is well known that the load type has an influence on the fatigue limit (difference between torsion, tension, rotative bending and plane bending). To design against fatigue, it is necessary to take into account the effects of the previous factors (*cf.* [131]).

4.2 Important effects on fatigue limit at small scale

4.2.1 Size effect and Gradient effect: difference and correlation

It has been known for a long time that fatigue limit depends on the spatial stress distribution (volumetric stress distribution) and also on the size of the component. Nevertheless, the so-called "stress

gradient effect" [1] and "size effect" are very closely linked and make confused; distinguishing them more clearly is necessary here for the further development of the study. A good review of these two effects was proposed by Papadopoulos and Panoskaltsis [135], and will be more analyzed in the Chapter 5. Furthermore, to study the stress gradient effect, studying the fatigue strength of notched components is not suitable because the presence of a notch produces in many cases high stress-strain concentrations and so local plastic strains. Pure stress gradient effect needs to be separated from the local plastic strain effect to avoid unnecessary confusion. The present investigation will be limited to macroscopically elastic behavior of components. In [135], the authors review a lot of experiments in tension, plane and rotative bending with smooth cylindrical specimens in different diameters and different lengths. For example, results from Pogoretskii and Karpenko [140] and from Pavan [136] show a decrease of the fatigue limit with the increase of the specimen diameter and with its length also. By noting that the moment in the four-point plane bending is independent of the specimen length, the Papadopoulos and Panoskaltsis explain that the dependence on the length of constant moment fatigue limits is a pure size effect; the gradient of normal stress is not length dependent. Fatigue data from [140] prove that the influence, on the fatigue limit, of the specimen diameter is an order of magnitude higher than the effect of its length. Experiments from Phillips and Heywood [138] under fully reversed tension show a very small size effect. Similarly, Weber in his work [179] synthesized results of Massonnet [104] to represent a very slight increase tendency in tension-compression fatigue limit with the decrease of specimen radius. This very slight variation is considered as a pure size effect because of the absence of stress gradient in that case. About the torsion fatigue, experiments of Massonnet [104] on specimens of different radii shows a decrease of the fully reversed torsion fatigue limits with the increase of the radius. Not the same as before, this variation is rather significant which is partially attributed to the pure size effect as usual, and in addition, the possible effect of the amplitude of the shear stress gradient which must be clarified further in this work.

Some following key points are synthesized (*cf.* [131; 17], along with the analyzes in Chapter 1):

- Similarly to the Part A dealing with constitutive models, in the Part B devoted to fatigue criteria here, the size and gradient effects will be also proved to be **two distinct phenomena**, although they are very confused in the literature because of their very close connection. Two well-known phenomena corresponding to them are clarified as follows: **"Higher Gradient is Stronger"** is only attributed to the gradient effect, whereas **"Smaller is Stronger"** in our cases actually is mainly attributed to the gradient effect related to the size - rather than totally to the pure size effect as usually believed. The size effect (at least pure size effect) always exists, while the gradient effect may be present or not, independently.

- On the one hand, it requires to consider that, taking into account the volumetric stress distribution

[1] The notion of "stress gradient" is incorrect and less strict than that of "spatial stress distribution" as two different volumetric stress distributions can have identical gradients at certain points. For example, in plane and rotating bending test of cylindrical specimens, both stress instant gradients are identical but volumetric stress distributions are not. However, this improper term will be kept in the thesis as it has been largely used.

in calculating fatigue life is generally more important than pure size effect. On the other hand, the pure size effect may be still not negligible in certain cases. This effect is also linked with the process used for machining components and for finishing their surface (grinding, polishing,...) as mentioned below. From probabilistic point of view of fatigue damage, the pure size effect inherently concerning material defects should be treated in probabilistic approach. In this thesis for cases considered, it will be shown that this effect can be negligible compared to the others.

In the next chapter (Chapter 5), we will return these issues to make more clear about these effects as well as corresponding phenomena in fatigue.

4.2.2 Loading effect

It is well known in high cycle fatigue, that the load type, i.e. the mode of loading on the object, has a significant influence on the fatigue strength. Different load types result in different stress states for components. For example, the volumetric stress distribution states in torsion, tension and bending tests are different. Even in bending test, although the stress gradient (or more precisely, stress instant distribution) in rotative bending and plane bending is the same, the volumetric stress distributions all over the loading cycle are not the same. Therefore, different load types lead to different fatigue strengths for components of the same geometry and material. Basing on the analyzes in Chapter 5, loading effect is shown naturally attached to the gradient effect.

4.2.3 Other factors

According to the synthesis of [17; 179; 112] and many other authors, some following factors also play particular role with respect to the fatigue of the metals.

- Machining: The machining process also has an important effect on fatigue strength because fatigue crack nucleation depends on the finishing state of the component surface (grinding, polishing, etc...). In this paper, this "technological effect" is not considered. The surface layer and roughness of both laboratory specimen and real industry component (with residual stresses if any) are presumed to be identical. If the states of the surface layers are not equal, the differences must be in principle taken into account in a suitable manner (empirical rules in general).

- Notches: The presence of notches causes high stress-strain concentrations and local plastic strain. Pure stress gradient effect has to be separated from the local plasticity effect for which a cyclic-plastic material behavior law must be considered to compute, by finite element analysis, the real stress-strain distributions. This is a complicated subject needing to be thoroughly treated in another framework of study.

- Defects (*cf.* [112]): Similarly to the presence of notches, that of defects causes a locally high stress concentration state and a high plasticity around here. In the material, the set of points where the equivalent stress is higher than a certain threshold (which value depends on each fatigue

criterion), can participate in fatigue crack nucleation because the stress level is high enough to allow microcracks and microdefects to grow up to a macrocrack. This is physical interpretation of the influence of defects. A probabilistic approach could be imagined to consider the distribution of defects in the volume influencing fatigue crack initiation.

- Inclusions: The presence of inclusions inside the material also causes a high stresses distribution and also leads to the supplementary boundary condition. Hence this is also a separate subject needing to be thoroughly treated in another framework of study.

- Environment (temperature variation, corrosion, etc.): the environment effect is left out in the present study.

4.2.4 Discussion

In the current study, three common effects ("size", gradient and loading effects) which are intimately correlative, will be investigated in order to be in some measure taken into account in the new models. In the next chapter, we will propose that the three effects are not necessary to be modeled in qualitative way for each one, but are modeled in the manner that, the pure size effect is proved negligible, loading mode is attached to gradient effect, and then the last is the only effect to be accounted for.

4.3 Brief review of conventional fatigue criteria: inefficacy at small scale

Many high-cycle multiaxial fatigue criteria for metals are proposed in the literature. After the brief classification by Banvillet 2003 [17], four categories of fatigue criteria can be distinguished. First, until the end of the fifties several empirical formulae were proposed to synthesize many fatigue data (Haigh, Gerber, Marin, Gough and Pollard, etc...). Second, from the observation that after nucleation a microcrack propagates first along a shear plane, many authors assumed that crack initiation is governed by the shear stress (McDiarmid, Findley) or by the second invariant of the deviatoric stress tensor (Sines, Crossland). Third, after the criterion proposed by Dang Van [41], other micro-macro approaches appeared (Papadopoulos, Deperrois, Morel). They consider that elastic shakedown is the condition needed to avoid fatigue crack initiation in unfavorably oriented grains. Fatigue crack initiation in polycrystalline metal is determined from the critical plane containing the easiest slip directions of the grain and experiencing the largest shear strain amplitude. Finally, some fatigue criteria are based on global energy quantities: elastic, plastic or total strain energy density. These approaches do not predict crack orientation, but the computation time of such a model is shorter than for critical plane criteria. All the above proposals are based on the stress (or strain) tensor at a critical point. Therefore none of them, after simple dimensional arguments, is able to predict the "size" and gradient effects, nor the load type effect (they treat indifferently the endurance limits in tension and in bending tests [22; 133]).

4.4 Survey of existing non-conventional fatigue criteria

4.4.1 Brief review

As said above, the conventional fatigue criteria do not capture the previous effects. Hence, it leads to the need of a new class of fatigue criteria to predict fatigue behaviors at small scale. This is the reason why, from about twenties years ago, a few fatigue criteria aim at modeling the previous effects. Examples are found, on the one hand in notches and fretting problems [9; 11; 139; 146; 101], and on the other hand in problems related to small electronic components and electro-mechanical devices. Existing approaches dealing with such problems are, (*cf.* syntheses of [131; 17; 132; 112; 179]): *(1)*- critical layer of Flavenot and Skally 1983 [51]; *(2)*- distance approaches such as: effective distance approach of Pluvinage 1997 [139], Qylafku *and al.* 1999 [146]; theory of critical distances Arauio 2007 [11]; *(3)*- nonlocal approaches such as: maximum stressed-strained volume $V90\%$ by Sonsino *and al.* 1997 [157]; energy based criterion (dealing with the volume V^* influencing fatigue crack initiation) of Palin-Luc and Lasserre 1998a [133]; volumetric energy based criterion of Banvillet *and al.* 2003 [17] and Palin-Luc 2004 [132] developed from Palin-Luc and Lasserre 1998a; gradient method proposed by Brand and Sutterlin 1980, 1981 [34; 33]; *(4)*- local approaches such as: the gradient dependent criterion of Ngargueudedjim and Robert *and al.* 2001 [115]; gradient dependent criterion of Papadopoulos and Panoskaltsis 1996 [135]; and serval derivatives based on the work of Papadopoulos and Panoskaltsis 1996 proposed by Weber 1999 [179] (gradient version of the criterion of Robert 1992 [148], and that of Fogue 1985, 1987 [59; 58]), etc.

Interesting literature reviews of such models are presented in [112; 132; 179]. It is reported in the next section the advantages and the limits of these methods concerning their capacity for predicting the "size", gradient and loading effects on high cycle multiaxial fatigue, are discussed.

In summary, a rough classification of fatigue criteria, after N. Caillet 2007 in his thesis [35], is given in the figure Fig. 4.1

4.4.2 Discussion

The fatigue criteria mentioned before illustrates different types of calculation methods available to predict the "size" and gradient effects in high cycle fatigue. Although this review is not exhaustive, one can notice that two ways are used in establishing non-conventional fatigue criteria. First, some criteria, are based on a characteristic length of the material such as the critical layer and the effective distance. Secondly, three-dimension approaches consider a real volume whose size is non-zero stress/strain state zone (e.g. the $W90\%$ and $W*$ methods).

Except the highly stressed volume $W90\%$ criterion, the size effect is not predicted by almost these methods. The effects of material machining (residual stresses, roughness of the surface layers...), notches, inclusions, defects,...are not predicted neither.

The pure gradient effect is considered by all the previous methods except by the critical layer one. The last approach do not predict the experimental difference between the fatigue limits in tension and in

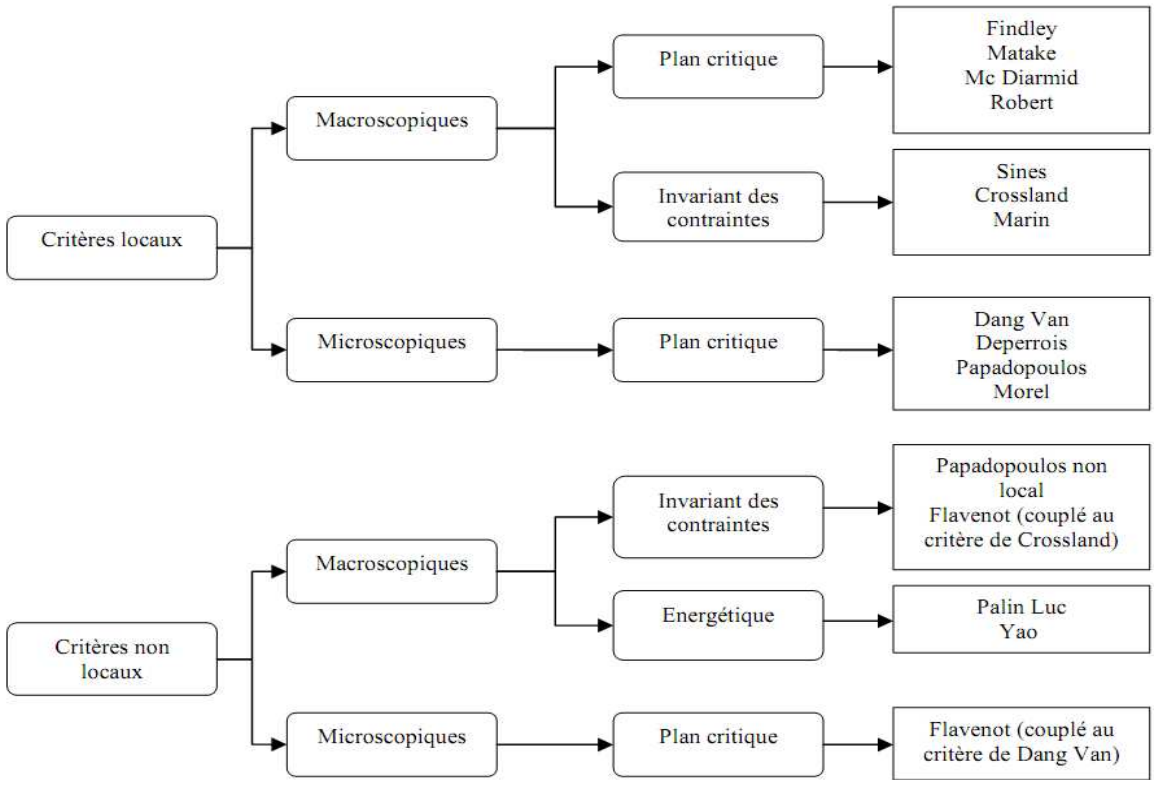

Figure 4.1 : *Classification of different fatigue criteria* (*cf.* Caillet [35])

bending. According to the effective distance approach, this difference can be predicted but the choice of the weight function is not clear. The $W90\%$ and $W*$ methods predict the differences between the endurance limits in tension and in bending but the distinction between plane and rotative bending is only predicted by the $W*$ criterion; while the other considers that this difference is due to a higher probability to find a material defect in rotative bending than in plane bending because of a larger maximum stressed/strained volume.

According to the authors of each proposal, there is a good agreement between experiments and predictions but there is no systematic study yet to compare their accuracy. Moreover, the effect of mean load is not always clear or can not be predicted by these gradient fatigue criteria. Almost the methods are tacitly limited to fully reversed multiaxial loadings. Publications on the effective distance criterion do not explain how to take into account mean loads. For the $W90\%$ criterion a mean stress correction has to be done, but in literature there is not many explanations on this. The critical layer is the only method with a direct mean stress consideration by using Dang Van's criterion.

Papadopoulos and Panoskaltsis 1996 gradient fatigue criterion and its derivatives later, introduce the gradient term into only the hydrostatic stress component of the conventional criteria. This approach is based on the well-established experimental fact for some metals, of the beneficial effect of the normal

stress gradient and the non-effect of the shear stress gradient, on fatigue limit. However, this has not enough the generality for all metals. Furthermore, in such a way, this excludes the possible role of the amplitude of the shear stress gradient.

In summary, among non-conventional fatigue criteria aforementioned, it seems that the criterion proposed by Palin-Luc and Lasserre [133] as well as its evolution later by Banvillet *et al.* [17] possess the most advantages and allow to almost capture the three important effects at small scale (size, gradient and loading effects). Therefore we do not have ambition in the thesis to develop such a kind of criterion, or even one more effective. The our main object here is just to establish another simple class of fatigue criteria extended from conventional ones, which are capable to model the some most important effects on fatigue at small scale.

4.5 Gradient Fatigue Approach proposed

Using as a basis the idea presented in the work of Papadopoulos and Panoskaltsis 1996 [135], we develop here a simple and phenomenological method to formulate an extension of conventional fatigue criteria in order to capture the previous effects.

With the presence of the unique gradient term in the hydrostatic stress part as proposed by Papadopoulos and Panoskaltsis 1996, the gradient fatigue criteria can successfully represent the difference between the fatigue limits in bending and in tension-compression tests. It is also expected to predict the fatigue limit in any other case providing the gradient of the normal stress is present. However, in the case of zero-gradient of normal stress (i.e. pure torsion), such a formulation is unable to represent the experimental results as the possible influence of shear gradient amplitude is ignored. An example is given in Fig.5.6 for the pure torsion test by Massonnet [105]. Differences in fatigue limit at various radii of the specimen are not reproduced using the criterion Papadopoulos and Panoskaltsis 1996.

This leads to the need of establishing a new class of gradient fatigue criteria where the presence of the gradient term in the shear stress part of any conventional local type criterion (Crossland, Sines, Dang-Van,...) is considered. In this way, we here propose a new class of fatigue criteria with the gradient term introduced not only in the normal stress part but also in the shear stress part. This spirit is elaborated in Chapter 5 followed with some typical application to show a good validation with experiment results.

4.6 Conclusion

At small scale, the previous effects on fatigue become important and must be taken into account. It is performed either by formulating new fatigue criteria, or extending conventional criteria where the latter is our objective in the present work. Among these effects, predicting the effects of manufacturing is a very important challenge and will be left out. In this thesis, a new class of gradient fatigue criteria are proposed to capture the three important effects ("size", gradient and loading effects), thereby to represent both well-known phenomena "Smaller is Stronger" and "Higher Gradient is Stronger".

CHAPTER 5

Gradient Fatigue Criteria: formulation and application

5.1 Introduction

In recent years there has been an increasing interest in developing fatigue criteria for metals capable of dealing with high stress gradient (around notches, voids, contacts, etc.) and particular issues related to small scales. Examples are found, on the one hand in notches and fretting problems [9; 165; 11; 139; 146; 101], and on the other hand in problems related to small electronic components and electro-mechanical devices. At sufficiently small sizes, some factors (size, gradient and loading effects) which effects on fatigue limits are inherently not captured by classical fatigue criteria, become important and must be taken into account through new criteria. Among them, experimental evidences show three interconnected ones: size effect, gradient effect[1] and loading effect (*cf.* [135; 131; 17; 132; 112; 179]). A visible general correlation between these factors is that, *"the smaller the size, the higher the gradient, then the higher fatigue resistance"*. There are also cases where the gradient exists but independent from the size, although both influence on material strength (e.g. residual surface stress cases). For the sake of further analyses, it requires to clarify what are the sources of the size effect by isolating it from the gradient effect. Size effect is commonly considered as the pure size effect related to the metallurgical defects and heterogeneity of material, and is proved insignificant compared to the other at the considered scale (e.g. tension-compression fatigue test in Fig. 5.5, [138; 135]). Then a preliminary qualitative remark is that, such a pure size effect just is a part, but not enough to explain the fact well known as *"Smaller is Stronger"* that we observe in fatigue tests.

The gradient effect is another factor which may help to interpret that fact. Such effect, termed here *"Higher Gradient is Stronger"*, is roughly related to three sources: boundary condition, loading mode and size. The first is associated with constraints on dislocation glide (passivated surfaces and interfaces, boundary layers, etc.); the second concerns loading type which decides the spatial stress distribution state in the solid (null gradient in tension-compression, non-zero gradient in bending, etc.); the last is associated with the size (e.g. geometry and grain sizes). For instance, in bending test, the smaller the beam radius the higher the stress gradient (and the higher the fatigue limit). Experimental results [140; 135] on the variation in fatigue strength at various radii conclude to the dominance of the gradient effect upon the pure size effect. Then the sources of the gradient effect prove two things: first, "Smaller is Stronger"

[1] In the current work, this must be understood as stress gradient effect.

experimentally observed is mainly attributed to the gradient effect in the cases considered here, rather than totally to the pure size effect as usually believed; second, the gradient effect, i.e. "Higher Gradient is Stronger", is really a phenomenon different from the size effect.

All previous analyses for both the size and gradient effects imply that although the size and gradient effects are intimately interconnected and usually confused in the literature, they are actually two distinct phenomena. The former only contributing in part to "Smaller is Stronger" and requiring to be modeled by other approach, is negligible compared to the latter and thus left out in the current study; whereas the latter is not only "Higher Gradient is Stronger" but also a main factor contributing to "Smaller is Stronger" that we observe, and is the object of study here. In brief, from phenomenological aspect, "Higher Gradient is Stronger" is naturally related to the gradient effect only, while "Smaller is Stronger" is related to both pure size and gradient effects where the latter is dominant. Then "Smaller is Stronger" here is just a "visible image" of gradient effect rather than the size effect from mechanical point of view. From phenomenological point of view, "Smaller is Stronger" is however an experimentally observed fact that evokes an intuitive relation to the size rather than the gradient. For this reason, henceforth in this research, the terminology *"size effect"* (placed within quotes) is still used for "Smaller is Stronger", but as an apparent size effect; and the terminology *gradient effect* is used for "Higher Gradient is Stronger". In such a sense, an important conclusion drawn is that, *taking into account only gradient effect (related to all its sources) is enough to capture both "size effect" and gradient effect on fatigue resistance*.

In this study, only cases where the gradient effect is present apart from the inherent pure size effect, are considered. As in [135], the notch effect - regarded as a particular case of the gradient effect, is left out in the study restricted to macroscopically elastic behavior or stabilized elastic shakedown state [102]. In such a context and along with the notable conclusion above, Gradient Fatigue Criteria with stress gradient terms introduced are capable to capture the "size", gradient and loading effects, and thus to model both phenomena "Smaller is Stronger" and "Higher Gradient is Stronger", as found in the applications considered here.

Classical fatigue criteria without material length scale predict no size, gradient neither loading effects. The objective is to establish a new class of fatigue criteria for considering the previous factors. Existing approaches dealing with such problems are (*cf.* [131; 17; 132; 112; 179]): *(i)* critical layer of Flavenot and Skally [51]; *(ii)* distance approaches such as: effective distance approach of Pluvinage [139], Qylafku *et al.* [146]; theory of critical distances, Taylor [165], Araujo *et al.* [11]; *(iii)* nonlocal approaches such as: maximum stressed-strained volume by Sonsino *et al.* [157]; energy based criterion of Palin-Luc and Lasserre [133]; volumetric energy based criterion of Banvillet *et al.* [17] and Palin-Luc [132]; gradient method proposed by Brand and Sutterlin [34; 33]; *(iv)* local approaches such as: gradient dependent criterion of Papadopoulos and Panoskaltsis [135]; that of Ngargueudedjim *et al.* [115], and several derivatives based on this work [135] proposed by Fouvry *et al.* [9; 49] and Weber [179] (gradient version of the criterion of Robert [148], and that of Fogue [59; 58]), etc.

The review of Papadopoulos and Panoskaltsis [135] is re-used and developed to make more clear the connection as well as the distinction between the effects by analyzing the role of each dimension of

specimen in fatigue resistance. It is shown that two issues remain: first, the non-effect of the shear stress gradient on fatigue limits is only found for some metals - but not all; second, the influence of the stress gradient amplitude must be clarified. Thereby, in the spirit of [135], gradient fatigue criteria extended from classical ones with stress gradient terms are proposed and validated to clarify the issues. The main idea is to maintain the general framework of the classical fatigue criteria, but to embed into it gradient terms which enable to describe the effects concerning the stress heterogeneous distribution. Three steps are done: first, the dependence of fatigue limit on the previous factors in the cases of uniaxial stress cyclic loadings is phenomenologically analyzed; second, the stress gradient fatigue criteria which capture the previous factors are established; and finally, a generalization to multiaxial loadings is performed and some applications are provided.

The outline of the work is as follows. Section (5.2) focuses on re-analyzing existing experiments on gradient, size and loading effects; in Section (5.3), basing on these analyses as well as notable observations and using as a basis classical fatigue criteria in the spirit of [135], new criteria with stress gradient terms entering not only in the normal stress but as well in the shear stress parts, are proposed in the context of macroscopic elasticity. Such a formulation allows the new criteria to capture the phenomena[2] only by means of gradient terms. These criteria are generalized under multiaxial loadings to be a new class of stress gradient multiaxial fatigue criteria; in Section (5.4) and (5.5), some classical fatigue criteria such as Crossland and Dang Van are extended within such framework; Formulation of gradient fatigue criteria for low-cycle fatigue (LCF) is given in Section (5.6); Section (5.7) is devoted to their numerical implementation; and finally, Sections (5.8) and (5.9) are discussions and conclusions. This work mainly deals with the multiaxial high-cycle fatigue limit (HCF). However some initial propositions will also be given for the multiaxial low-cycle fatigue limit (LCF).

5.2 Analyses of gradient fatigue tests: size, gradient and loading effects

In this section, analyses on single component zero and non-zero gradient fatigue tests from the literature, including two groups, uniaxial normal stress and shear stress tests, are made to clarify the size, stress gradient and loading effects on fatigue limits. The tests exempt from the size and gradient effects, are used as reference. A special attention is also paid on the interpretation of the three effects and their relation as well as the capacity of either eliminating or integrating them into "gradient terms" for some cases. Analyses and preliminary conclusions drawn here for single component fatigue tests are generalized to formulate new gradient fatigue criteria under multiaxial cyclic loadings.

5.2.1 Uniaxial normal stress cyclic loading

a) Experimental observations and interpretation of stress gradient effect

Some analyses of [135] and [179] are reported here on fatigue endurance of metals in bending or tension-compression tests. Two respective distinct groups of results, uniaxial normal cyclic stress states

[2] In this study, these effects are captured in the sense that the gradient effect has to be present as prerequisite - to which the loading effect is naturally attached, whereas and the pure size effect is proved unimportant compared to the others.

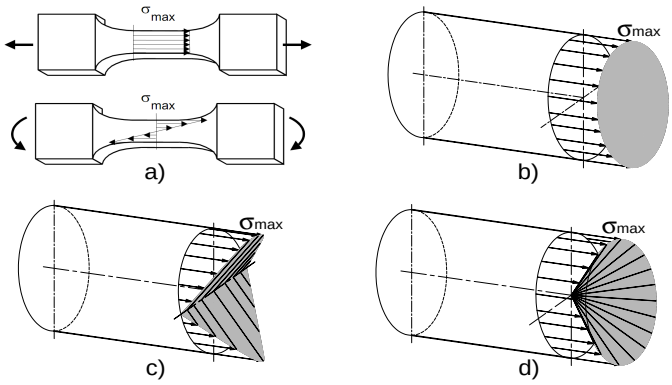

Figure 5.1 : *Stress distribution types in fatigue tests of the same specimen: (a) tension-compression vs. bending tests; (b-c-d) tension-compression vs. rotative bending vs. plane bending* (*cf.* Weber [179])

with non-zero and zero normal stress gradients, respectively, allow to draw some comments about the normal stress gradient effect and about the possibility of integrating the loading effect into gradient effect. In the first example, a well-established experimental fact is always found: for the same smooth geometry and material, and the same nominal stress $\sigma_{\max}$ (Fig. 5.1(a)), the specimen in fully reversed tension-compression test sustains lower nominal fatigue stress than in fully reversed bending test. Or similarly but in another observation [130; 179; 135]: a large number of experiments proved that the fully reversed bending fatigue limit f_{-1} (rotative bending, or plane bending) is always higher than the homologue σ_{-1} in fully reversed tension-compression test for smooth samples with the same geometry and material (Tab. 5.1). This experimental fact is attributed to the *"beneficial gradient effect"* [135], which exists in bending but not in tension. The second experimental example illustrates and makes more clear

Materials	N_D (cycles)	σ_{-1} (MPa)	f_{-1} (rotative bending) (MPa)	Difference between σ_{-1} and f_{-1} (%)
Steel 30NCD16	10^6	560	658	+17.5
Steel XC18	10^6	273	310	+13.6
Iron cast GS61	10^6	245	280	+14.3
Steel 35CD4	10^7	558	581	+4.1

Table 5.1 : *Comparison between the fully reversed tension-compression and rotative bending fatigue limits of smooth specimens with the same geometry and material, for different materials* (Results of Palin-Luc [130], synthesized by Weber [179])

the point of view *"beneficial gradient effect"* and also roughly deals with the *size effect* discussed more in detail in the next analyses. Fig. 5.2 presents the experimental results obtained on smooth circular tubes subjected to tension-compression or rotating bending. In tension-compression the stress gradient

is zero, the results exhibit a *slight increase tendency in fatigue limit* when the radius of test specimens decreases. Because of the absence of stress gradient, this variation of the fatigue limit may be considered as a *pure size effect* analyzed later. With the counterparts in rotative bending, however, a *strong increase tendency in fatigue limit* with decreasing radius and an asymptotic value when the radius increases, are found. Apart from the pure size effect as in the tension-compression case, this strong increase tendency of fatigue limit with the small radius as well as the saturation or insensitivity tendency with the large enough radius again, can be only attributed to the beneficial gradient effect which increases as the radius decreases and vice versa. The two examples above only sketched the *influence of the pure size and gradi-*

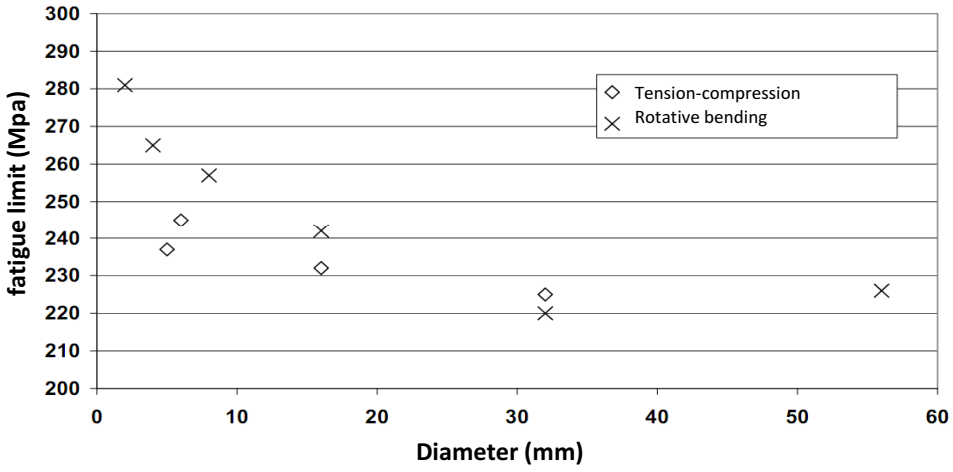

Figure 5.2 : *Evolution of the fully reversed tension-compression and rotative bending fatigue limits of smooth specimens with the same geometry and material according to their radii* (Results of Massonnet [104], synthesized by Weber [179])

ent effects on fatigue limits. Besides these two factors, it remains the loading effect within the context of the current treatment. The study of the loading effect needs to be now put into the consistent framework with the previous others, to thoroughly examine all of three, *from probabilistic point of view of fatigue damage* related to metallurgical defects. Indeed, the difference in fatigue limit in the various test cases of the above examples can be explained from a statistical point of view: the larger these volumes are, the larger the number of defects, i.e. the more the probability of fatigue damage of the specimen is.

First, consider the *pure size effect* through constant moment tests on samples of the same material, bending moment and radius - i.e. the same nominal maximum stress σ and stress gradient, but different lengths (data of [140], represented by [135]). As shown in Fig. 5.4(a), the bending fatigue limit always increases with the decrease in the specimen length. For the same radius, the volume of the most loaded zone decreases with the decrease in the length. Hence, a conclusion drawn about the "pure size effect" is: for the same instant stress distribution as well as nominal maximum stress and material, the smaller the sample size is, the smaller the volume of the most stressed zone is, the higher the fatigue limit is.

Second, three types of tests, in tension-compression, rotative bending and plane bending, for the smooth

specimens with the same geometry and material, subjected to the same nominal maximum stress σ_{max}, are now examined (Fig. 5.1(b-c-d)) in order to make clear the *stress gradient effect*. The fatigue limits [104] are respectively decreasing as as reported in Fig. 5.2 and Tab. 5.2, [179]. For materials with defects, this phenomenon can be explained from a probabilistic point of view. In fact, the common feature of the three tests is, the critical points on their cross-section are subjected to the same stress state. However, the volumes of the most loaded zones are different. In descending volume order, they are tension-compression, rotative bending and plane bending, corresponding to increasing order of fatigue limits. The stress gradient leads to a disparity of the stress distribution, and with the same nominal maximum stress, that also leads to the diminution of the volumes of the most stressed zones, i.e. to the raise of fatigue resistance. The stress gradient is then a quantity able to represent and model all those informations, notably fatigue resistance. Another explanation is related to the average stress in a representative volume element (RVE) [101], which is different between the three tests for the critical point, during a fatigue cycle. This stress is equal to the maximum stress for the tension-compression tests, whereas it is reduced by the presence of a gradient for the bending tests. Therefore, the maximum stress in the RVE and the stress gradient are two relevant quantities for the fatigue resistance; they will be used in the formulation of fatigue criteria taking these phenomena into account.

Third, the *loading effect* implies the influence of loading mode on fatigue limit. For instance, for the same geometry, material and nominal maximum stress, plane bending and rotative bending give different fatigue limits. In fact, the rotative bending induces a more important circumferential stress gradient due to rotation. The loading effect of the rotative bending, as just explained, can be captured by using probabilistic approach or possibly by averaging stresses on a relevant RVE.
To summarize, the pure size, stress gradient and loading mode are three factors influencing on fatigue. Their close connection can be interpreted either under the probabilistic failure aspect as just discussed, or under the average stress in the RVE, although their manifestations are not totally identical. In this study, gradient approaches will be developed to represent some of these phenomena.

Materials	N_D (cycles)	$f_{-1}^{rotative}$ (rotative bending) (MPa)	f_{-1}^{plane} (plane bending) (MPa)	Difference between $f_{-1}^{rotative}$ and f_{-1}^{plane} (%)
Steel 30NCD16	10^6	658	690	+4.9
Steel XC18	10^6	310	332	+7.1
Iron cast GS61	10^6	280	294	+5.0
Steel 35CD4	10^7	581	620	+6.7

Table 5.2 : *Comparison between the fully reversed rotative bending and plane bending fatigue limits for different metals of smooth specimens of the same geometry and material* (Results of Palin-Luc [130], synthesized by Weber [179])

b) Typical fatigue tests

The differences between four-point bending tests and cantilever bending experiments allow to point out the distinction between pure size and gradient effects. In the former, the bending moment is the same at any time in the interval $L \leq x \leq L+l$ and equal to $M = FL$ (Fig. 5.3(a)). The bending stress $\boldsymbol{\sigma}$ and its gradient $\boldsymbol{Y}$ for $L \leq x \leq L+l$ and $-R \leq y \leq R$ are then:

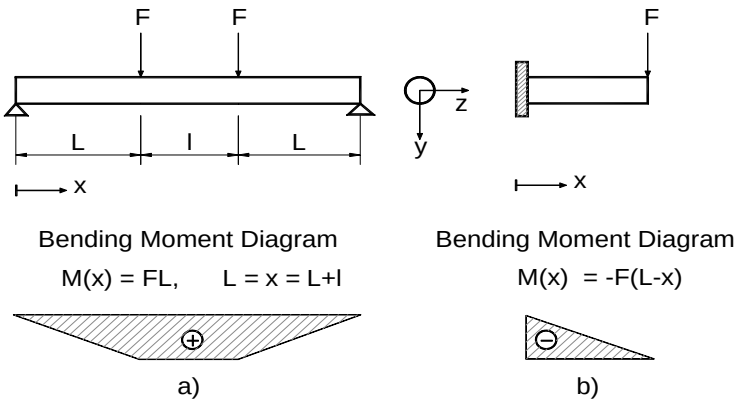

Figure 5.3 : *Four-point bending (constant moment) and cantilever bending tests: (a) four-point bending; (b) cantilever bending [135].*

$$\boldsymbol{\sigma} = \sigma_{xx}\, e_x \otimes e_x \ , \quad \sigma_{xx} = \frac{FL}{I} y \tag{5.1}$$

$$\boldsymbol{Y} = \nabla \boldsymbol{\sigma} \ \text{ with } \ \sigma_{xx,x} = 0 \ , \ \ \sigma_{xx,y} = \frac{FL}{I} = \frac{\sigma_{xx}}{R} \ , \ \ \sigma_{xx,z} = 0 \tag{5.2}$$

in which Eq. (5.2) is written for the most stressed points, i.e. points located at $L \leq x \leq L+l$ and at $y = \pm R$. In both Eqs. (5.1) and (5.2), all components not mentioned are null. The notations $\sigma_{xx,x}, \sigma_{xx,y}$ and $\sigma_{xx,z}$ mean partial derivative of σ_{xx} relative to respectively x, y and z.
In the cantilever bending test the bending moment is: $M = -F(L-x)$ (Fig. 5.3(b)). The bending stress and its gradient for $0 \leq x \leq L$ and $-R \leq y \leq R$ are given by:

$$\boldsymbol{\sigma} = \sigma_{xx}\, e_x \otimes e_x \ , \quad \sigma_{xx} = \frac{-F(L-x)}{I} y \tag{5.3}$$

$$\boldsymbol{Y} = \nabla \boldsymbol{\sigma} \ ; \quad \sigma_{xx,x} = \frac{F}{I} y = \frac{-\sigma_{xx}}{L} \ , \ \sigma_{xx,y} = \frac{-F(L-x)}{I} = \frac{\sigma_{xx}}{R} \ , \ \sigma_{xx,z} = 0 \tag{5.4}$$

Eq. (5.4) is written for the critical points, i.e. those at $x = 0$ and $y = \pm R$.
In their work, [135] did distinguish clearly the pure size and gradient effects on fatigue limits, and both obviously concern the specimen size in diverse manners. Now it is worthy recalling and making more clear the role each specimen size (such as the length L and radius R of the beam) plays in the pure size and gradient effects on fatigue strength. The aim of such analysis is to answer to a question: "Is it possible to formulate fatigue criteria which can include these both effects in a certain sense just by introducing in classical criteria appropriate "gradient terms"? As well-known, according to many authors the pure size effect should be addressed within the context of statistical approaches. To answer to the question, the

role of each sample dimension must be clarified. First of all, it is confirmed that both length and radius of specimens affect on the fatigue limit (Fig. 5.4): the larger the radius and/or the length, the lower the fatigue endurance. But a more important question is: by means of which effect they influence on the fatigue resistance (through the pure size effect, or the gradient effect, or even both simultaneously)? On the one hand, the influence of L on the fatigue limit is a well-established experimental fact after the results of [140] synthesized by [135] in Fig. 5.4(a). On the other hand, in view of Eq. (5.2) showing the independence of the normal stress gradient on L, thus the role of L in the fatigue limit in four-point bending is clearly realized through solely the pure size effect not gradient effect.

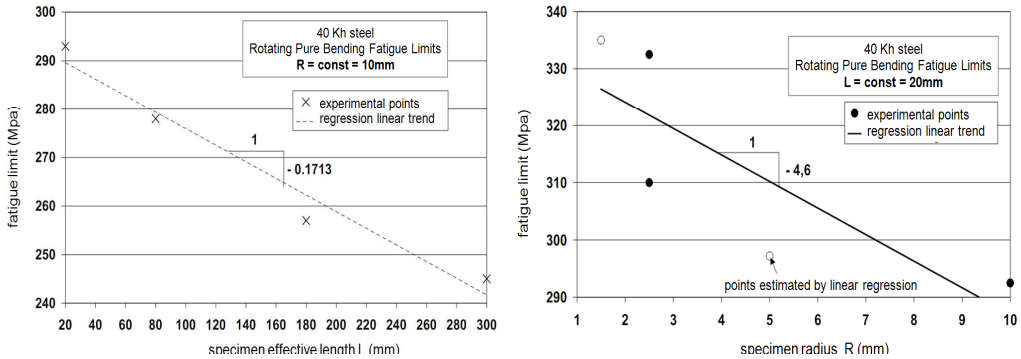

Figure 5.4 : *Constant moment bending fatigue limit data: (a) constant radius R; (b) constant length L* (Results of Pogoretskii and Karpenko [140], represented by Weber [179])

On the contrary, apart from the pure size effect, the gradient effect is present as the normal stress gradient is not zero and is also R dependent (Eq. 5.2).

The quantitative estimate of the contribution of the pure size effect made in [135], using the results of the constant moment tests on specimens of the same radius but different lengths, is recalled and used. The slope of the linear trend observed for the (fatigue limit-R) data in Fig. 5.4(a) is much higher than the one for the (fatigue limit-L) data in Fig. 5.4(b). This shows that the gradient effect is an order of magnitude higher than the pure size effect. It eventually results in, for the case of constant moment tests, a preliminary conclusion that, an appropriate introduction of the normal stress gradient terms in the expression of fatigue criteria is enough to reproduce the experimental results.

The influence of L and R on the fatigue limit are now realized by means of the inherent pure size effect and the gradient effect as both the length L and the radius R are present in the expression of the normal stress gradient (Eq. 5.4). From the previous observations, one can conclude that a presence of normal stress gradient terms in the formula of fatigue criteria, such as Eq. (5.4), is enough to accurately model these fatigue tests.

Besides this analysis, the experiments of [138], performed under fully reversed tension-compression on specimens of various sizes, manifested a negligibly small pure size effect on the observed fatigue limits. These experimental data are depicted in Fig. 5.5 for cylindrical specimens of a mild steel and a nickel-chromium steel, where the observed fatigue limits are plotted against the specimen radii. It seems

that no systematic pure size effect related to R exists. In another class of results, Fig. 5.2 indicates a slight increase tendency of tension-compression fatigue limit with the decrease in specimen radius. A conclusion drawn from these results is, the pure size effect is negligible, at least within the size range under consideration.

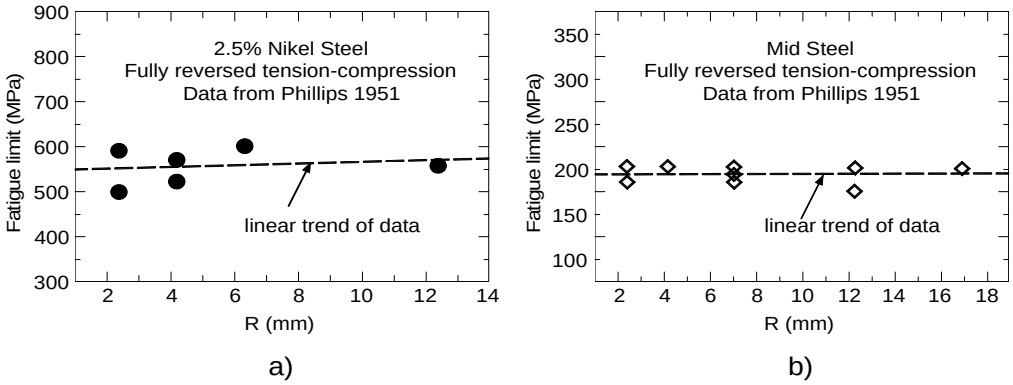

Figure 5.5 : *Fully reversed tension-compression fatigue limit data* (Results of Phillips and Heywood [138], represented by Papadopoulos and Panoskaltsis [135])

5.2.2 Shear stress cyclic loading

Cyclic torsion tests (fully reversed and/or asymmetrical torsion tests) from the literature are examined in this section. Torsion tests intrinsically exhibit shear stress gradients, which are therefore always present in the cases considered here. The comparison of the torsion fatigue limit between different superimposed mean torque tests, i.e. different mean shear stresses as well as its gradients for the same smooth geometry and material, is re-analyzed.

The experimental result, clearly demonstrated by the compilation in [156], is that the fatigue limit in torsion is the same in fully reversed and in any asymmetrical torsion tests for the same smooth geometry and material. Basing on this fact, [135] did conclude the independence of the fatigue limit from the shear stress gradient effect for some metals. In view of this, [135] did not introduce any gradient term concerning shear stresses in their fatigue criteria. Departing from this result, we add the argument that such an independence of the fatigue limit does not ensure a similar independence from the amplitude of the shear stress gradient. Thus, the amplitude of the shear stress gradient is introduced in the relevant component of fatigue criteria (sec. 5.4.3).

To consider this capability, the shear stress state and its gradient in torsion tests for $-R \leq r \leq R$, are written down:

$$\boldsymbol{\sigma} = \sigma_{xz}\,(e_x \otimes e_z + e_z \otimes e_x); \quad \sigma_{xz} = \frac{M}{I} r = \frac{M}{I}\sqrt{x^2+y^2} \tag{5.5}$$

$$\boldsymbol{Y} = \nabla\boldsymbol{\sigma}\ ; \quad \left[\sigma_{xz,x} = \frac{M}{I}\frac{x}{\sqrt{x^2+y^2}} = \sigma_{xz}\frac{x}{R^2}, \sigma_{xz,y} = \frac{M}{I}\frac{y}{\sqrt{x^2+y^2}} = \sigma_{xz}\frac{y}{R^2}, \sigma_{xz,z} = 0\right] \tag{5.6}$$

where Eq. (5.6) is written for the maximum strained points, i.e. $r = R$.

The influence of R on the fatigue limit, experimentally observed as in Fig. 5.6 after [104] is concretized

through the pure size effect and the shear stress gradient amplitude effect presumably. According to the previous analyses, the pure size effect concerning R is regarded as negligible compared to the latter. Therefore the introduction of a shear stress gradient amplitude term is sufficient to reproduce the experimental results.

5.2.3 Discussion

Analyses in the section 5.2.1 show that: (i) the gradient effect on four-point bending fatigue limits related to the length is null whereas the pure size effect related to the length is negligible compared to both pure size and gradient effects related to the radius. (ii) the gradient effect on tension-compression fatigue limits related to all dimensions is null whereas the pure size effect related to the radius can also be negligible, at least within the radius size range under consideration. Analyses in the section 5.2.2 prove that: (iii) for the considered metallic materials, the shear stress gradient effect on torsion fatigue limits through all dimensions is null and the role of the stress gradient amplitude effect is possible.

These estimations allow to preliminarily confirm the possibility to formulate new gradient fatigue criteria well reproducing the analyzed experimental results. In brief, the above indepth comparative analysis demonstrates the negligibility of the pure size effect, whereas affirms the strong influence of the normal stress gradient as well as the non-influence of the shear stress gradient, and especially allows supposing the possible role of the shear stress gradient amplitude. Indeed, a dependence of the pure torsion fatigue limit of a cylinder on its radius is only attributed to the shear stress gradient amplitude effect as both normal and shear stress gradient effects are here null while the pure size effect is always insignificant. Hence, apart from a gradient term introduced into the normal stress component as proposed in [135], another term of gradient amplitude into the shear stress component of any fatigue criterion is indispensable (most visibly for the case of the pure torsion). The rationale of introducing a gradient term into the shear stress part is more reinforced if one notes that the non-effect of the shear stress gradient on fatigue interpreted by [135] is only found for some metals considered, but not meaning for all, thus such a presence of gradient is generally reasonable.

5.3 Formulation of gradient multiaxial high-cycle fatigue criteria

5.3.1 General form of the classical fatigue endurance criteria

A general form of the fatigue limit criteria can be written as follows:

$$f\big(C_a(\boldsymbol{n}^*), N_a(\boldsymbol{n}^*), N_m(\boldsymbol{n}^*)\big) \leq 0 \tag{5.7}$$

f is a function, chosen in many cases as linear; and $\boldsymbol{n}^*$ is the normal vector of the *"critical plane"*; and $C_a(\boldsymbol{n}^*), N_a(\boldsymbol{n}^*), N_m(\boldsymbol{n}^*)$ are the amplitudes of shear stress and normal stress, and the mean value of normal stress, respectively. The shear stress generally appears in fatigue criteria through its amplitude $C_a(\boldsymbol{n}^*)$, due to the independence of the fatigue limit with respect to the mean shear stress for a large

number of metallic materials. And if one considers that the amplitude and the mean value of normal stress appear in form of their sum, i.e. $N_{max}(\boldsymbol{n}^*)$, (5.7) can be rewritten:

$$f\big(C_a(\boldsymbol{n}^*), N_{max}(\boldsymbol{n}^*)\big) = C_a(\boldsymbol{n}^*) + aN_{max}(\boldsymbol{n}^*) - b \leq 0 \tag{5.8}$$

with a, b being two material parameters.

5.3.2 General form of the stress gradient fatigue criteria

The classical criteria (Crossland, Dang Van, ...) will now be modified to include the "size effect" [3] experimentally observed and beneficial influence of the stress gradient in the cases analyzed and corresponding to the surface fatigue and "decreasing stress gradient". At this stage it is reminded two crucial points. First, even if the torsion fatigue limit is generally independent from the shear stress gradient, it is not sure that it is also independent from the amplitude of the last. Second, the small pure size effect and the influence of the normal stress gradient on the bending fatigue limit show that adding only gradient terms could allow to model the fatigue tests results. Basing on these analyses, under multiaxial loading a generalization of the above experimental fact will be done.

With the presence of the unique gradient term (e.g. in P_{max} as Papadopoulos' proposal), the gradient fatigue criteria successfully represent the difference in the fatigue limit of uniaxial normal stress cyclic loadings, between fully reversed bending tests and fully reversed tension-compression tests. However, because of the vanishing of the gradient term of the model [135] in the case of pure torsion, such a formulation with the unique gradient term is not able to represent the possible influence of shear stress gradient amplitude and the "size effect" on the fatigue limit in torsion. For example, for torsion tests performed on specimen with various radii, the fatigue between the "reference test" (without any effect) and test at a certain radius is found identical using such an approach, which is contrary to experimental facts. The criterion adopted in [135] with only one stress gradient term in the normal stress part can describe gradient effects for tension-compression loadings with non zero hydrostatic stress, but not for shear stress loadings. Thus it leads to the necessity of adding a second gradient term to the shear stress part. Besides the stress gradient term appearing in the normal stress part in form of $G = \nabla\sigma_{kk}$, another gradient term, the gradient of stress tensor (or alternatively of deviatoric stress tensor) $\|\boldsymbol{Y}\|_{,a} = \|\nabla\boldsymbol{\sigma}\|_{,a}$, is added to the shear stress part. Basing on all these analyses a new form of fatigue criteria taking into account gradient effects, is proposed:

$$f\big(\widetilde{C_a}(\boldsymbol{n}^*), \widetilde{N}_{max}(\boldsymbol{n}^*)\big) = \widetilde{C_a}(\boldsymbol{n}^*) + a\widetilde{N}_{max}(\boldsymbol{n}^*) - b \leq 0 \tag{5.9}$$

where $\widetilde{C_a}(\boldsymbol{n}^*)$ and $\widetilde{N}_{max}(\boldsymbol{n}^*)$ are extended definitions of the counterparts in the classical criteria. We propose the following forms for these quantities:

$$\widetilde{C_a}(\boldsymbol{n}^*) = C_a(\boldsymbol{n}^*) f_c\left(l_\tau^* \frac{\|\boldsymbol{Y}\|_{,a}}{C_a(\boldsymbol{n}^*)}\right) \tag{5.10}$$

[3] in the sense as discussed right from the introduction, actually it implies rather the gradient effect related to the size.

$$\widetilde{N}_{max}(\boldsymbol{n}^*) = N_{max}(\boldsymbol{n}^*) f_n\left(l_\sigma^* \frac{\max_t \sum_{k=1}^3 n_i^* n_j^* n_k^* Y_{ijk}}{N_{max}(\boldsymbol{n}^*)}\right) \tag{5.11}$$

The two functions f_c and f_n including the stress gradient terms, can have the following forms :

$$f_c\left(l_\tau^* \frac{\|\boldsymbol{Y}\|_{,a}}{C_a(\boldsymbol{n}^*)}\right) = \sqrt{1 - \left(l_\tau^* \frac{\|\boldsymbol{Y}\|_{,a}}{C_a(\boldsymbol{n}^*)}\right)^{n_\tau}} \tag{5.12}$$

$$f_n\left(l_\sigma^* \frac{\max_t \sum_{k=1}^3 n_i^* n_j^* n_k^* Y_{ijk}}{N_{max}(\boldsymbol{n}^*)}\right) = \sqrt{1 - \left(l_\sigma^* \frac{\max_t \sum_{k=1}^3 n_i^* n_j^* n_k^* Y_{ijk}}{N_{max}(\boldsymbol{n}^*)}\right)^{n_\sigma}} \tag{5.13}$$

Note that f_c could alternatively be function of the gradient of the stress deviator. These expressions will be specified for the two criteria considered in the next sections. l_τ^* and l_σ^* are two *material characteristic lengths*; n_τ and n_σ are two *material characteristic exponents*, or actually *gradient-amplifying exponents* introduced to get a more flexibility in capturing any large experimental data class.

To sum up, it is clear to confirm the necessity of the simultaneous presence of the two gradient terms in fatigue criteria, one for the normal stress part through G and the other for the shear stress part through $\|Y\|_{,a}$. These criteria are used to describe fatigue limits under different kinds of loading (loading effect) in which the gradient effect is taken into account and the pure size effect is insignificant compared to the other. After all, using as a basis the classical fatigue criteria for formulating the stress gradient dependent fatigue criteria after the above methodology, some illustrations will be made in the following, one for Crossland criterion and the other for Dang Van criterion. The same approach could be in principle applied to other classical fatigue criteria.

5.4 Gradient Crossland criterion

5.4.1 Classical Crossland criterion

The Crossland criterion [39] is used as a basis for the development of a gradient dependent criterion. The classical Crossland criterion defines the fatigue limit of metallic specimens subjected to multiaxial in-phase cyclic stress states as, *cf.* [134]:

$$\sqrt{J_2}_{,a} + \alpha_c P_{max} \leq \gamma_c \tag{5.14}$$

where α_c and γ_c are material parameters, $\sqrt{J_2}_{,a}$ is the amplitude of the square root of the second invariant of the stress deviator tensor and P_{max} is the maximum hydrostatic stress during a loading cycle.

The amplitude of the square root of the second invariant of the stress deviator can be defined, in general case, as the half-length of the longest chord of the deviatoric stress path by :

$$\sqrt{J_2}_{,a} = \frac{1}{2\sqrt{2}} \max_{t_1}\left\{\max_{t_2} \left\|\boldsymbol{s}(t_2) - \boldsymbol{s}(t_1)\right\|\right\} = \frac{1}{2\sqrt{2}} \max_{t_1}\left\{\max_{t_2} \sqrt{\left(\boldsymbol{s}(t_2) - \boldsymbol{s}(t_1)\right) : \left(\boldsymbol{s}(t_2) - \boldsymbol{s}(t_1)\right)}\right\} \tag{5.15}$$

or as the radius of the smallest hypersphere circumscribed to the deviatoric stress path by :

$$\sqrt{J_2}_{,a} = \frac{1}{\sqrt{2}} \min_{\boldsymbol{s}_1}\left\{\max_{t} \left\|\boldsymbol{s}(t) - \boldsymbol{s}_1\right\|\right\} = \frac{1}{\sqrt{2}} \min_{\boldsymbol{s}_1}\left\{\max_{t} \sqrt{\left(\boldsymbol{s}(t) - \boldsymbol{s}_1\right) : \left(\boldsymbol{s}(t) - \boldsymbol{s}_1\right)}\right\} \tag{5.16}$$

The maximum value that the hydrostatic stress reaches during the loading cycle is:

$$P_{max} = \max_t \left\{ \frac{1}{3} tr\big(\sigma(t)\big) \right\} = \frac{\sigma_{kk}}{3} \tag{5.17}$$

In these equations, the summation convention over repeated indices holds and $\boldsymbol{s}$ and p are respectively the deviatoric and spherical part of the stress tensor:

$$p(t) = \frac{1}{3} tr\big(\sigma(t)\big) \quad \text{and} \quad \boldsymbol{s}(t) = \boldsymbol{\sigma}(t) - p(t)\boldsymbol{I} \tag{5.18}$$

and $\boldsymbol{I}$ is the second order unit tensor.

The material parameters α_c and γ_c can be related to the fully reversed tension-compression fatigue limit, denoted by s_{ref}, and to the torsion fatigue limit, denoted by t_{ref}, by:

$$\gamma_c = \mathrm{t}_{ref}; \quad \alpha_c = \frac{3\mathrm{t}_{ref}}{s_{ref}} - \sqrt{3} \tag{5.19}$$

As well-known, to obtain the observed detrimental effect of a tensile mean stress state, the parameter α_c in Eq. (5.19), must be positive, and therefore: $\mathrm{t}_{ref} > s_{ref}/\sqrt{3}$.
Furthermore, since the "size" and gradient effects are not captured in the classical Crossland criterion, it is only valid for the specimen large enough and smooth enough. For this reason, the subscript *"ref"* used for the fatigue limits s_{ref} and t_{ref} means material constants independent of the "size" and gradient effects which will be used as references for other case-studies. Concretely, in the case where these effects could be important, new fatigue criteria to include them are required. As well for this reason, in Eq. (5.19) just $\mathbf{s_{ref}}$ is chosen instead of $\mathbf{f}$ because in size range under consideration where the gradient effects can be significant, just $\mathbf{s_{ref}}$ is regarded as a characteristic constant intrinsic to material but not $\mathbf{f}$ in the sense that only that is exempt from the gradient effect.

5.4.2 Formulation of the gradient Crossland criterion

Using as a basis the classical Crossland criterion, Eq. (5.14) and the general framework for the development of a gradient dependent fatigue limit criterion (Eq. 5.9), a new version can be written in the form:

$$\sqrt{\widetilde{J_2}_{,a}} + \alpha_g \widetilde{P_{max}} \leq \gamma_g \tag{5.20}$$

From the classical expression of $\sqrt{J_2}$, a new form *embedded with gradient term* is proposed:

$$\sqrt{\widetilde{J_2}} = \sqrt{\frac{1}{2}\|\boldsymbol{s}\|^2 \left[1 - \left(l_\tau \frac{\|\boldsymbol{Z}\|}{\|\boldsymbol{s}\|}\right)^{n_\tau}\right]} = \sqrt{J_2}\sqrt{1 - \left(l_\tau \frac{\|\boldsymbol{Z}\|}{\|\boldsymbol{s}\|}\right)^{n_\tau}} \tag{5.21}$$

l_τ is a *material characteristic length*, and n_τ is a *material characteristic exponent*. The quantity $\|\boldsymbol{Z}\| = \|\nabla \boldsymbol{s}\|$ is used as an indicator of the influence of the gradient of the stress deviator which reflects the spatial non-uniform distribution of stress state. Similarly to [135], the ratio of the norm $\|\boldsymbol{Z}\|$ over the norm $\|\boldsymbol{s}\|$ is called reduced gradient too. However in the current work that is more exactly understood as

the shear reduced gradient of the new fatigue criterion.
Eq. (5.21) can be found in more familiar and visible way when setting $n_\tau = 2$:

$$\sqrt{\widetilde{J_2}} = \sqrt{\frac{1}{2}\left[\|\boldsymbol{s}\|^2 - l_\tau^2\|\boldsymbol{Z}\|^2\right]} \tag{5.22}$$

which is similar to the expression of *plasticity criteria* within the framework of *gradient dependent models*, see e.g. [118]. However, the present study will not fix $n_\tau = 2$ but let it be a material parameter to calibrate experimentally.

In the spirit of Eq. (5.22), and taking account of the recent proposition of Amargier *et al* [9] which expression includes the product of $\sqrt{J_2}_{,a}$ and a function of the hydrostatic stress gradient, we define the following amplitude $\sqrt{\widetilde{J_2}}_{,a}$ which combines $\sqrt{J_2}_{,a}$ and the full stress gradient $\|\boldsymbol{Y}\|_{,a}$ is the form:

$$\sqrt{\widetilde{J_2}}_{,a} = \sqrt{J_2}_{,a}\ \sqrt{1 - \left(l_\tau \frac{\|\boldsymbol{Y}\|_{,a}}{\|\boldsymbol{s}\|_{,a}}\right)^{n_\tau}} \tag{5.23}$$

For the sake of illustration, the following treatment is performed for in-phase loading where simple expressions can be obtained. The stress state at a point is written as:

$$\sigma_{ij}(t) = \widehat{\sigma}_{ij}\, sin(\omega t) + \overline{\sigma}_{ij}, \quad i,j = x,y,z, \tag{5.24}$$

where $\widehat{\sigma}_{ij}$ is the amplitude of the (ij) stress component oscillating around a $\overline{\sigma}_{ij}$- mean value and over T-the loading period.

The expression of the third order tensor $\boldsymbol{Y}$ and the amplitude of its norm $\|\boldsymbol{Y}\|_{,a}$ are elaborated in the present case-study, as Eq. (5.25) or (5.26):

$$\begin{aligned}
&\boldsymbol{Y}(t) = \nabla\boldsymbol{\sigma}(t) \Longrightarrow Y_{ijk}(t) = \sigma_{ij,k}(t) = \widehat{\sigma}_{ij,k}\, sin(\omega t) + \overline{\sigma}_{ij,k}, \quad i,j,k = x,y,z,\\
&\|\boldsymbol{Y}\|_{,a} = \min_{\boldsymbol{Y}_1}\left\{\max_t \left\|\boldsymbol{Y}(t) - \boldsymbol{Y}_1\right\|\right\} = \min_{\boldsymbol{Y}_1}\left\{\max_t \sqrt{\left(\boldsymbol{Y}(t) - \boldsymbol{Y}_1\right) \bullet \left(\boldsymbol{Y}(t) - \boldsymbol{Y}_1\right)}\right\} \qquad (5.25)\\
\text{or}\ \ &\|\boldsymbol{Y}\|_{,a} = \max_{t_1}\left\{\max_{t_2} \sqrt{\left(\boldsymbol{Y}(t_2) - \boldsymbol{Y}(t_1)\right) \bullet \left(\boldsymbol{Y}(t_2) - \boldsymbol{Y}(t_1)\right)}\right\} = \sqrt{4\widehat{Y}_{ijk}\widehat{Y}_{ijk}} \qquad (5.26)
\end{aligned}$$

with $\widehat{Y}_{ijk} = \widehat{\sigma}_{ij,k}$, and the product definition: $\boldsymbol{Y} \bullet \boldsymbol{Y} = Y_{ijk}Y_{ijk}$.
Thus, from Eq. (5.16) with the expression of $\sqrt{J_2}_{,a}$ and of $\|s\|_{,a} = \sqrt{4\widehat{s}_{ij}\widehat{s}_{ij}}$, and Eq. (5.25) with the expression of $\|Y\|_{,a}$, $\sqrt{\widetilde{J_2}}_{,a}$ is elaborated as Eq. (5.23):

$$\sqrt{\widetilde{J_2}}_{,a} = \sqrt{\frac{1}{2}\widehat{s}_{ij}\widehat{s}_{ij}\left[1 - \left(l_\tau \frac{\sqrt{\widehat{Y}_{ijk}\widehat{Y}_{ijk}}}{\sqrt{\widehat{s}_{ij}\widehat{s}_{ij}}}\right)^{n_\tau}\right]} \tag{5.27}$$

With respect to $\widetilde{P_{max}}$, the same form as the one of [135] is proposed:

$$\widetilde{P_{max}} = P_{max}\left[1 - \left\langle l_\sigma \frac{\|\boldsymbol{G}\|}{P_{max}}\right\rangle^{n_\sigma}\right] \tag{5.28}$$

with G, the gradient of P_{max} being the vector:

$$\boldsymbol{G} = \nabla P_{max} = {}^{T}\left[P_{max,x}, P_{max,y}, P_{max,z}\right] \tag{5.29}$$

which norm $\|\boldsymbol{G}\|$ is:

$$\|\boldsymbol{G}\| = \sqrt{(P_{max,x})^2 + (P_{max,y})^2 + (P_{max,z})^2} \tag{5.30}$$

The norm of the gradient of P_{max}, i.e. $\|\boldsymbol{G}\|$, is used as an indicator of the influence of the normal stresses gradient. One more again, the ratio of the norm $\|\boldsymbol{G}\|$ over P_{max} is called here hydrostatic reduced gradient.

Moreover, in Eq. (5.28), l_σ and n_σ are also *material characteristic parameters* with the same signification as l_τ and n_τ. as in [135], to avoid the degradation in the case of null value of P_{max} but non-zero value of its gradient, an extended definition of the McCauley bracket $\langle \circ \rangle$ is adopted:

$$\begin{aligned} &\left\langle l_\sigma \frac{\|\boldsymbol{G}\|}{P_{max}} \right\rangle = l_\sigma \frac{\|\boldsymbol{G}\|}{P_{max}} \text{ if } l_\sigma \frac{\|\boldsymbol{G}\|}{P_{max}} > 0, \text{ and } \left\langle l_\sigma \frac{\|\boldsymbol{G}\|}{P_{max}} \right\rangle = 0 \text{ if } l_\sigma \frac{\|\boldsymbol{G}\|}{P_{max}} \leq 0 \\ &\left\langle l_\sigma \frac{\|\boldsymbol{G}\|}{P_{max}} \right\rangle = 0 \text{ if } P_{max} = 0 \end{aligned} \tag{5.31}$$

The properties expressed by Eq. (5.31) have been used to deliberately neglect the gradient effect in the case of a fully compressive cycle of the hydrostatic stress (i.e. $P_{max} < 0$). This assumption can be disregarded if experimental facts show that it is irrelevant.

Finally, the criteria written as:

$$\sqrt{J_2}_{,a} \sqrt{1 - \left(l_\tau \frac{\|\boldsymbol{Y}\|_{,a}}{\|\boldsymbol{s}\|_{,a}} \right)^{n_\tau}} + \alpha_g P_{max} \left[1 - \left\langle l_\sigma \frac{\|\boldsymbol{G}\|}{P_{max}} \right\rangle^{n_\sigma} \right] - \gamma_g < 0 \tag{5.32}$$

has six materials parameters $(\alpha_g, \gamma_g, l_\tau, l_\sigma, n_\tau, n_\sigma)$ to be identified experimentally.

5.4.3 Calibration of the material parameters

As the proposed criterion reduces to the classical Crossland one in the absence of "size" and gradient effects, the parameters α_g et γ_g are the same as those in the classical version, and given by $\gamma_g = \gamma_c = \mathrm{t}_{ref}$, and $\alpha_g = \alpha_c = \dfrac{3\mathrm{t}_{ref}}{s_{ref}} - \sqrt{3}$.

A procedure for obtaining the parameters from fully reversed torsion and fully reversed constant moment bending tests is detailed hereafter.

a) Fully reversed torsion tests

The criterion described by Eq. (5.20) is applied, first, to the case of fully reversed torsion tests. Let us denote by $\mathrm{t}(R)$ the fatigue limit of a specimen of radius R. Considering the critical points (located at $r = \pm R$), their relevant quantities are:

$$\boldsymbol{\sigma} = \widehat{\sigma}_{x\theta}\, sin(\omega t)\, (e_x \otimes e_\theta + e_\theta \otimes e_x) = \mathrm{t}(R)\, sin(\omega t)\, (e_x \otimes e_\theta + e_\theta \otimes e_x)$$

$$\widehat{s}_{ij}\,\widehat{s}_{ij} = 2\big(\mathrm{t}(R)\big)^2 \quad \text{and} \quad \widehat{Y}_{ijk}\,\widehat{Y}_{ijk} = 2\big(\frac{\widehat{\sigma}_{x\theta}}{R}\big)^2 = 2\left(\frac{\mathrm{t}(R)}{R}\right)^2$$

$$\widetilde{P_{max}} = 0 \quad \text{and} \quad \sqrt{\widetilde{J}_{2,a}} = \mathrm{t}(R)\,L_\tau(R) \tag{5.33}$$

$$\text{with} \quad L_\tau(R) = \sqrt{1-(l_\tau/R)^{n_\tau}} : \textit{shear reduced gradient} \tag{5.34}$$

And using Eqs. (5.33) the proposed fatigue criterion, Eq. (5.20), leads to:

$$\mathrm{t}(R) = \frac{\mathrm{t}_{ref}}{\sqrt{1-(l_\tau/R)^{n_\tau}}} \tag{5.35}$$

This formula is used to calibrate the three material parameters τ_{ref}, l_τ and n_τ, using the experiment curve relating the fatigue limit t(R) to the radius of the specimen. The material parameters are then calibrated using the least square method on the tests points; and therefore the optimal parameters (i.e. the values which minimize the scatter between the predicted and experimental points) for the criterion are obtained. As an illustration, the torsion fatigue tests given by Massonnet [104] are used to identify τ_{ref}, l_τ and n_τ, as shown in Fig. 5.6. A visual image of t_{ref} aforementioned is as well found in this graph. The values obtained are: $\tau_{ref} = 115$MPa, $l_\tau = 1.6$mm and $n_\tau = 0.5$.

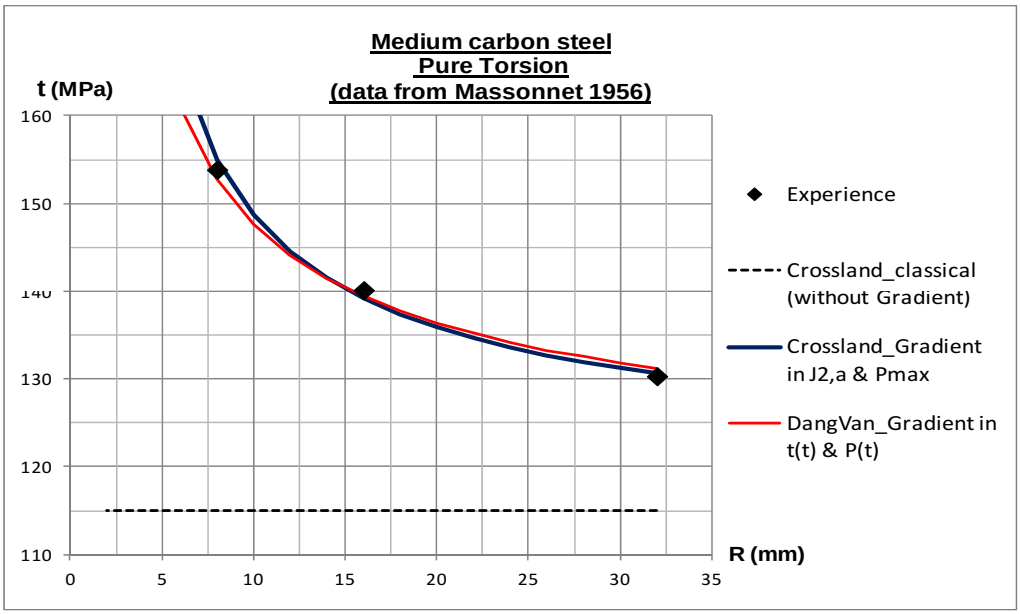

Figure 5.6 : *Fully reversed torsion fatigue limit of smooth cylindrical samples* (*cf.* Massonnet [105])

We notice that the fatigue limit tends toward infinity as the radius tends toward the characteristic length l_τ. It defines the limit of the model. Nevertheless, it indicates a tendency consistent with the fact *"Smaller is Stronger"*.

b) Fully reversed constant moment bending tests (four-point bending tests)

To calibrate the other parameters (l_σ, n_σ) the criterion Eq. (5.20) is now applied to the case of fully reversed four-point bending tests. The fatigue limit of a specimen of radius R is denoted $\mathrm{f}(R)$. Considering the most stressed points, i.e. points lying at $L \leq x \leq L + l$ and at $y = \pm R$, relevant quantities, in particular $\sqrt{\widetilde{J_2}_{,a}}$, calculated by Eq. (5.27) are given by:

$$\boldsymbol{\sigma} = \sigma_{xx}\ e_x \otimes e_x = \widehat{\sigma}_{xx}\ sin(\omega t)\ e_x \otimes e_x = \mathrm{f}(R)\ sin(\omega t)\ e_x \otimes e_x$$

$$\sqrt{\widetilde{J_2}_{,a}} = \frac{\mathrm{f}(R)}{\sqrt{3}} L_{\tau f}(R) \tag{5.36}$$

$$\text{with} \quad L_{\tau f}(R) = \sqrt{1 - (3/2)^{n_\tau/2}\ (l_\tau/R)^{n_\tau}} = L_{\tau f}(L_\tau) \tag{5.37}$$

Similarly, with the help of Eq. (5.28), $\widetilde{P_{max}}$ can be elaborated, in this case-study, as:

$$P_{max} = \frac{\widehat{\sigma}_{xx}}{3} = \frac{\mathrm{f}(R)}{3} \quad \text{and} \quad \widetilde{P_{max}} = \frac{\mathrm{f}(R)}{3} L_{\sigma f}(R) \tag{5.38}$$

$$\text{with} \quad L_{\sigma f}(R) = 1 - (l_\sigma/R)^{n_\sigma} \text{ : } \textit{normal reduced gradient} \tag{5.39}$$

$$\text{and} \quad \boldsymbol{G} = \left[P_{max,x} = 0, P_{max,y} = \frac{\widehat{\sigma}_{xx,y}}{3} = \frac{\widehat{F} L}{3I} = \frac{\widehat{\sigma}_{xx}}{3R} = \frac{\mathrm{f}}{3R}, P_{max,z} = 0\right] \tag{5.40}$$

$$\text{and} \quad \|\boldsymbol{G}\| = \frac{\mathrm{f}}{3R} \tag{5.41}$$

Finally, the fatigue criterion (5.20), lead to the following expression of the fatigue limit f:

$$\mathrm{f}(R) = \frac{s_{ref}}{1 - l_\sigma R^{-n_\sigma} \left(1 - \dfrac{s_{ref}}{\sqrt{3}\ \mathrm{t}_{ref}}\right) - \dfrac{s_{ref}}{\sqrt{3}\ \mathrm{t}_{ref}} \left(1 - L_{\tau f}(R)\right)} \geq s_{ref} \tag{5.42}$$

As previously, this formula is used to calibrate the three material parameters s_{ref}, l_σ and n_σ, using the experiment curve relating the fatigue limit $\mathrm{f}(R)$ to the radius of the specimen. The material parameters are calibrated using the least square method on the tests points to obtain the optimal parameters. As an illustration, the four-point bending tests given by Pogoretskii [140] are used to identify s_{ref}, l_σ and n_σ assuming that t_{ref} and $L_{\tau f}(R)$ are known from the previous calibration. The result is shown in Fig. 5.7d. A visual image of s_{ref} aforementioned is as well found in this graph.

c) Application to the fully reversed cantilever bending tests

It is of more interest to apply the criterion Eq. (5.20) to the case of fully reversed cantilever bending tests to see, besides the well-known role of R, the role of L. The difference and similarity in fatigue limit between two kinds of bending, i.e. four-point bending and cantilever bending is analyzed. Let us denote the corresponding fatigue limit $f'(R)$. Considering the most stressed points, i.e. points at $x = 0$ and at $y = \pm R$ (Fig. 5.3), again, respective quantities and then $\sqrt{\widetilde{J_2}_{,a}}$ determined by Eq. (5.27) are given:

$$\boldsymbol{\sigma} = \sigma_{xx}\ e_x \otimes e_x = \widehat{\sigma}_{xx}\ sin(\omega t)\ e_x \otimes e_x = f'\ sin(\omega t)\ e_x \otimes e_x \tag{5.43}$$

$$\sqrt{\widetilde{J_2}}_{,a} = \frac{f'(R)}{\sqrt{3}}\, L_{\tau f'}(R,L) \tag{5.44}$$

$$\text{with} \quad L_{\tau f'}(R,L) = \sqrt{1-(3/2)^{n_\tau/2}\,(l_\tau/R)^{n_\tau}\left(1+\frac{R^2}{L^2}\right)^{n_\tau/2}} \tag{5.45}$$

Similarly, with the help of Eq. (5.28), $\widetilde{P_{max}}$ can be evaluated for this case:

$$\boldsymbol{G} = \left[P_{max,x} = \frac{\widehat{\sigma}_{xx,x}}{3} = \frac{-f'(R)}{3L}, P_{max,y} = \frac{\widehat{\sigma}_{xx,y}}{3} = \frac{f'(R)}{3R}, P_{max,z} = 0\right] \tag{5.46}$$

$$\|\boldsymbol{G}\| = \frac{f'(R)}{3R}\sqrt{1+\frac{R^2}{L^2}} \tag{5.47}$$

$$\widetilde{P_{max}} = \frac{f'(R)}{3}\, L_{\sigma f'}(R,L) \tag{5.48}$$

$$\text{with} \quad L_{\sigma f'}(R,L) = 1-(l_\sigma/R)^{n_\sigma}\left(1+\frac{R^2}{L^2}\right)^{n_\tau/2} \tag{5.49}$$

Finally, from Eq. (5.20), f' is obtained as:

$$f'(R) = \frac{s_{ref}}{L_{\sigma f'}(R,L) - \dfrac{s_{ref}}{\sqrt{3}\,\mathrm{t}_{ref}}\left(L_{\sigma f'}(R,L) - L_{\tau f'}(R,L)\right)} \geq s_{ref} \tag{5.50}$$

Using the Eq. (5.50), a class of experimental data of the cantilever bending fatigue tests are successfully reproduced, as shown in Fig. 5.7(a-c).

On the other hand, for specimens with $R \ll L$, the ratio (R^2/L^2) is negligible. Under these circumstances the fatigue limit in fully reversed constant moment and cantilever bending of specimens of the same radius, coincide and are related to the tension-compression fatigue limit by Eq. (5.42). Using this assumption an important number of bending fatigue limits has been analyzed. It turned out that the value $1/2$ for the exponents n_τ and n_σ brought adequate predictions for the experiments studied. The criterion is then:

$$\sqrt{J_2}_{,a}\ \sqrt{1-\left(l_\tau\frac{\|\boldsymbol{Y}\|_{,a}}{\|s\|_{,a}}\right)^{1/2}} + \alpha_g P_{max}\left[1-\sqrt{l_\sigma\left\langle\frac{\|\boldsymbol{G}\|}{P_{max}}\right\rangle}\right] - \gamma_g < 0 \tag{5.51}$$

with four materials parameters $(\alpha_g, \gamma_g, l_\tau, l_\sigma)$ to be identified experimentally.

Figure 5.7 shows some test results of rotating bending fatigue limits from the literature in which the fatigue limits are plotted against the specimen radii. Figures 5.7(a-c) are related to cantilever bending tests and Fig. 5.7(d) depicts constant moment tests. The solid curves in these graphs present the simulation with the proposed criterion, where the value $n = 1/2$ has been assumed. As shown, the accordance with the experimental data is satisfactory.

d) Application to the fully reversed combined bending-twisting tests

The criterion (5.20) is now applied to the case of fully reversed in-phase bending and torsion fatigue tests [135]. Specimens of toroidal shape are usually used for these tests. Considering the most stressed

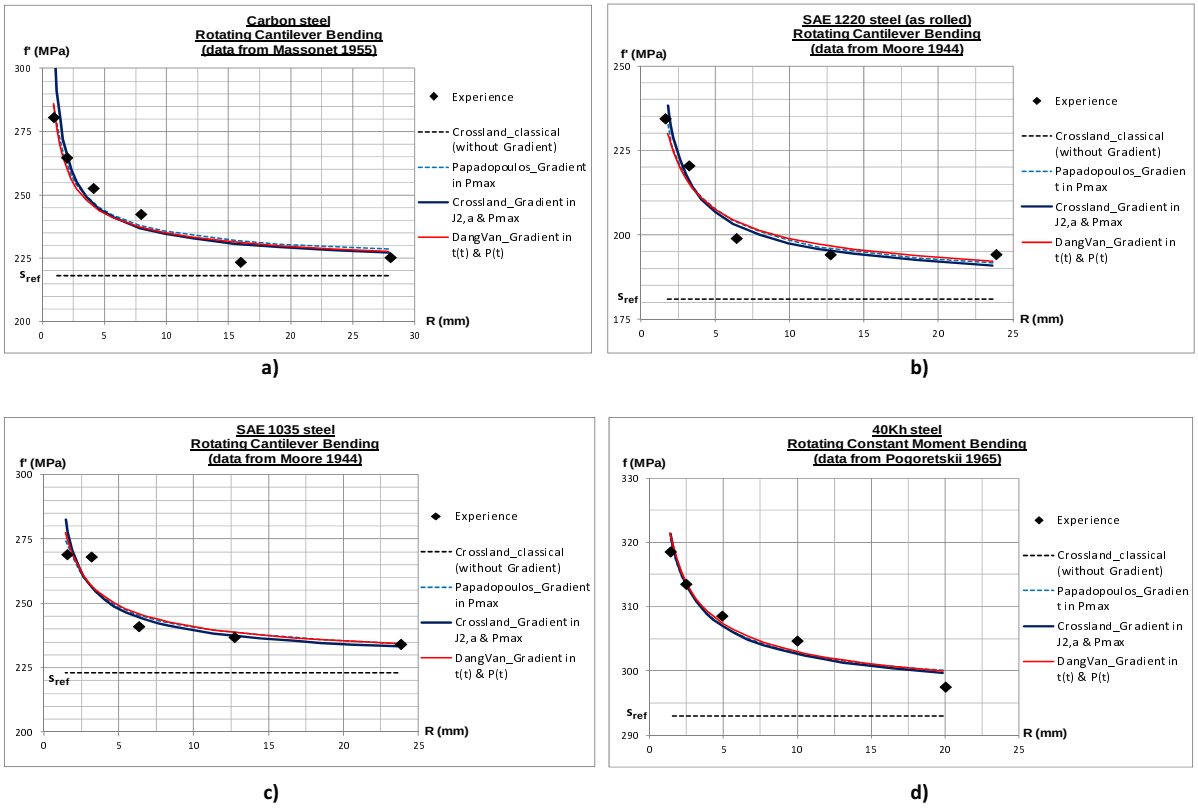

Figure 5.7 : *Fully reversed bending fatigue limits of cylindrical specimen* (Massonnet [104], Moore & Morkovin [110], Pogoretskii & Karpenko [140], Papadopoulos & Panoskaltsis [135])

points, i.e. points at $y=\pm R, z=0$ and denoting by σ_a and τ_a the limit amplitudes of the normal and shear stresses respectively, related quantities especially $\sqrt{\widetilde{J_2}_{,a}}$, by Eq. (5.27), are given:

$$\boldsymbol{\sigma}=\sigma_a\ sin(\omega t)\ e_x\otimes e_x+\tau_a\ sin(\omega t)\ (e_x\otimes e_\theta+e_\theta\otimes e_x)$$

$$\sqrt{\widetilde{J_2}_{,a}}=\sqrt{\frac{\sigma_a^2}{3}+\tau_a^2}\ L_{\tau c}(\sigma_a,\tau_a,R) \tag{5.52}$$

with:

$$L_{\tau c}(\sigma_a,\tau_a,R)=\sqrt{1-(l_{\tau c}/R)^{n_\tau}}\quad\text{with}\quad l_{\tau c}=l_\tau^{n_\tau}\left(\frac{3\sigma_a^2+6\tau_a^2}{2\sigma_a^2+6\tau_a^2}\right)^{n_\tau/2} \tag{5.53}$$

For the maximum hydrostatic stress $\widetilde{P_{max}}$, the same expression as the case of bending tests, Eq. (5.38), is here given:

$$\widetilde{P_{max}}=\frac{\sigma_a}{3}L_{\sigma c}(R)\quad\text{with}\qquad L_{\sigma c}=1-(l_\sigma/R)^{n_\sigma}=L_{\sigma f} \tag{5.54}$$

The criterion is therefore expressed as:

$$\sqrt{\left(\frac{\sigma_a^2}{3}+\tau_a^2\right)}\,L_{\tau c}+\alpha_g\,\frac{\sigma_a}{3}\,L_{\sigma c}<\gamma_g\ ,\qquad \text{or more concretely,}$$
$$\sqrt{\left(\frac{\sigma_a^2}{3}+\tau_a^2\right)}\sqrt{1-(l_\tau/R)^{n_\tau}\left(\frac{3\sigma_a^2+6\tau_a^2}{2\sigma_a^2+6\tau_a^2}\right)^{n_\tau/2}}+\alpha_g\,\frac{\sigma_a}{3}\left(1-(l_\sigma/R)^{n_\sigma}\right)<\gamma_g \tag{5.55}$$

Comparison with classical and Papadopoulos results

The application of the classical Crossland criterion in the case of fully reversed in-phase combined tension-compression and torsion fatigue tests gives the following *"ellipse arc equation"*:

$$\left(\frac{\tau_a}{\mathrm{t}_{ref}}\right)^2+\left(\frac{2\,s_{ref}}{\sqrt{3}\,\mathrm{t}_{ref}}-1\right)\left(\frac{\sigma_a}{s_{ref}}\right)^2+\left(2-\frac{2\,s_{ref}}{\sqrt{3}\,\mathrm{t}_{ref}}\right)\left(\frac{\sigma_a}{s_{ref}}\right)\leq 1 \tag{5.56}$$

which delimits in the $\sigma_a-\tau_a$ plane the safe domain. Eq. (5.56) shows high discrepancies between predictions and experiments for the fatigue limit in combined bending-twisting with the "size" and gradient effects (Fig. 5.8). As in [135], to bypass this trouble, modified material parameters α_g and γ_g related to the bending fatigue limit $\mathrm{f}(R)$ and torsion fatigue limit $\mathrm{t}(R)$ (instead of s_{ref} and t_{ref}), experimentally determined on specimens (radius R) of the same geometry as used for the combined tension-compression and torsion tests, can be used. Two things different from [135] are, first, the use of $\mathrm{f}(R)$ and $\mathrm{t}(R)$ determined at the specific radius R of specimens under consideration, and second, the substitution of both s_{ref} and t_{ref} by $\mathrm{f}(R)$ and $\mathrm{t}(R)$, instead of only one s_{ref} by f. Then $\gamma_g=\mathrm{t}(R)$ and $\alpha_g=\dfrac{3\mathrm{t}(R)}{f(R)}-\sqrt{3}$, and the application of the Crossland criterion using these new values of α_g and γ_g leads to the new ellipse arc equation:

$$\left(\frac{\tau_a}{\mathrm{t}(R)}\right)^2+\left(\frac{2\,\mathrm{f}(R)}{\sqrt{3}\,\mathrm{t}(R)}-1\right)\left(\frac{\sigma_a}{\mathrm{f}(R)}\right)^2+\left(2-\frac{2\,\mathrm{f}(R)}{\sqrt{3}\,\mathrm{t}(R)}\right)\left(\frac{\sigma_a}{\mathrm{f}(R)}\right)\leq 1 \tag{5.57}$$

It is noticed that this formula is very similar to the well known ellipse arc formula of Gough and Pollard.

In the following, we show that Eq. (5.55) obtained with the proposed criterion, reduces to Eq. (5.57) for certain values of the material parameters. Indeed, first let us review the constant moment bending case. Assuming $n_\tau=0.5$ as validated by a large number of experiment, Eq. (5.37) yields:

$$L_{\tau f}(R)\approx\sqrt{1-(l_\tau/R)^{n_\tau}}=L_\tau \tag{5.58}$$

Resulting from Eqs. (5.35, 5.34) and (5.42, 5.39), the expressions of L_τ and $L_{\sigma f}$ are reported below for completeness:

$$L_\tau=\frac{\mathrm{t}_{ref}}{\mathrm{t}};\quad L_{\sigma f}=\frac{1/\mathrm{f}-1/\sqrt{3}\,\mathrm{t}}{1/s_{ref}-1/\sqrt{3}\,\mathrm{t}_{ref}} \tag{5.59}$$

And second, consider now again the combined bending-twisting case by evaluating the function $h(\tau_a)=\left(\dfrac{3\sigma_a^2+6\tau_a^2}{2\sigma_a^2+6\tau_a^2}\right)^{n_\tau/2}$ to get an approximation for $L_{\tau c}$ and $l_{\tau c}$ defined in Eq. (5.53). Again, for $n_\tau=0.5$ assumed before, $h(\tau_a)$ is in the interval $[1,1.1)$, we take $h(\tau_a)\approx 1$, so that $l_{\tau c}\approx l_\tau^{n_\tau}$. Therefore,

$$L_{\tau c}(R)=\sqrt{1-(l_{\tau c}/R)^{n_\tau}}\approx L_\tau \tag{5.60}$$

Finally, replacing $L_{\tau c}$ and $L_{\sigma c}$ in Eq. (5.55) by their approximations, with the help of Eq. (5.59), Eq. (5.57), is recovered.

In Fig. 5.8 the test results of bending-twisting conducted by [50] on $SAE4340$ steel, are depicted. In the same figure, the Crossland analytical ellipse arc based on the $s_{ref} - \mathrm{t}_{ref}$ fatigue limits, Eq. (5.56), is plotted too. As we can see, all the test points fall considerably outside this analytical ellipse arc. This demonstrates the effect of the normal stress gradient, as the analytical ellipse arc (Eq. 5.56) is obtained with zero normal stress gradient, whereas the experimental data for combined bending-twisting tests have a non-zero stress gradient. Furthermore, it is interesting to re-consider some analyses of [135] when stated that *"the higher the normal stress due to bending, the higher the difference between test points and Crossland ellipse arc, whereas the higher the shear stress, the smaller the difference between test points and Crossland ellipse arc becomes..."*. First, the difference between test points and classical Crossland ellipse arc near the x-axis where the normal load is predominant, is a proof of the beneficial "size" and gradient effects. Indeed, the difference between two kinds of fatigue test can be clearly seen: the bending test (test points) includes the beneficial effects of the normal stress gradient; the tension-compression test (Crossland ellipse arc) excludes these effects due to the gradient-free stress state. Second, the coincidence between test points and Crossland ellipse arc near the y-axis with predominant shear stress is actually natural due to the fact that t_{ref} used to depict the Crossland ellipse arc after Eq. (5.56) and corresponding test point on the y-axis are actually the same, thus this coincidence really does not reflect the "lack of sensitivity of the limiting fatigue stress on the gradient of the shear stress" [135] due to the fact that the "size" and gradient effects in torsion test were not accounted for. Third, to account for the "size" and shear gradient amplitude effect, a clear distinction must be made between t_{ref} determined at the radius R_∞ of specimen large enough and $\mathrm{t}(R)$ determined at the radius R of the considered specimen. Then all these above analyses affirm, first, the "size effect" on fatigue limits (Smaller is Stronger) as well as the beneficial effect of the normal stress gradient (Higher Gradient is Stronger), and second, the necessity of a distinction between $\mathrm{t}_{ref} = \mathrm{t}(R_\infty)$ and $\mathrm{t}(R)$) when applied to the classical Crossland criterion and the new gradient criterion, respectively. With all such conceptions, the experimental data now agree very well with the ellipse arc based on the f–t limits of the new criterion proposed (Eq. 5.57), as plotted in Fig. 5.8. It is also recalled [135] that the substitution of the material parameters by the bending and torsion limits is an unorthodox way to bypass the above described problems for classical criterion. The same ellipse formula is obtained in a more intrinsic way using the proposed criterion. The same approach can be applied to any other classical fatigue criterion.

5.5 Gradient Dang Van criterion

A stress gradient dependent version of Dang Van criterion is proposed here in the same spirit as that of Crossland.

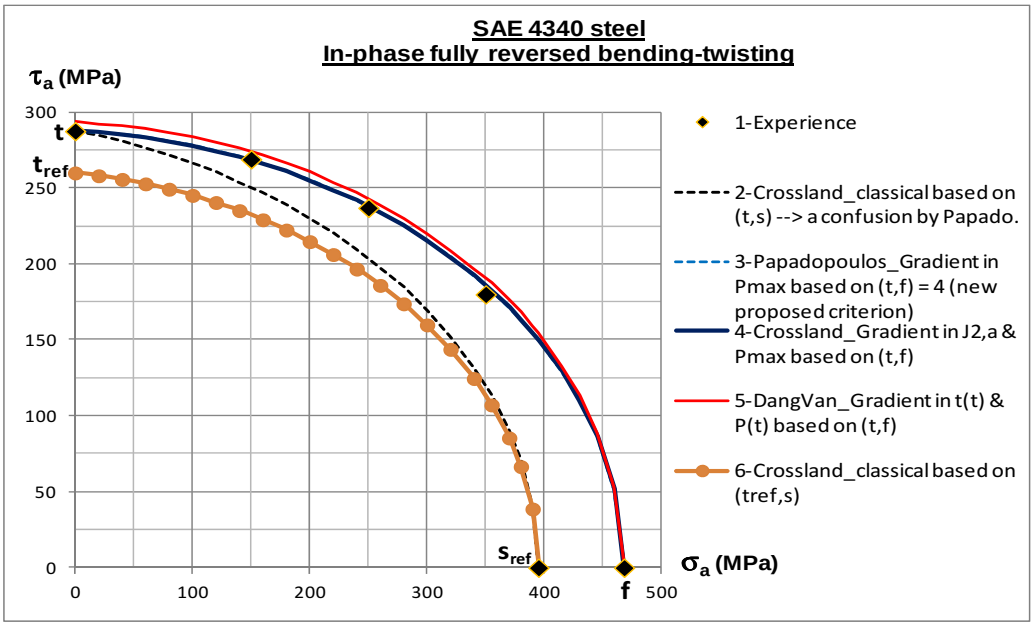

Figure 5.8 : *Fully reversed combined bending-twisting fatigue limit data* (Findley *et al.* [50], Papadopoulos and Panoskaltsis [135])

5.5.1 Classical Dang Van criterion

The Dang Van criterion presented in [16] is expressed as:

$$\max_t \left\{\tau(t) + a_D\, P(t)\right\} \leq b_D \tag{5.61}$$

$\tau(t)$ denotes the *mesoscopic shear stress amplitude* and is obtained from a mesoscopic stress tensor $\hat{\boldsymbol{\sigma}}$ defined by:

$$\hat{\boldsymbol{\sigma}}(t) = \left(\boldsymbol{\sigma}(t) - \boldsymbol{s}^*\right) \tag{5.62}$$

$\boldsymbol{s}^*$ is the center of the smallest hypersphere circumscribed to the loading path in deviatoric stress space. It is obtained by solving a *"min-max" problem* as follows:

$$\boldsymbol{s}^* = arg \min_{\boldsymbol{s}_1} \left\{ \max_t \|\boldsymbol{s}(t) - \boldsymbol{s}_1\| \right\} \tag{5.63}$$

In the case of fully reversed loading, the value $\boldsymbol{s}^* = 0$ can be directly deduced without solving the *"min-max problem"* as in general case.

Denoting by $\hat{\sigma}_{III}(t) \leq \hat{\sigma}_{II}(t) \leq \hat{\sigma}_I(t)$ the principal stress values of stress tensor $\widetilde{\sigma}$, one gets the amplitude of shear stress by:

$$\tau(t) = \frac{1}{2}(\hat{\sigma}_I(t) - \hat{\sigma}_{III}(t)) \tag{5.64}$$

$P(t)$ is the hydrostatic stress as a function of the time, given by:

$$P(t) = \frac{\sigma_{kk}(t)}{3} \tag{5.65}$$

The material characteristic parameters a_D and b_D of the Dang Van criterion, can be related to the fully reversed bending (or tension-compression because of the same stress state between them) fatigue limit , denoted by f_{ref} (or s_{ref}), and to the torsion fatigue limit, denoted by t_{ref},

$$a_D = \frac{3\mathrm{t}_{ref}}{s_{ref}} - 3/2; \quad b_D = \mathrm{t}_{ref} \tag{5.66}$$

5.5.2 Formulation of gradient Dang Van criterion

Using as a basis the classical Dang Van criterion, Eq. (5.61), along with the general spirit, Eq. (5.9), for the development of a gradient version as below:

$$\max_t \left\{\widetilde{\tau(t)} + a_g \widetilde{P(t)}\right\} \leq b_g \tag{5.67}$$

The material parameters a_g, b_g are actually equal to a_D, b_D respectively, as was the case of the gradient Crossland criterion (sec. 5.4.2).
Using $\tau(t)$ as a basis, a new form $\widetilde{\tau(t)}$ *embedded with gradient term* is proposed:

$$\widetilde{\tau(t)} = \tau(t)\left[1 - \left(l_\tau \frac{\|\boldsymbol{Y}(t)\|}{\tau(t)}\right)^{n_\tau}\right] \tag{5.68}$$

where $\boldsymbol{Y}(t) = \nabla\boldsymbol{\sigma}(t)$ and the definitions as well as significance of n_τ, l_τ are the same as for the case of the Crossland (sec. 5.4.2). For $\widetilde{P(t)}$, the same form as that of [135] is proposed again:

$$\widetilde{P(t)} = P(t)\left[1 - \left\langle l_\sigma \frac{\|\boldsymbol{G}(t)\|}{P(t)}\right\rangle^{n_\sigma}\right] \tag{5.69}$$

with the expressions of $\boldsymbol{G}(t), \|\boldsymbol{G}(t)\|$ similar to Eqs. (5.29, 5.30), the McCauley bracket $\langle \circ \rangle$ similar to Eq. (5.31), and the definitions as well as significance of n_σ, l_σ are the same.

The proposed criterion has six materials parameters $(a_g, b_g, l_\tau, l_\sigma, n_\tau, n_\sigma)$ to be identified experimentally.

5.5.3 Calibration of the material parameters

As previously, a procedure for obtaining the parameters from fully reversed torsion and fully reversed constant moment bending tests is detailed hereafter.

a) Fully reversed torsion tests

Applying first the gradient version described by Eq. (5.67) to the case of fully reversed torsion tests on specimen of radius R, with the fatigue limit denoted by $\mathrm{t}(R)$ and considering the most stressed points,

relevant quantities are:

$$\begin{aligned}
&\boldsymbol{\sigma}(t) = \sigma_{x\theta}(t)\ (e_x \otimes e_\theta + e_\theta \otimes e_x) = \mathrm{t}(R)\ sin(\omega t)\ (e_x \otimes e_\theta + e_\theta \otimes e_x) \\
&\hat{\sigma}_I = \mathrm{t}(R)\ \big|sin(\omega t)\big|,\ \ \hat{\sigma}_{II} = 0,\ \ \hat{\sigma}_{III} = -\mathrm{t}(R)\ \big|sin(\omega t)\big| \\
&\tau(t) = \frac{1}{2}(\hat{\sigma}_I - \hat{\sigma}_{III}) = \mathrm{t}(R)\ \big|sin(\omega t)\big| \\
&Y_{ijk}\, Y_{ijk} = 2\ \Big(\frac{\mathrm{t}(R) sin(\omega t)}{R}\Big)^2 \quad \text{and} \quad \|Y(t)\| = \sqrt{2}\ \frac{\mathrm{t}(R)}{R}\big|sin(\omega t)\big| \\
&\widetilde{\tau(t)} = \mathrm{t}(R)\ \big|sin(\omega t)\big|\ L_\tau(R) \qquad (5.70) \\
&\widetilde{P(t)} = 0 \qquad (5.71)
\end{aligned}$$

$$\text{with:} \qquad L_\tau(R) = 1 - 2^{n_\tau/2}(l_\tau/R)^{n_\tau} \qquad (5.72)$$

And using Eqs. (5.70, 5.71), the proposed fatigue criterion yields:

$$\mathrm{t}(R) = \frac{b_D}{L_\tau(R)} \approx \frac{\mathrm{t}_{ref}}{1 - (l_\tau/R)^{n_\tau}} \qquad (5.73)$$

between two kinds of fatigue test can be clearly seen. As for the gradient Crossland criterion, this formula is used to calibrate the three material parameters τ_{ref}, l_τ and n_τ, using the experiment curve relating the fatigue limit $\mathrm{t}(R)$ to the radius of the specimen. The material parameters are then calibrated using the least square method on the tests points; and therefore the optimal parameters (i.e. the values which minimize the scatter between the predicted and experimental points) for the criterion are obtained. As an illustration, the torsion fatigue tests given by Massonnet [104] are used to identify τ_{ref}, l_τ and n_τ, as shown in Fig. 5.6. A visual image of t_{ref} aforementioned is as well found in this graph. The values obtained are: $\tau_{ref} = 115$ MPa, $l_\tau = 9.8\ 10^{-1}$mm and $n_\tau = 0.5$.

b) Fully reversed cantilever bending tests

With the same notation and most stressed points to consider as in Sec. (5.4.3.c), all quantities are given by:

$$\begin{aligned}
&\boldsymbol{\sigma}(t) = \sigma_{xx}(t)\ e_x \otimes e_x = f'(R)\ sin(\omega t)\ e_x \otimes e_x \\
&\|Y(t)\| = \frac{f'(R)}{R}\big|sin(\omega t)\big|\sqrt{1 + \frac{R^2}{L^2}} \\
&\widetilde{\tau(t)} = \frac{f'}{2}\big|sin(\omega t)\big|\ L_{\tau f'}(R,L) \qquad (5.74)
\end{aligned}$$

$$\text{with:} \qquad L_{\tau f'}(R,L) = 1 - 2^{n_\tau}\ (l_\tau/R)^{n_\tau}\Big(1 + \frac{R^2}{L^2}\Big)^{n_\tau/2} \qquad (5.75)$$

Similarly, using Eq. (5.69):

$$\widetilde{P(t)} = \frac{f'(R)}{3} sin(\omega t)\ L_{\sigma f'}(R,L) \qquad (5.76)$$

$$\text{with:} \qquad L_{\sigma f'}(R,L) = 1 - (l_\sigma/R)^{n_\sigma}\Big(1 + \frac{R^2}{L^2}\Big)^{n_\tau/2} \qquad (5.77)$$

Finally, from Eq. (5.67), an equation with respect to the variable f' is solved to give:

$$f'(R) = \frac{s_{ref}}{L_{\sigma f'} - \dfrac{s_{ref}}{2\,\mathrm{t}_{ref}}(L_{\sigma f'} - L_{\tau f'})} \geq s_{ref} \tag{5.78}$$

The fatigue limit of four-point bending tests $f(R)$ can be directly obtained by imposing L large enough such that $\frac{R^2}{L^2}$ in Eq. (5.78) is negligible and then $f'(R) \equiv f(R)$.

5.6 Formulation of the gradient dependent multiaxial low-cycle fatigue criteria

In addition to what are dealt with before for HCF case, now some development will be made for the *multiaxial low-cycle fatigue* case which does not require a macroscopically elastic stress state as in HCF case. Thus the application is larger, even to notched specimen fatigue problems in principle. The following will be confined in some proposals and without any validation because of lack of experimental data.

5.6.1 Strain gradient dependent Manson-Coffin fatigue criterion

The classical Manson-Coffin fatigue criterion relates the number of cycle in fatigue rupture N_R to the amplitude of plastic strain in stabilized cycle $E_a^p = \Delta\varepsilon^p/2$ according to the formula (*cf.* [100]):

$$E_a^p = \frac{\Delta\varepsilon^p}{2} = \varepsilon_f^{/}(N_R)^c \tag{5.79}$$

where the exponent c varies between $0.5-0.7$ whereas the ductility coefficient in fatigue $\varepsilon_f^{/}$ for most metals, is equal to the elongation in fatigue.
With a general extension of the plastic strain in the case of multiaxial loading defined as,

$$E^p = \sqrt{\frac{2}{3}\|\varepsilon^p\|^2} = \sqrt{\frac{2}{3}}\|\varepsilon^p\| \tag{5.80}$$

an extension of this criterion can be made using a general extension of the amplitude of the plastic strain defined as the radius of the smallest hypersphere circumscribed to the plastic strain path by:

$$E_{,a}^p = \sqrt{\frac{2}{3}}\min_{\varepsilon_1^p}\left\{\max_t \left\|\varepsilon^p(t)-\varepsilon_1^p\right\|\right\} = \min_{\varepsilon_1^p}\left\{\max_t \sqrt{\frac{2}{3}\left(\varepsilon^p(t)-\varepsilon_1^p\right):\left(\varepsilon^p(t)-\varepsilon_1^p\right)}\right\} \tag{5.81}$$

or as the half-length of the longest chord of the plastic strain path by:

$$E_{,a}^p = \frac{1}{2}\sqrt{\frac{2}{3}}\max_{t_1}\left\{\max_{t_2} \left\|\varepsilon^p(t_2)-\varepsilon^p(t_1)\right\|\right\} = \frac{1}{2}\max_{t_1}\left\{\max_{t_2} \sqrt{\frac{2}{3}\left(\varepsilon^p(t_2)-\varepsilon^p(t_1)\right):\left(\varepsilon^p(t_2)-\varepsilon^p(t_1)\right)}\right\} \tag{5.82}$$

Using as a basis the classical criterion, eq. (5.79), for the development of the gradient version, yields:

$$\widetilde{E_a^p} = \frac{\Delta\widetilde{\varepsilon^p}}{2} = \varepsilon_f^{/}(N_R)^c \tag{5.83}$$

where the gradient dependent modified versions of E^p and E^p_a, denoted as $\widetilde{E^p}$ and $\widetilde{E^p_a}$, respectively, is introduced by taking inspiration from eqs. (5.21) and (5.23):

$$\widetilde{E^p} = \sqrt{\frac{2}{3}\|\varepsilon^p\|^2\left[1 - l\left(\frac{\|\nabla\varepsilon^p\|}{\|\varepsilon^p\|}\right)^n\right]} = E^p\sqrt{1 - l\left(\frac{\|\nabla\varepsilon^p\|}{\|\varepsilon^p\|}\right)^n} \tag{5.84}$$

$$\widetilde{E^p_a} = E^p_a\sqrt{1 - l\left(\frac{\|\nabla\varepsilon^p\|_a}{\|\varepsilon^p\|_a}\right)^n} \tag{5.85}$$

5.6.2 Strain gradient dependent fatigue energy criterion

A second family of LCF criterion relating an energy calculated at stabilized cycle W_R to the number of cycle in fatigue rupture, *cf.* [100], and its corresponding gradient version, are given below:

$$w_R = C(N_R)^{-\gamma}, \implies \widetilde{w_R} = C(N_R)^{-\gamma} \tag{5.86}$$

where C and γ are two characteristic constants intrinsic to materials. Several expressions for w_R were proposed, in which the two followings are rather common:

- Plastically dissipated energy on stabilized cycle:

$$w_R = \Delta W_p = \int_{stabilized\ cycle} \sigma : \dot{\varepsilon^p} dt, \implies \widetilde{w_R} = \int_{stabilized\ cycle} \widetilde{\sigma} : \dot{\widetilde{\varepsilon^p}} dt \tag{5.87}$$

- Sum of plastically dissipated energy and elastic energy in tension phase of stabilized cycle:

$$w_R = (\Delta W_p + \Delta W_e^+)/A + B, \implies \widetilde{w_R} = \left(\widetilde{\Delta W_p} + \widetilde{\Delta W_e^+}\right)/A + B \tag{5.88}$$

where ΔW_e^+ is the elastic energy accumulated during tension phase of stabilized cycle; $A and B$ are two characteristic constants intrinsic to materials. Again taking inspiration from eqs. (5.21) and (5.23), the proposals for $\sigma, \dot{\varepsilon^p}$ can be:

$$\widetilde{\varepsilon^p} = \varepsilon^p\left[1 - l\left(\frac{\|\nabla\varepsilon^p\|}{\|\varepsilon^p\|}\right)^n\right], \quad \widetilde{\sigma} = \sigma\left[1 - l\left(\frac{\|\nabla\sigma\|}{\|\sigma\|}\right)^n\right]$$

5.7 Numerical implementation

The stress gradient Crossland criterion, Eqs. (5.20), is considered as an illustration. The calculation of $\sqrt{\widetilde{J_2}_{,a}}$, as described by Eq. (5.23), with the help of Eq. (5.16) or Eq. (5.15) for $\sqrt{J_{2,a}}$, and of Eq. (5.25) or (5.26) for $\left\|\boldsymbol{Y}(t)\right\|_{,a}$, is *"min-max"* or *"max-max"* problems in a 5-dimension space for $\sqrt{J_{2,a}}$ and 18-dimension space for $\|\boldsymbol{Y}\|_{,a}$. Therefore, in numerical aspect, the calculation of $\sqrt{\widetilde{J_2}_{,a}}$ is actually *"min-max"* or *"max-max"* problems with 23 variables. It is solved using user-written program under Matlab. It remains $\widetilde{P_{max}}$ which evaluation through Eq. (5.28) is straightforward. Just using suitable operators in any available finite element code (i.e. Cast3M, [36]), the quantities $G = \nabla P_{max}$ after Eq.

(5.29) and then $\|\boldsymbol{G}\|$ after Eq. (5.30) are estimated quickly.
So the proposed gradient fatigue criteria, Eqs. (5.20) and (5.67), can be numerically implemented within any available finite element code along with a user-written program to solve *"min-max"* or *"max-max"* problems.

5.8 Discussion

***Remark* 1 (Gradient terms)** Limits of classical fatigue criteria in the literature are that the "size", gradient and loading effects are not captured. Even in the gradient fatigue criterion proposed by a number of authors such as the typical work of [135], the role of the shear stress gradient as well as the shear stress gradient amplitude in fatigue strength has not been made clear and thereby temporarily still neglected. In [135], the role of the shear stress gradient which is inherently assumed null only for some metals considered, but has been generally omitted even when applied to any other metal.
This study, as reasoned in the section 5.3.2, show that in some special cases where just one kind of load appears (e.g. pure torsion test, pure bending test), *a unique gradient term* is enough to model the gradient and loading effects. This is introduced either in the normal stress component of the classical fatigue criterion as [135] proposed, or in the shear stress part as presented in the current work. However, in multiaxial fatigue tests, concomitant two types of stress gradient terms are in principle indispensable to capture the previous effects.

***Remark* 2 (Material characteristic length scale ℓ)** The values of ℓ of the model proposed extend from several hundredths of a millimeter to about a millimeter for cases considered, while the one of the model proposed very recently by Ferré *et al.* 2013 [49] takes about a micron. The very difference between them is physically explained by the following reason: we study here the fatigue endurance of macroscopic specimens and components for which the crack initiation is generally detected by loss of stiffness corresponding to crack length which can reach a millimeter; whereas Ferré *et al.* consider crack nucleation in the scale is few dozen microns.

***Remark* 3 (Insensitive threshold of effects)** The dependence of fatigue limits on both "size" and gradient effects according to the specimen size (*e.g.* L, R) has a "saturated" or "insensitive" threshold. That means, there always exists a certain "saturated" value for the specimen size (L_∞, R_∞) from which the fatigue behavior is insensitive to both effects and the proposed criteria exactly reduce to the respective classical ones.

***Remark* 4 (Approximation of some formulae)** In the illustration through Crossland criterion, using a priori the exponent $n = 0.5$ for some approximations (Eqs. (5.37), (5.53)) results in the very simple formulas for relevant quantities, especially in the combined bending-twisting case. This value of n was afterwards affirmed reasonable through very good validation with some experimental classes. In the general case, however, n could have another value for other experimental classes, then the proposed

criteria may require to use the exact formulae, Eqs. (5.75, 5.77) e.g., to express consistently all relevant quantities (such as $L_{\tau f}, L_{\tau f'}, L_{\sigma f}, L_{\sigma f'}...$) in any case of test according to their analogues in calibration tests (torsion and bending tests).

5.9 Conclusion

The present study develops a simple formulation of gradient multiaxial fatigue criteria extending the classical HCF criteria. The objective is to model the "size", surface gradient and loading effects, not included yet in classical mechanics but become important at small scale, by taking into account just the gradient effect.

Basing on some experimental observations, and departing from classical fatigue criteria, new class of criteria with stress gradient terms entering not only in the normal stress but also in the shear stress amplitude, are proposed. Such a formulation allows the new criteria to capture the "size" and gradient effects, and to cover a large range of loading mode (traction, bending, shearing). These new criteria are then generalized to multiaxial cases to capture both well-known phenomena *"Smaller is Stronger" and "Higher Gradient is Stronger"* and thus can reproduce fatigue experimental data even at small scale. Here in this work, the nature of these two phenomena is also clarified. "Higher Gradient is Stronger" is only related to the gradient effect, while "Smaller is Stronger" is related to both pure size and gradient effects where the latter is dominant - rather than totally to the pure size effect as usually believed.

Extensions of some classical fatigue limit criteria such Crossland and Dang Van are done as illustrations. The proposed criteria shown a good agreement with a number of experiments from the literature. A more comprehensive validation for complex loading (real multiaxial loads) could be perspective for this research direction.

Nevertheless, in this work only cases with critical points located at the specimens surfaces have been examined. In these cases, the gradient is such that it has a beneficial effect on fatigue. However, cases where the effect can be presumably negative, especially with the presence of residual stresses, can be encountered. A reexamination of the approach will be the object of the further work. Besides, for notched fatigue problems, this approach may be still applicable.

In conclusion, the extension of classical fatigue criteria embedding into them two gradient terms, one corresponds to normal stress part, the other to shear stress part, leads to new versions able to describe common effects on multiaxial fatigue endurance.

CHAPTER 6

General conclusions and perspectives

6.1 Conclusion

The work deals with two grand classes of gradient models: elastoplastic constitutive models and high/low cycle fatigue (HCF/LCF) models. Its main motivation is that the micro- and nanomechanical issues are becoming increasingly important in MEMS engineering and technologies. For problems at these small scale, "size"[1] and gradient effects become significant. Taking them into account in the design and therefore in models of mechanical behavior and fatigue life is necessary for a good estimation of the reliability of such devices. This thesis is devoted to study on the one hand gradient models of elastoplastic behavior in a generalized standard framework, on the other hand the possibility of extending the classical HCF/LCF criteria. These two themes consist of two parts (A and B) of the thesis, respectively.

Part A- Standard Gradient Constitutive Models: Application in Micro-Mechanics

After an analysis of the abundant literature on the gradient theories of elastoplastic behavior, those proposed by QS Nguyen (2000, 2005, 2011 and 2012) has chosen to develop. It is based on a consistent global approach, implemented in the generalized standard framework (from the thermodynamic potential and the dissipation potential). It allows obtaining the constitutive equations, evolution and associated variational principles. The framework also makes it easy to address issues relating to the uniqueness of solutions. Gradient elastoplastic models considered include different types of hardening (kinematic and isotropic). When the dissipation potential depends on the gradient of the internal variables, the numerical implementation of these models present difficulties. A method of regularization energy allow to overcome them. The presence of the gradient leads to a non-standard evolution problem with a Laplace equation and boundary conditions governed by differential equations of second order. The resolution method chosen and implemented in the CAST3M code is similar to that used for diffusion problems. Some typical examples as illustration are then processed and compared to reference results from the literature to show the relevance of the models. These are the problems of thin wire torsion, thin film shearing and microvoid growth. Using the model, "size" and gradient effects are taken into account and both well-known phenomena "Smaller is Stronger" and "Higher Gradient is Stronger" are reproduced.

Part B- Gradient Fatigue Criteria at Small Scale

The effects of the "size", gradient and loading mode, are well known in the research of material fatigue. They are often highlighted in the notches, fretting fatigue problems and micromechanics. If there is a

[1] in the sense that it mainly results from the gradient effect related to the size rather than the size effect by Dislocation Starvation and the pure size effect by material metallurgical defects-heterogeneity which are negligible.

large number of fatigue criteria, very few of them are able to capture these effects. A relevant work is that done by Papadopoulos and Panoskaltsis in 1996. From an analysis of fatigue experiment data in the literature, they made clear the pure size and gradient effect and proposed a fatigue criterion taking into account only the hydrostatic stress gradient. Such a model does not cover large enough loading cases (rotative bending and torsion left), i.e. loading effect is not captured. The work in the thesis departs from this analysis and formulates gradient multiaxial fatigue criteria in more general framework where the loading mode (except rotative bending) is included. The idea is to introduce the stress gradients into two main components of the criteria (one related to the amplitude of the shear stress and the other to the hydrostatic stress) by defining the gradient versions of both shear stress amplitude and hydrostatic stress. In this way, the loading effect is naturally directly attached to the gradient effect, whereas the pure size effect is insignificant and thus negligible, and then three factors, "size", gradient and loading effects, are taken into account. Two classical criteria widely used, Crossland and Dang Van, are particularly formulated in the new framework to their give gradient versions. A validation of these proposals is then made using the experiment results from the literature. A very good correlations are obtained. Two well-known phenomena "Smaller is Stronger" and "Higher Gradient is Stronger" are reproduced.

The above is a very brief conclusion of the work. More detailed conclusions for each part (A and B) are also given at the end of each one.

6.2 Perspectives

For both classes of models:

The pure size effect has not been really included yet, thus maybe make trouble if this effect is considerable in certain cases. Another approach, or even a certain approach combined with the method presented in this work, can be a solution.

The validity range of the gradient models adopted is micron or sub-micron for the constitutive model and about millimeters for fatigue model, not smaller. At smaller scale other approaches are required.

6.2.1 Standard Gradient Constitutive Model

The "size" and gradient effect concerning specimen size (microsystems problems) are affirmed to be modeled with the model adopted. Those concerning the material grain size (microstructure problems) are expected to be also captured via the *material characteristic length* related to the grain size. However, validation for these problems are temporarily left out for a further work. Moreover, since the SGP model in general and the SSGP model in particular are based on the strain gradient plasticity, they are not usable in purely elastic cases. In this kind of problems, a class of models based on **stress gradient** approach or, equivalently, **total strain gradient** approach (as it is linear problem), may be valid instead. It suggests that a class of models based on total strain gradient approach, could be more general to deal with both plastic and purely elastic problems.

6.2.2 Gradient Fatigue Criteria

In methodological aspect, gradient approach just allow modeling the volumetric stresses instant distribution (related to loading case such as: tension-compression, torsion, plane bending), not volumetric stresses distribution all over the loading cycle (related to rotative bending). Thus the adopted criteria indifferently deal with the plane bending and the rotative bending tests, although their fatigue limits are actually different.

Fatigue problems concerning other factors (machining, notches, defects, inclusions, corrosion, etc.) have been left out in this approach and need another approach to address. In particular for notched fatigue problems, this approach may be still applicable. A validation by means of experimental data is needed to examine this possibility.

Cases with critical points located inside specimens where the gradient effect can be presumably negative on fatigue resistance, for instance those with presence of residual stresses, can be encountered and have not examined yet. A reexamination of the approach will be the object of the further work.

Appendix

.1 Numerical implementation

.1.1 Parameters of material

k, κ, H, J, G, r are known through experiments (identification experiments).

.1.2 Initiation for quantities

The Hencky algorithm is an 1-step increment schema with regard to a given load. A certain number of mechanical iterations will be necessary until the numerical convergence of the solutions.

But in the case of needing to draw the evolution of certain quantities versus load, the algorithm would be used many times, independently, corresponding to many different loading levels (i.e. to independent problems). For such each time of using Hencky algorithm, an 1-step increment schema is obviously still available.

At a certain loading level n, with the notation k assigned to the mechanical iteration and t to the list of loading time of the whole problem, the initiation of quantities in a series of mechanical iterations will be:

$$\begin{cases} k = 1 \\ F_d^{ext\,(n)} = t^{(n)}\, F_d^{ext} \qquad (F_d^{ext}\text{-total load, i.e final load, putting on the object}) \\ W^{(k=1)} = 0 \ \text{(total free energy stocked in the considered system)} \\ \text{Other quantities: } x_{(k=1)}^{(n)} = \left(\varepsilon_1^{p\,(n)}, \gamma_1^{(n)}\right) = 0 \end{cases}$$

The maximum number of mechanical iterations for each loading level, denoted as k_{max}, is necessary to reasonably chose in advance. If the computer code could not attain its convergence for each loading step, then it must be raised k_{max}.

.1.3 Calculation via LOOPs: Algorithm schema (Fig.1)

The following schema is established for a general case where the algorithm will be used many times, independently, corresponding to many different loading levels, to draw the evolution of certain quantities against load. Index n_{max} corresponds to the final loading level.

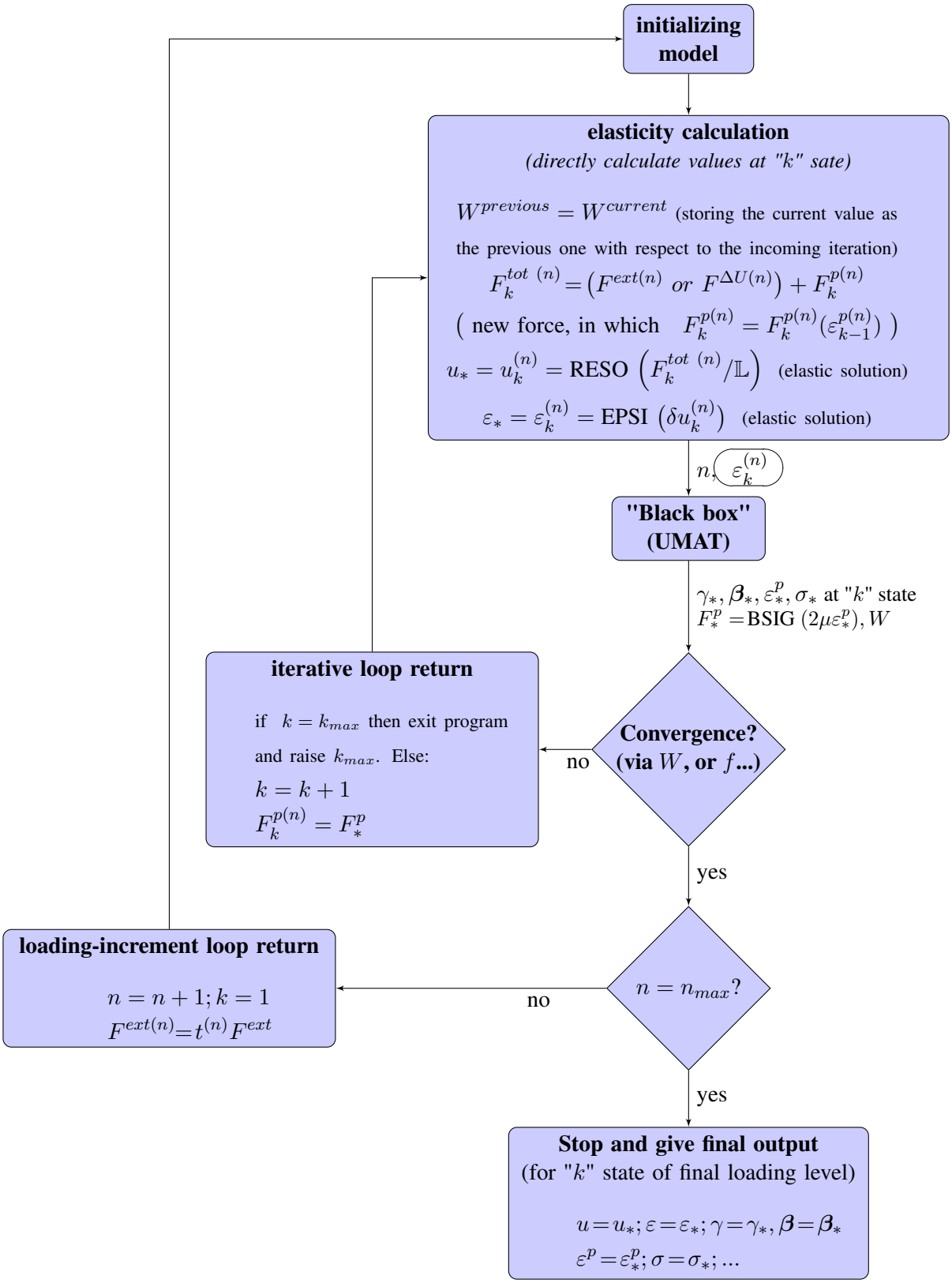

Note: see more detailed about UMAT at Fig 2 (a user code for mechanical behavior model).

Figure 1 : *Calculation via LOOPs - Algorithm schema*

.1.4 Detail of UMAT in CAST3M (Fig.2)

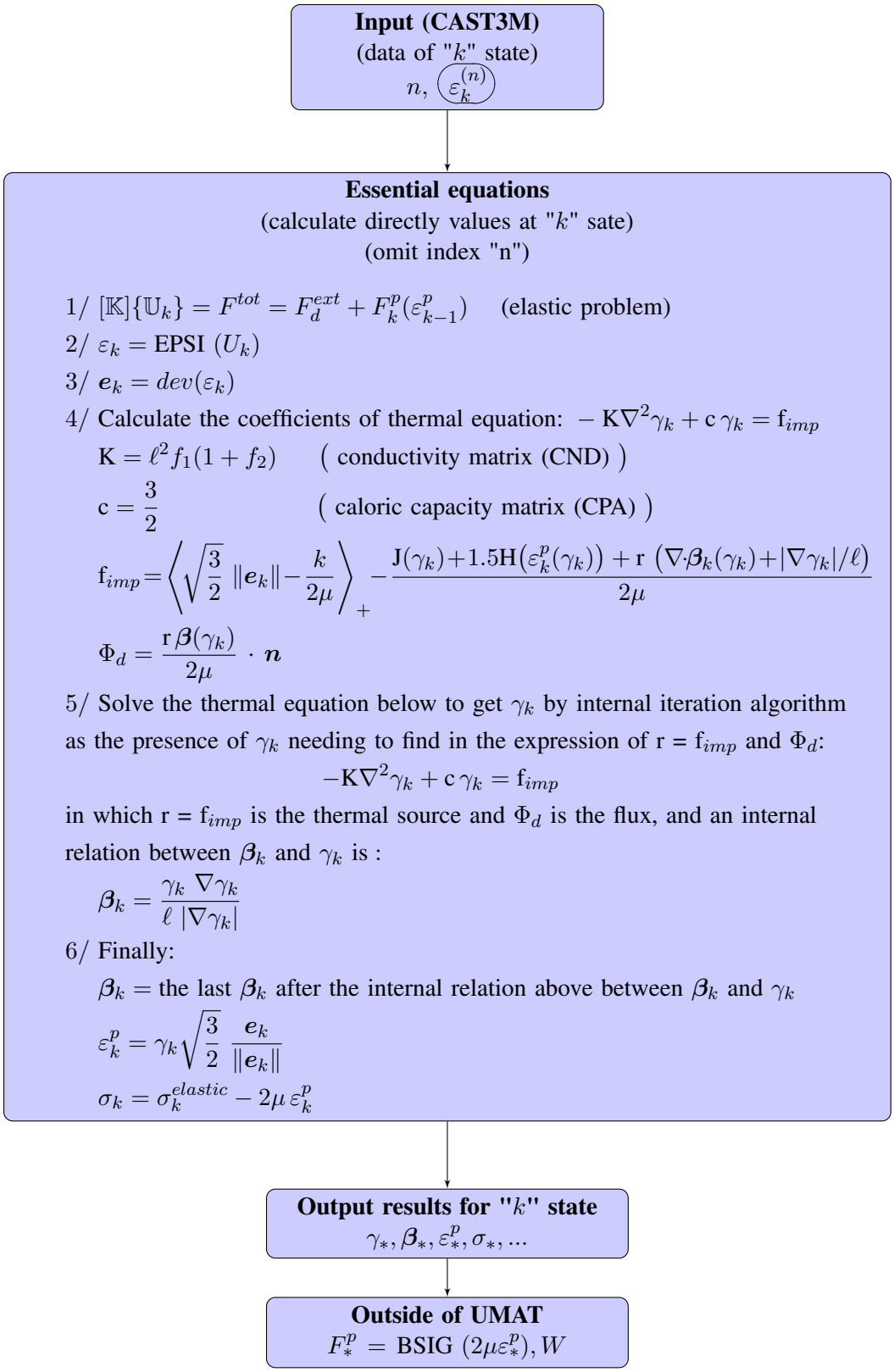

Figure 2 : *Detail of UMAT in CAST3M (for implicit schema)*

.1.5 Implementation in CAST3M

1. ***Calculation operators***

   Calculate f_{imp} at global level using operators in CAST3M such as:

   $$\text{div V} = \text{tr (grad V)} = \text{(grad V)}_{xx} + \text{(grad V)}_{yy} + \text{(grad V)}_{zz}$$

   where V is a 1-order tensor, i.e a vector, and $grad\, V$ is considered gradient operator for a displacement vector field in CAST3M (vector u)

2. ***Global solution for Laplace equation***

   Solve at global level the Laplace equations (3.85) or (3.89) with the boundary condition in (3.70) which is rewritten under a more familiar form:

   $$\begin{cases} -\text{K}\nabla^2 z + \text{c}\, z = \text{f}_{imp}, \quad (z = \gamma_k = \lambda), \quad \forall x \in V \\ -\text{appropriate boundary conditon (it will be clarified later)} \end{cases} \tag{1}$$

   Solve (1) by taking spirit of the thermic problem in CAST3M [21]-page 14:

   $$\begin{cases} -\text{K}\,\nabla^2 T + \rho\,\text{c}\,\dfrac{\partial T}{\partial t} = \text{r} & \forall x \in V \\ (\text{K}\,\nabla T)\,\cdot\,\boldsymbol{n} = \Phi_d & \forall x\ on\ \partial V_q \\ T = T_d & \forall x\ on\ \partial V_T \end{cases}$$

   or under the form:

   $$\begin{cases} -div\,(\text{K}\,\nabla T) + \rho\,\text{c}\,\dot{T} = \text{r} & \forall x \in V \\ (\text{K}\,\nabla T)\,\cdot\,\boldsymbol{n} = \Phi_d & \forall x\ on\ \partial V_q \\ T = T_d & \forall x\ on\ \partial V_T \end{cases} \tag{2}$$

   The same spirit as that of quasi-harmonic equations allows to obtain the weak formulation as below:

   Find T such that $T = T_d$ on ∂V_T in order that:

   $$-\int_V \delta T\, div\,(\text{K}\,\nabla T) + \int_V \delta T \rho\,\text{c}\,\dot{T} = \int_V \delta T\,\text{r} \tag{3}$$
   $$\forall \delta T \text{ such that } \delta T = 0 \ \ on\ \ \partial V_T$$

   Note that:

   $$div\,(\delta T\,.\,\text{K}\,\nabla T) = \delta T\,.\,div\,(\text{K}\,\nabla T) + \text{K}\,\nabla T\,\cdot\,\nabla \delta T$$

   So (3) can be rewritten:

   $$-\int_V div\,(\delta T\,.\,\text{K}\,\nabla T) + \int_V \text{K}\,\nabla T \cdot \nabla \delta T + \int_V \delta T \rho\,\text{c}\,\dot{T} = \int_V \delta T\,\text{r} \tag{4}$$
   $$\forall \delta T \text{ such that } \delta T = 0 \ \ on\ \ \partial V_T$$

Green theorem brings:

$$\int_V div\,(\delta T\,.\,\mathrm{K}\,\nabla T) = \int_{\partial V} \delta T\,.\,\mathrm{K}\,\nabla T \cdot \boldsymbol{n}$$
$$= \int_{\partial V_q} \delta T\,.\,\mathrm{K}\,\nabla T\,\cdot\,\boldsymbol{n} + \int_{\partial V_T} \delta T\,.\,\mathrm{K}\,\nabla T\,\cdot\,\boldsymbol{n} = \int_{\partial V_q} \delta T\,.\,\mathrm{K}\,\nabla T\,\cdot\,\boldsymbol{n}$$
$$= \int_{\partial V_q} \delta T\,.\,\Phi_d \quad \text{(thanks to (2.b) and } \delta T = 0\ on\ \partial V_T)$$

Finally (4) can be expressed:

$$\int_V (\nabla \delta T)^T\,\cdot\,\mathrm{K}\,\nabla T + \int_V \delta T \rho\,\mathrm{c}\,\dot{T} = \int_V \delta T\,\mathrm{r} + \int_{\partial V_q} \delta T\,.\,\Phi_d \qquad (5)$$
$$\forall \delta T \text{ such that } \delta T = 0\ \ on\ \ \partial V_T$$

Temperature field is estimated within each element V^e of the mesh and every moment from the values in nodes associated with this element at this time. The temperature is approached in the following manner via nodal values:

$$T(\underline{X}, t) = \left\{N^e(\underline{X})\right\}.\left\{T^e(t)\right\}$$

The application of the nodal approximations in the problem (5) allows to obtain (after discretized):

$$\int_{V^e} \delta T_h^e\ \nabla \mathrm{N}_j^e\ \mathrm{K}\ \nabla \mathrm{N}_i^e\ T_h^e\ dV + \int_{V^e} \mathrm{N}_j^e\ \delta T_h^e\ \rho\,\mathrm{c}\ \mathrm{N}_i^e\ \dot{T}_h^e\ dV$$
$$= \int_{V^e} \mathrm{N}_j^e\ \delta T_h^e\ \mathrm{r}\ dV + \int_{\partial V_q^e} \mathrm{N}_j^e\ \delta T_h^e\ \Phi_d\ d\Gamma \quad \forall\ \delta T_h^e$$

Or under the matrix form:

$$\left(\int_{V^e} \{\nabla \mathrm{N}_i^e\}^T\ \mathrm{K}\ \{\nabla \mathrm{N}_j^e\}\ dV\right)\{T^e\} + \left(\int_{V^e} \{\mathrm{N}_i^e\}^T\ \rho\,\mathrm{c}\ \{\mathrm{N}_j^e\}\ dV\right)\{\dot{T^e}\}$$
$$= \int_{V^e} \{\mathrm{N}_j^e\}\ \mathrm{r}\ dV + \int_{\partial V_q^e} \{\mathrm{N}_j^e\}\ \Phi_d\ d\Gamma$$

As well known in thermal problem, one defines:

$$\begin{cases} [\mathbb{K}^e] = \int_{V^e} \{\nabla \mathrm{N}_i^e\}^T \mathrm{K}\ \{\nabla \mathrm{N}_j^e\}\ dV & \text{conductivity matrix (CND)} \\ [\mathbb{C}^e] = \int_{V^e} \{\mathrm{N}_i^e\}^T \rho\,\mathrm{c}\ \{\mathrm{N}_j^e\}\ dV & \text{caloric capacity matrix (CPA)} \\ \{\mathbb{F}^e\} = \int_{V^e} \{\mathrm{N}_j^e\}\ \mathrm{r}\ dV + \int_{\partial V_q^e} \{\mathrm{N}_j^e\} \Phi_d\ d\Gamma & \text{thermal force/source} \end{cases} \qquad (6)$$

Finally after assembling the element matrix, the considered problem becomes:

$$[\mathbb{K}]\{\mathbb{T}\} + [\mathbb{C}]\{\dot{\mathbb{T}}\} = \{\mathbb{F}\} \qquad (7)$$

with:

$$\begin{cases} [\mathbb{K}] = \sum_{e=1}^{m} [\mathbb{A}^e]^T [\mathbb{K}^e] [\mathbb{A}^e] \\ [\mathbb{C}] = \sum_{e=1}^{m} [\mathbb{A}^e]^T [\mathbb{C}^e] [\mathbb{A}^e] \\ \{\mathbb{F}\} = \sum_{e=1}^{m} [\mathbb{A}^e]^T \{\mathbb{F}^e\} \end{cases} \tag{8}$$

Note that calculation of these above matrix CND, CPA and $\{\mathbb{F}\}$ is available without any difficulty in CAST3M in the framework of thermic problem.
Return now to (1) which really must be solved for our mechanic problem.

The same approach as in thermal problem but much more simple because of the presence of the variable z instead of $\dot{z}$, all (1), (2) and (7) lead to (9) which is a linear form (after discretized) of the considered eq. (1) and easy to solve:

$$\Big[[\mathbb{K}] + [\mathbb{C}] \Big] \{\mathbb{Z}\} = \{\mathbb{F}\} \tag{9}$$

where $\{\mathbb{F}\}$ is determined after (6.c) with r replaced with f_{imp} and Φ_d needing to be determined after the boundary condition of (1).

Comparing (3.86) with (2.b), Φ_d necessary for the calculation of $\{\mathbb{F}\}$ in (6.c) to solve (9) and also (1), is:

$$\Phi_d = \mathrm{K}\nabla z \cdot \boldsymbol{n} = \left[\ell^2 f_1 f_2 \boldsymbol{\beta} \right] \cdot \boldsymbol{n} = \frac{\mathrm{r}\boldsymbol{\beta}}{2\mu} \cdot \boldsymbol{n} \tag{10}$$

Such a Φ_d can be easily calculated by the operator "FLUX" in CAST3M for example.

Therefore finally, the considered Laplace equation (1) can be solved in implicit way under the linear form (9) **at global level** of the system.

Comment on the boundary condition (see eq. (2.b)):

Some particular cases are now discussed.

1/ *For the Mode-I problem* ($\mathrm{r} = 0$, that means $f_2 = 0$):

The boundary condition (2.b) at the mechanical iteration "k" after (10) becomes:

$$\begin{aligned} \Phi_d &= \mathrm{K}\nabla z \cdot \boldsymbol{n} = \mathrm{K}\nabla\gamma_k \cdot \boldsymbol{n} \ \text{(after the definition in (2.b))} \\ &= 0 \ \text{(after (10) with } f_2 = 0) \end{aligned}$$

Hence it follows that $\mathrm{K}\nabla\gamma \,.\, \boldsymbol{n} = 0$ (because $\mathrm{K}\nabla\gamma_k \,.\, \boldsymbol{n} = 0 \ \ \forall k$), that means $\gamma_{,n} = 0$ on ∂V, and the familiar boundary condition of Mode-I problem is then recovered as expected.

2/ *For the classical problem* ($\ell = 0$, that means $\mathrm{G} = 0, \ \ \mathrm{r} = 0$):

Naturally $\Phi_d = \mathrm{K}\nabla z \cdot \boldsymbol{n} = \mathrm{K}\nabla\gamma_k \cdot \boldsymbol{n} = 0$ (because $\mathrm{K} = 0$) and the boundary condition (2.b) do not result in $\gamma_{,n} = 0$ which is really logical with a classical problem as expected too.

.1.6 Remarks on the algorithm schemata used; Numerical convergence question

It is noteworthy to distinguish algorithm schemata used in both mechanical and numerical aspects.

• In mechanical aspect:

In the present work, the deformation plasticity method with the implicit algorithm is used, and as aforementioned (page 119).

• In purely numerical aspect:

An explicit schema (actually *internal iteration algorithm*), as presented in the page 117, is required to numerically solve the nonlocal Laplace equation in which the variable γ also appears in the right side.

• Numerical convergence question:

The difficulty in convergence when dealing with the nonlinear hardening problem is that, once a functional of uniaxial tensile stress-strain such as Ramberg-Osgood is used, it may sometimes cause non-convergence due to its very sharp slope around the zone close to co-ordinate origin where the uniaxial strain is very tiny. In order to overcome this inconvenience, a smoother functional as an exponential type as presented in (3.88), is strongly recommended. Even though an available referencial/experimental database would be given in terms of a Ramberg-Osgood curve, an equivalent conversion to an exponential hardening functional is still recommended thanks to the identification between them (see Fig. 3). This conversion does not considerably affect the final result because the segment different between each other lies within the zone where the uniaxial strain is very tiny. That also means, a priority for the range of strain predicted for the problem under consideration, while identifying two curves, is really more important. This conversion was carried out in Section "Applications" as commented in (.2)- page 124.

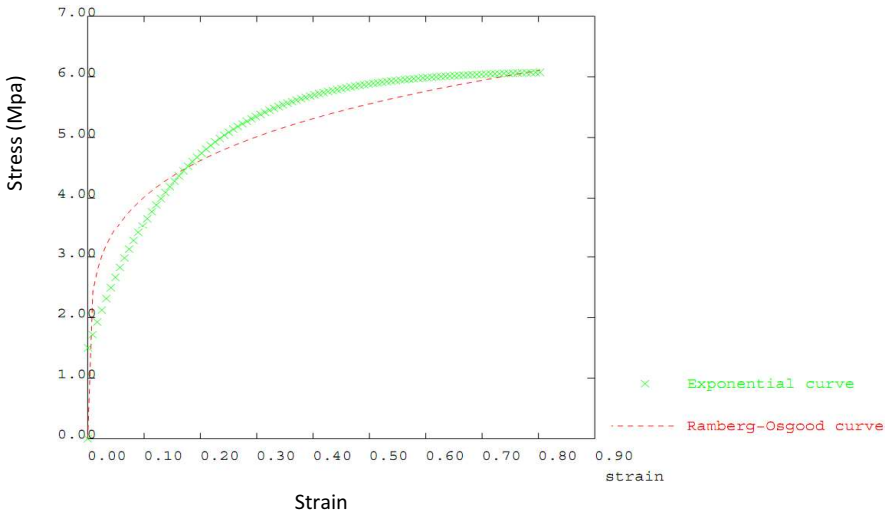

Figure 3 : *Conversion of a "uniaxial tensile stress-strain curve" of Ramberg-Osgood to an exponential curve* (*cf.* Fleck and Hutchinson 2001 [54])

.2 Procedure to validate the reference numerical results of Fleck & Hutchinson 2001

First of all, here are some conventions for what follows:

- The following presentation takes micro-void growth test as typical example. Thereby the corresponding notions do not need to be mentioned again.

- The *basic dimension of microsystems* means the key size of the problem under consideration. These are the radius R of micro-void, the thickness L of thin film, or the radius R of thin wire, etc.

The reference numerical results in [54] are obtained basing on the Ramberg-Osgood uniaxial tensile stress-strain curve in which the set of parameters $(\sigma_0, \varepsilon_0, n)$ are determined from the uniaxial tensile experiment. However, this curve causes numerical non-convergence sometimes, as aforementioned in (.1.6), thus the model proposed uses the exponential uniaxial stress-strain curve with its set of parameters (J_∞, b) as a substitution. Therefore it requires first of all to identify the latter after the former, that means (J_∞, b) after $(\sigma_0, \varepsilon_0, n)$.

All results of [54] plotted on diagrams are actually normalized by the values of $(\sigma_0, \varepsilon_0, n)$, then the specific values of these parameters are not important. They can take any values and then the corresponding load assumed to be used in [54] (pressure p in micro-void growth test) can be deduced after such a set of $(\sigma_0, \varepsilon_0, n)$ already chosen.

This load is then used again in the model proposed, with the set of parameters (J_∞, b) identified before. The simulation results by the adopted model is in reality only dependent on the ratio of the basic dimension against the *material intrinsic length* (R/ℓ_m) but not on their proper specific values. In order to numerically function the model, it needs to temporarily take a certain value for ℓ_m (with order of micrometer, normally). This chose does not affect on the final results.

Denote (R_i/ℓ_r) as the ratio of the i^{th} curve of [54], and (R_i/ℓ_m) the ratio of the i^{th} curve by the model. It requires to find an optimal set of parameters (G or f_1, r or f_2,...) in order that the "mod" curves fit as well as possible the "ref" ones, provided that the proportions between (R_{i+1}/ℓ_m) and (R_i/ℓ_m) have to be equal to those between $R_{i+1}/\ell_r)$ and (R_i/ℓ_r) respectively, with any of i. That means (R_i/ℓ_m) is not obligatory to be equal to (R_i/ℓ_r), but just their proper proportions when varying i must be equal. In that way the micro-void growth is simulated for all R_i.

In summary, three steps are performed to validate reference results of [54]:

• Determine a set of (J_∞, b) of the exponential curve after a set of $(\sigma_0, \varepsilon_0, n)$ of Ramberg-Osgood curve.

• Determine the corresponding load p assumed to be used in [54].

• Identify an optimal set of parameters for the model such that the simulation curves fit as well as possible those of the reference where the ratios between R_{i+1}/ℓ and R_i/ℓ are preserved from the one to the other of "ref" and "mod" curves for any i^{th}.

The simulation results prove a good agreement with those of the reference and the set of parameters identified in such way shows that the values of $(\sigma_0, \varepsilon_0)$, n, ℓ_m and even R only play the role "symbolic", not really important to the final results. It is the ratio R_i/ℓ_m which really play an important role as it decides simulation curves.

Bibliography

[1] A. Acharya. A nonlinear generalization of the koiter-sanders-budiansky bending strain measure. *International Journal of Solids and Structures*, 37(39):5517 – 5528, 2000.

[2] A. Acharya and A.J. Beaudoin. Grain-size effect in viscoplastic polycrystals at moderate strains. *Journal of the Mechanics and Physics of Solids*, 48(10):2213 – 2230, 2000.

[3] A. Acharya, H. Tang, S. Saigal, and J.L. Bassani. On boundary conditions and plastic strain-gradient discontinuity in lower-order gradient plasticity. *Journal of the Mechanics and Physics of Solids*, 52(8):1793 – 1826, 2004.

[4] E.C. Aifantis. On the microstructural origin of certain inelastic models. *Trans. ASME J. Eng. Mat. Tech.*, 106:326–330, 1984.

[5] E.C. Aifantis. The physics of plastic deformations. *Int. J. Plasticity*, 3:211–247, 1987.

[6] K.E. Aifantis, W.A. Soer, J.T.M. De Hosson, and J.R. Willis. The role of interface within strain gradient plasticity and nanoindentation. *Acta Mater*, 54:5077–5085, 2006.

[7] K.E. Aifantis and J.R. Willis. The role of interfaces in enhancing the yield strength of composites and polycrystals. *Journal of the Mechanics and Physics of Solids*, 53(5):1047 – 1070, 2005.

[8] R.K. Abu Al-Rub, G.Z. Voyiadjis, and D.J. Bammann. A thermodynamic based higher-order gradient theory for size dependent plasticity. *International Journal of Solids and Structures*, 44(9):2888 – 2923, 2007.

[9] R. Amargier, S. Fouvry, L. Chambon, C. Schwob, and C. Poupon. Stress gradient effect on crack initiation in fretting using a multiaxial fatigue framework. *Int. J of Fatigue*, 32(12):1904–1912, 2010.

[10] L. Anand, M.E. Gurtin, S.P. Lele, and C. Gething. A one-dimensional theory of strain-gradient plasticity: Formulation, analysis, numerical results. *Journal of the Mechanics and Physics of Solids*, 53(8):1789 – 1826, 2005.

[11] J.A. Araujo, L. Susmel, D. Taylor, J.C.T. Ferro, and E.N. Mamiya. On the use of the theory of critical distances and the modified wohler curve method to estimate fretting fatigue strength of cylindrical contacts. *Int J of Fatigue*, 29(1):95–107, 2007.

[12] M.F. Ashby. The deformation of plastically non-homogeneous alloys. *Philosophical Magazine*, 21(8):399–424, 1970.

[13] M.F. Ashby. The deformation of plastically non-homogeneous alloys. *Strengthening Methods of Crystals (A Kelly and R. B. Nicholson, eds.), John Wiley and Sons*, (8):137–192, 1971.

[14] M. Atkinson. Further analysis of the size effect in indentation hardness tests of some metals. *Journal of Materials Research*, 10:2908–2915, 10 1995.

[15] D.S. Balint, V.S. Deshpande, A. Needleman, and E. Van der Giessen. Discrete dislocation plasticity analysis of the grain size dependence of the flow strength of polycrystals. *International Journal of Plasticity*, 24(12):2149 – 2172, 2008.

[16] P. Ballard, K.D. Van, A. Deperrois, and Y.V. Papadopoulos. High cycle fatigue and a finite element analysis. *Fatigue & Fracture of Engineering Materials & Structures*, 18:397–411, 1995.

[17] A. Banvillet, T. Palin-Luc, and S. Lasserre. A volumetric energy based high cycle multiaxial fatigue citerion. *International Journal of Fatigue*, 25(8):755 – 769, 2003.

[18] L. Bardella. A deformation theory of strain gradient crystal plasticity that accounts for geometrically necessary dislocations. *Journal of the Mechanics and Physics of Solids*, 54(1):128 – 160, 2006.

[19] L. Bardella. Some remarks on the strain gradient crystal plasticity modelling, with particular reference to the material length scales involved. *International Journal of Plasticity*, 23(2):296 – 322, 2007.

[20] S.J. Basinski and Z.S. Basinski. Chapter1, the nature of the cold worked state. *Recrystallization, Grain Growth and Textures, A.S.M.*, 26:1–44, 1966.

[21] S. Basseville and F. Feyel. *Méthodes de résolution en éléments finis (Enseignement spécialisé "Eléments Finis" S3733-S3735).* Ecole Nationale Suprieure des Mines de Paris, 2005 - 2006.

[22] C. Bathias and J-P. Bailon. *La fatigue des matériaux et des structures*. Paris, France: Hermes, 1997.

[23] M.R. Begley and J.W. Hutchinson. The mechanics of size-dependent indentation. *Journal of the Mechanics and Physics of Solids*, 46(10):2049 – 2068, 1998.

[24] A. Benallal and C. Comi. On interfacial properties in gradient damaging continua. *Comptes Rendus Mecanique*, 333(4):319 – 324, 2005.

[25] A. Benallal, C.A. Fudoli, and W.S. Venturini. An implicit bem formulation for gradient plasticity and localization phenomena. *International Journal for Numerical Methods in Engineering*, 53-8:1853–1869, 2001.

[26] A. Benallal and J.-J. Marigo. Bifurcation and stability issues in gradient theories with softening. *Modelling and Simulation in Materials Science and Engineering*, 15, 1:283–295, 2007.

[27] A. Benallal and V. Tvergaard. Nonlocal continuum effects on bifurcation in the plane strain tension-compression test. *Journal of the Mechanics and Physics of Solids*, 43(5):741 – 770, 1995.

[28] M.A. Biot. *Mechanics of incremental deformation*. Wiley, New York, 1965.

[29] E. Bittencourt, A. Needleman, M.E. Gurtin, and E. Van der Giessen. A comparison of nonlocal continuum and discrete dislocation plasticity predictions. *Journal of the Mechanics and Physics of Solids*, 51(2):281–310, 2003.

[30] U. Borg and N.A. Fleck. Strain gradient effect in surface roughing. *Modell. Simul. Mater. Sci. Eng.*, 15:1–12, 2007.

[31] U. Borg, C.F. Niordson, and J.W. Kysar. Size effects on void growth in single crystals with distributed voids. *International Journal of Plasticity*, 24(4):688–701, 2008.

[32] B. Bourdin, G.A. Francfort, and J-J. Marigo. Numerical experiments in revisited brittle fracture. *Journal of the Mechanics and Physics of Solids*, 48(4):797 – 826, 2000.

[33] A. Brand. Nouvelle méthode de calcul en fatigue faisant intervenir le gradient de contraintes. *Mécanique Matériaux Electricité*, N^0 375-376-377:pp. 136–143, 1981.

[34] A. Brand and R.Sutterlin. Calcul des piéces a la fatigue. méthode du gradient. In *Senlis : Editions du CETIM, 157 p*, 1980.

[35] N. Caillet. *Prise en compte des spécificités des pieces forgées en fatigue illimitée*. PhD thesis, Ecole des Mines de Paris, 2007.

[36] Cast3M. *CEA, DEN, DM2S, SEMT, <http://www-cast3m.cea.fr/>*.

[37] P. Cermelli and M.E. Gurtin. Geometrically necessary dislocations in viscoplastic single crystals and bicrystals undergoing small deformations. *International Journal of Solids and Structures*, 39(26):6281 – 6309, 2002.

[38] S.H. Chen and T.C. Wang. A new deformation theory with strain gradient effects. *International Journal of Plasticity*, 18(8):971 – 995, 2002.

[39] B. Crossland. Effect of large hydrostatic pressures on the torsional fatigue strength of an alloy steel. In *International Conference on Fatigue of Metals, I. Mech. E.*, pages 138–149, London, U.K., 1956.

[40] H. Dai and D.M. Parks. Geometrically necessary dislocation density and scale dependent crystal plasticity. *Ed., Proceeding of Plasticity 97*, pages 17–18, 1997.

[41] K. DangVan, G. Cailletaud, J-F Flavenot, A. Le Douaron, and H-P. Lieurade. Amorcage des fissure de fatigue sous solicitations complexes. *Paris SF2M*, pages 301–337, 1984.

[42] R. de Borst, M.G.D. Geers, R.H.J. Peerlings, and A. Benallal. Some remarks on gradient and non-local damage theories. In Jiann-Wen Woody Ju George Z. Voyiadjis and Jean-Louis Chaboche,

editors, *Damage Mechanics in Engineering Materials*, volume 46 of *Studies in Applied Mechanics*, pages 223 – 236. Elsevier, 1998.

[43] R. de Borst and H.B. Muhlhaus. Gradient-dependent plasticity: Formulation and algorithmic aspects. *Int. J. Num. Meth. Engrg*, 35:521–539, 1992.

[44] F.M. de Sciarra. A general theory for nonlocal softening plasticity of integral-type. *International Journal of Plasticity*, 24(8):1411 – 1439, 2008.

[45] F.M. de Sciarra. Novel variational formulations for nonlocal plasticity. *International Journal of Plasticity*, 25(2):302 – 331, 2009.

[46] V.S. Deshpande, A. Needleman, and E. Van der Giessen. Plasticity size effects in tension and compression of single crystals. *Journal of the Mechanics and Physics of Solids*, 53(12):2661 – 2691, 2005.

[47] G. Duvaut and J.L. Lions. *Les inéquations en m´ecanique et en physique*. Dunod, Paris, 1972.

[48] H.D. Espinosa, M. Panico, S. Berbenni, and K.W. Schwarz. Discrete dislocation dynamics simulations to interpret plasticity size and surface effects in freestanding fcc thin films. *International Journal of Plasticity*, 22(11):2091–2117, 2006.

[49] R. Ferre, S. Fouvry, B. Berthel, and J-A. Ruiz-sabariego. Stress gradient effect on the crack nucleation process of a ti-6al-4v titanium alloy under fretting loading: comparison between nonlocal fatigue approaches. *International Journal of Fatigue*, (0):–, 2013.

[50] W.N. Findley, J.J. Coleman, and B.C. Hanley. Theory for combined bending and torsion fatigue with data for sae 4340 steel. In *International Conference on Fatigue of Metals, I. Mech. E.*, pages 150–157, London, England, 1956.

[51] J-F. Flavenot and N. Skally. L'épaisseur de couche critique ou une nouvelle approche du calcul en fatigue a long terme des structures soumises a des solicitations multiaxialles en présence de gradient de contraintes. *Rev. Méca. Matériaux et Electricité*, 397:15–25, 1983.

[52] N.A. Fleck and J.W. Hutchinson. A phenomenological theory for strain gradient effects in plasticity. *Journal of the Mechanics and Physics of Solids*, 41(12):1825 – 1857, 1993.

[53] N.A. Fleck and J.W. Hutchinson. Strain gradient plasticity. *Advances in Applied Mechanics Journal*, 33:295 – 361, 1997.

[54] N.A. Fleck and J.W. Hutchinson. A reformulation of strain gradient plasticity. *Journal of the Mechanics and Physics of Solids*, 49(10):2245 – 2271, 2001.

[55] N.A. Fleck, G.M. Muller, M.F. Ashby, and J.W. Hutchinson. Strain gradient plasticity: Theory and experiment. *Acta Metallurgica et Materialia*, 42(2):475 – 487, 1994.

[56] N.A. Fleck and J.R. Willis. A mathematical basis for strain-gradient plasticity theory. part i: Scalar plastic multiplier. *Journal of the Mechanics and Physics of Solids*, 57(1):161 – 177, 2009.

[57] N.A. Fleck and J.R. Willis. A mathematical basis for strain-gradient plasticity theory. part ii: Tensorial plastic multiplier. *Journal of the Mechanics and Physics of Solids*, 57(7):1045 – 1057, 2009.

[58] M. Fogue. *Critere de fatigue a longue durée de vie pour des états multiaxiaux de contraintes sinusoidales en phase et hors phase*. PhD thesis, These de l'Institut National des Sciences Appliquées (INSA) de Lyon, N^0 ordre 87 ISAL 0030, 189 p, 1987.

[59] M. Fogue and J. Bahuaud. Fatigue multiaxiale a durée de vie illimitée. In *7eme Congres Franais de Mécanique, Bordeaux, pp. 30-31*, 1985.

[60] S. Forest, J.M. Cardona, and R. Sievert. *Thermoelasticity of second-grade media*. Kluwer, Dordrecht, continuum thermodynamics edition, 2000.

[61] G. Francfort and A. Mielke. Existence results for a class of rate-independent material models with nonconvex elastic energies. *J. R. A. Math. Mech.*, 595:55–91, 2006.

[62] G.A. Francfort and J.-J. Marigo. Revisiting brittle fracture as an energy minimization problem. *Journal of the Mechanics and Physics of Solids*, 46(8):1319 – 1342, 1998.

[63] P. Fredriksson and P. Gudmundson. Size-dependent yield strength of thin films. *International Journal of Plasticity*, 21(9):1834 – 1854, 2005.

[64] P. Fredriksson and P. Gudmundson. Competition between interface and bulk dominated plastic deformation in strain gradient plasticity. *Modell. Simul. Mater. Sci. Eng.*, 15:S61–S69, 2007.

[65] M. Frémond. *Contact unilatéral avec adhérence. une théorie du premier gradient*, volume CISM Course 304. Springer-Verlag, Wien, unilateral problems in structural analysis edition, 1985.

[66] M. Frémond. Shape memory alloy: a thermo-mechanical macroscopic theory. *Shape memory alloys*, CISM Course 351, Springer-Verlag, Wien:3–68, 1996.

[67] M. Frémond and B. Nedjar. Damage, gradient of damage and principle of virtual power. *International Journal of Solids and Structures*, 33(8):1083–1103, 1996.

[68] H. Gao and Y. Huang. Taylor-based nonlocal theory of plasticity. *International Journal of Solids and Structures*, 38(15):2615 – 2637, 2001.

[69] H. Gao, Y. Huang, W.D. Nix, and J.W. Hutchinson. Mechanism-based strain gradient plasticity-i. theory. *Journal of the Mechanics and Physics of Solids*, 47(6):1239 – 1263, 1999.

[70] P. Germain. *Cours de mécanique des milieux continus*. Masson, Paris, 1973.

[71] A. Giacomini and A. Musesti. Two-scale homogenization for a model in strain gradient plasticity. In *ESAIM: Control, Optimisation and Calculus of Variations, doi:10.1051/cocv/2010036*, 2011.

[72] J.R. Greer, W.C. Oliver, and W.D. Nix. Size dependence of mechanical properties of gold at the micron scale in the absence of strain gradients. *Acta Materialia*, 53(6):1821–1830, 2005.

[73] S. Groh, E.B. Marin, M.F. Horstemeyer, and H.M. Zbib. Multiscale modeling of the plasticity in an aluminum single crystal. *International Journal of Plasticity*, 25(8):1456–1473, 2009.

[74] P. Gudmundson. A unified treatment of strain gradient plasticity. *Journal of the Mechanics and Physics of Solids*, 52(6):1379 – 1406, 2004.

[75] A.L. Gurson. Continuum theory of ductile rupture by void nucleation and growth: part i-yield criteria and flow rules for porous ductile media. *J. Eng. Mater. Technol.*, 99:2–15, 1977.

[76] M.E. Gurtin. Generalized ginzburg-landau and cahn-hilliard equations based on a microforce balance. *Physica D: Nonlinear Phenomena*, 92(3-4):178–192, 1996.

[77] M.E. Gurtin. A gradient theory of single-crystal viscoplasticity that accounts for geometrically necessary dislocations. *Journal of the Mechanics and Physics of Solids*, 50(1):5 – 32, 2002.

[78] M.E. Gurtin. A gradient theory of small-deformation isotropic plasticity that accounts for the burgers vector and for dissipation due to plastic spin. *Journal of the Mechanics and Physics of Solids*, 52(11):2545 – 2568, 2004.

[79] M.E. Gurtin. A theory of grain boundaries that accounts automatically for grain misorientation and grain-boundary orientation. *Journal of the Mechanics and Physics of Solids*, 56(2):640 – 662, 2008.

[80] M.E. Gurtin and L. Anand. A theory of strain-gradient plasticity for isotropic, plastically irrotational materials. part i: Small deformations. *Journal of the Mechanics and Physics of Solids*, 53(7):1624–1649, 2005.

[81] M.E. Gurtin and L. Anand. Thermodynamics applied to gradient theories involving the accumulated plastic strain: The theories of aifantis and fleck and hutchinson and their generalization. *Journal of the Mechanics and Physics of Solids*, 57(3):405 – 421, 2009.

[82] M.E. Gurtin and A. Needleman. Boundary conditions in small-deformation, single-crystal plasticity that account for the burgers vector. *Journal of the Mechanics and Physics of Solids*, 53(1):1 – 31, 2005.

[83] M.S. De Guzman, G. Neubauer, P. Flinn, and W.D. Nix. The role of indentation depth on the measured hardness of materials. *MRS Proceedings*, 308:613–618, 0 1993.

[84] B. Halphen and Q.S. Nguyen. Sur les matériaux standard généralisés. *Journal Mecanique*, 14:1–37, 1975.

[85] M.A. Haque and M.T.A. Saif. Strain gradient effect in nanoscale thin films. *Acta Materialia*, 51:3053–3061, 2003.

[86] H. Henry and H. Levine. Dynamic instabilities of fracture under biaxial strain using a phase field model. *Phys. Rev. Let.*, 93:105504, 2004.

[87] R. Hill. A general theory of uniqueness and stability in elastic-plastic solids. *Journal of the Mechanics and Physics of Solids*, 6(3):236–249, 1958.

[88] Y. Huang, H. Gao, W.D. Nix, and J.W. Hutchinson. Mechanism-based strain gradient plasticity - ii. analysis. *Journal of the Mechanics and Physics of Solids*, 48(1):99 – 128, 2000.

[89] J.W. Hutchinson. Plasticity at the micron scale. *International Journal of Solids and Structures*, 37(1 - 2):225 – 238, 2000.

[90] M.I. Idiart, V.S. Deshpande, N.A. Fleck, and J.R. Willis. Size effects in the bending of thin foils. *International Journal of Engineering Science*, 47(11-12):1251 – 1264, 2009.

[91] Y.Y. Jiang. An experimental study of inhomogeneous cyclic plastic deformation. *J of Eng. Materials and Tech.-Transactions of the ASME*, 123:274–280, 2001.

[92] D.M. Kochmann and K.C. Le. Dislocation pile-ups in bicrystals within continuum dislocation theory. *International Journal of Plasticity*, 24(11):2125 – 2147, 2008.

[93] D. Kostas, V. Deshpande, and N.A. Fleck. Discrete dislocation dynamics and strain gradient formulations: a way to modelsize effects in plasticity. In *Seminar at LMS, Ecole Polytechnique de Palaiseau, France*, 2010.

[94] T. Liebe, P. Steinmann, and A. Benallal. Theoretical and computational aspects of a thermodynamically consistent framework for geometrically linear gradient damage. *Computer Methods in Applied Mechanics and Engineering*, 190(4950):6555 – 6576, 2001.

[95] Z.L. Liu, X.M. Liu, Z. Zhuang, and X.C. You. A multi-scale computational model of crystal plasticity at submicron-to-nanometer scales. *International Journal of Plasticity*, 25(8):1436–1455, 2009.

[96] E. Lorentz and S. Andrieux. A variational formulation for nonlocal damage models. *International Journal of Plasticity*, 15(2):119–138, 2003.

[97] E. Lorentz and A. Benallal. Gradient constitutives relations: numerical aspect and application to gradient damage. *Comp. Meth. Appl. Mech. Engng.*, 194:5191–5220, 2005.

[98] Q. Ma and D.R. Clarke. Size dependent hardness of silver single crystals. *Journal of Materials Research*, 10:853–863, 3 1995.

[99] A. Mainik and A. Mielke. Global existence for rate-independent gradient plasticity at finite strain. *J. Nonlinear Sci.*, 19:221–248, 2009.

[100] M.H. Maitournam. *Mcanique des structures anlastiques: Comportement, chargements cycliques et fatigue*. Laboratoire de Mcanique des Solides (LMS) - Ecole Polytechnique, polytechnique edition, 2010.

[101] MH. Maitournam, V. Ky Dang, and J-F. Flavenot. Fatigue design of notched components with stress gradients and cyclic plasticity. *Advanced Engineering Materials*, 11(9):750–754, 2009.

[102] MH. Maitournam, B. Pommier, and JJ. Thomas. Determination of the asymptotic response of a structure under cyclic thermomechanical loading. *Comp Rend Meca*, 330(10):703-8, 2002.

[103] J. Mandel. *Cours de mécanique des milieux continus*. Gauthier-Villars, Paris, 1966.

[104] Ch. Massonnet. Le dimensionnement des pices de machines soumises la fatigue. contribution exprimentale l'tude de l'effet de l'chelle et des entailles. *Revue Universelle des Mines*, 9:203–222, 1955.

[105] Ch. Massonnet. The effect of size, shape and grain size on the fatigue strength of medium carbon steel. In *ASTM (American Society for Testing and Materials International)*, volume 56, pages 954–978, 1956.

[106] G.A. Maugin and W. Muschik. Thermodynamics with internal variables, part 1: General concepts. *Journal of Non-equilibrium Thermodynamics*, 19:217–249, 1994.

[107] T. Mayama, T. Ohashi, and R. Kondou. Geometrically necessary dislocation structure organization in fcc bicrystal subjected to cyclic plasticity. *International Journal of Plasticity*, 25(11):2122–2140, 2009.

[108] K. W. McElhaney, J.J. Vlassak, and W.D. Nix. Determination of indenter tip geometry and indentation contact area for depth-sensing indentation experiments. *Journal of Materials Research*, 13:1300–1306, 4 1998.

[109] R.D. Mindlin. Micro-structure in linear elasticity. *Arch. Ration. Mech. Anal*, 16:51–78, 1964.

[110] H.F. Moore and D. Morkovin. Third progress report on the effect of size of specimen on fatigue strength of three types of steel. In *ASTM (American Society for Testing and Materials International)*, number 44, pages 137–158, 1944.

[111] J.J. Moreau. Sur les lois de frottement, de plasticité et de viscosité. *C. R. Acad. Sciences*, 271:608–611, 1970.

[112] F. Morel and T. Palin-Luc. A non-local theory devoted to high cycle multiaxial fatigue. *Int J Fatigue*, 25:649–65, 2002.

[113] A.K. Nair, E. Parker, P. Gaudreau, D. Farkas, and R.D. Kriz. Size effects in indentation response of thin films at the nanoscale: A molecular dynamics study. *International Journal of Plasticity*, 24(11):2016–2031, 2008.

[114] A. Needleman, V. Tvergaard, and J.W. Hutchinson. Void growth in plastic solids. in "topics in fracture and fatigue". *Springer-Verlag, New York.*, pages 145–178, 1992.

[115] K. Ngargueudedjim, B. Weber, and J-L. Robert. Accounting for stress gradient effect in multiaxial fatigue criteria. In *de Freitas M, editor. Sixth International Conference on Biaxial/Multiaxial Fatigue and Fracture. ESIS; p. 143-50*, 2001.

[116] Q.S. Nguyen. Standard gradient models and gradient plasticity. (Unplished manuscript: A revisit of Q.S. Nguyen 2005 and 2011).

[117] Q.S. Nguyen. *Stability and Nonlinear Solid Mechanics*. Wiley, Chichester, 2000.

[118] Q.S. Nguyen. Variational principles in the theory of gradient plasticity. *Comptes Rendus Mcanique*, 339(12):743 – 750, 2011.

[119] Q.S. Nguyen and S. Andrieux. The non-local generalized standard approach: a consistent gradient theory. *Comptes Rendus Mécanique*, 333(2):139 – 145, 2005.

[120] L. Nicola, E. Van der Giessen, and A. Needleman. Discrete dislocation analysis of size effects in thin films. *Journal of Applied Physics*, 93(10):5920–5928, 2003.

[121] C. Nilsson. On nonlocal rate-independent plasticity. *International Journal of Plasticity*, 14(6):551–575, 1998.

[122] C.F. Niordson and J.W. Hutchinson. On lower order strain gradient plasticity theories. *European Journal of Mechanics a-Solids*, 22:771–778, 2003.

[123] W.D. Nix. Mechanical properties of thin films. *Metall. Trans. A*, 201:2217–2245, 1988.

[124] W.D. Nix and H. Gao. Indentation size effects in crystalline materials: A law for strain gradient plasticity. *Journal of the Mechanics and Physics of Solids*, 46(3):411 – 425, 1998.

[125] W.D. Nix, J.R. Greer, G. Feng, and E.T. Lilleodden. Deformation at the nanometer and micrometer length scales: Effects of strain gradients and dislocation starvation. *Thin Solid Films*, 515(6):3152 – 3157, 2006.

[126] J.F. Nye. Some geometrical relations in dislocated crystals. *Acta Metallurgica*, 1(2):153 – 162, 1953.

[127] T. Ohashi. Three dimensional structures of the geometrically necessary dislocations in matrix-inclusion systems under uniaxial tensile loading. *International Journal of Plasticity*, 20(6):1093–1109, 2004. <ce:title>Recent Advances in Multiscale Modeling of Plasticity</ce:title>.

[128] T. Ohashi. Crystal plasticity analysis of dislocation emission from micro voids. *International Journal of Plasticity*, 21(11):2071–2088, 2005. <ce:title>Plasticity of Heterogeneous Materials</ce:title>.

[129] T. Ohashi, M. Kawamukai, and H. Zbib. A multiscale approach for modeling scale-dependent yield stress in polycrystalline metals. *International Journal of Plasticity*, 23(5):897–914, 2007.

[130] T. Palin-Luc. *Fatigue multiaxiale d'une fonte GS sous sollicitations combinées d'amplitude variable*. PhD thesis, ENSAM, Talence, 1996.

[131] T. Palin-Luc. Stress gradient and size effects in multiaxial fatigue. In *Materials Week (Munich, Germany)*, 2000.

[132] T. Palin-Luc. *Approche énergétique et volumique de la fatigue multiaxiale des mtaux*. Habilitation diriger des recherches (hdr), 2004.

[133] T. Palin-Luc and S. Lasserre. An energy based criterion for high cycle multiaxial fatigue. *European Journal of Mechanics - A/Solids*, 17(2):237–251, 1998.

[134] I.V. Papadopoulos, P. Davoli, C. Gorla, M. Filippini, and A. Bernasconi. A comparative study of multiaxial high-cycle fatigue criteria for metals. *International Journal of Fatigue*, 19(3):219–235, 1997.

[135] I.V. Papadopoulos and V.P. Panoskaltsis. Invariant formulation of a gradient dependent multiaxial high-cycle fatigue criterion. *Engineering Fracture Mechanics*, 55(4):513 – 528, 1996.

[136] A. Pavan. *Contribution aux calculs d'organes d'ensembles mcaniques par rapport a la limite de fatigue. Explication des principaux facteurs*. PhD thesis, Universit de Reims, Reims, France, 1979.

[137] G. Pekmezi. *Nonlocal gradient-dependent modeling of plasticity with anisotropic hardening*. PhD thesis, Supervised by Prof. G.Z. Voyiadjis, Louisiana State University, 2008.

[138] C.E. Phillips and R.B. Heywood. The size effect in fatigue of plain and notched steel specimens loaded under reversed direct stress. In *I. Mech. E.*, volume 165, pages 113–124, 1951.

[139] G. Pluvinage. Notch effect in high cycle fatigue. *ICF 9 Proceedings*, 3:1237–50, 1997.

[140] R.G. Pogoretskii and G.V. Karpenko. Effect of test piece length on the fatigue strength of steel in air. *Fiziko Khimicheskaya Mekhanika Materialov*, 1:90–94, 1965.

[141] C. Polizzotto. Unified thermodynamic framework for nonlocal/gradient continuum theories. *European Journal of Mechanics - A/Solids*, 22(5):651 – 668, 2003.

[142] C. Polizzotto. A nonlocal strain gradient plasticity theory for finite deformations. *International Journal of Plasticity*, 25(7):1280 – 1300, 2009.

[143] C. Polizzotto. Size effects on the plastic collapse limit load of thin foils in bending and thin wires in torsion. *European Journal of Mechanics - A/Solids*, 30(6):854 – 864, 2011.

[144] Castrenze Polizzotto. A unified residual-based thermodynamic framework for strain gradient theories of plasticity. *International Journal of Plasticity*, 27(3):388–413, 2011.

[145] W.J. Poole, M.F. Ashby, and N.A. Fleck. Micro-hardness of annealed and work-hardened copper polycrystals. *Scripta Materialia*, 34(4):559 – 564, 1996.

[146] G. Qylafku, Z. Azari, N. Kadi, M. Gjonaj, and G. Pluvinage. Application of a new model proposal for fatigue life prediction on notches and key-seats. *International Journal of Fatigue*, 21(8):753–760, 1999.

[147] J.R. Rice and D.M. Tracey. On the ductile enlargement of holes in triaxial stress fields. *J. Meeh. Phys. Solids*, 17:201–217, 1969.

[148] J.L. Robert. *Contribution a l'étude de la fatigue multiaxiale sous sollicitations périodiques ou aléatoires*. PhD thesis, These de l'Institut National des Sciences Appliquées (INSA) de Lyon - N^0 ordre 92 ISAL 0004, 229 p., 1992.

[149] R. Saha, Z. Xue, Y. Huang, and W.D. Nix. Indentation of a soft metal film on a hard substrate: strain gradient hardening effects. *Journal of the Mechanics and Physics of Solids*, 49(9):1997 – 2014, 2001. <ce:title>The JW Hutchinson and JR Rice 60th Anniversary Issue</ce:title>.

[150] J. Schiotz, F.D. Di Tolla, and K.W. Jacobsen. Softening of nanocrystalline metals at very small grain sizes. *Nature*, 391:561–563, 1998.

[151] D. Shan, C. Wang, B. Guo, and X. Wang. Effect of thickness and grain size on material behavior in micro-bending. *Transactions of Nonferrous Metals Society of China*, 19, Supplement 2(0):s507 – s510, 2009.

[152] M.X. Shi, Y. Huang, and K.C. Hwang. Plastic flow localization in mechanism-based strain gradient plasticity. *International Journal of Mechanical Sciences*, 42(11):2115 – 2131, 2000.

[153] X.H. Shi and Y.G. Gao. Generalization of response number for dynamic plastic response of shells subjected to impulsive loading. *International Journal of Pressure Vessels and Piping*, 78(6):453 – 459, 2001.

[154] Z.F. Shi, B. Huang, H. Tan, Y. Huang, T.Y. Zhang, P.D. Wu, K.C. Hwang, and H. Gao. Determination of the microscale stress-strain curve and strain gradient effect from the micro-bend of ultra-thin beams. *International Journal of Plasticity*, 24(9):1606 – 1624, 2008.

[155] B. Shubhra. *Characterization of nanostructured metals and metal nanowires for chip-to-package interconnections*. PhD thesis, Georgia Institute of Technology, 2006.

[156] G. Sines. Behavior of metals under complex static and alternating stresses. *Metal Fatigue*, pages 145–169, 1959.

[157] C.M. Sonsino, H. Kaufmann, and V. Grubisic. Transferability of material data for the example of a randomly loaded forged truck stub axle. *SAE Technical Paper -Journal of Materials and Manufacturing*, No. 970708:1–22, 1997.

[158] N.A. Stelmashenko, M.G. Walls, L.M. Brown, and Yu.V. Milman. Microindentations on w and mo oriented single crystals: An stm study. *Acta Metallurgica et Materialia*, 41(10):2855–2865, 1993.

[159] J.S. Stolken and A.G. Evans. A microbend test method for measuring the plasticity length scale. *Acta Materialia*, 46(14):5109 – 5115, 1998.

[160] L. Stromberg and M. Ristinmaa. Fe-formulation of a nonlocal plasticity theory. *Computer Methods in Applied Mechanics and Engineering*, 136(12):127 – 144, 1996.

[161] S. Sun, B.L. Adams, and W.E. King. Observations of lattice curvature near the interface of a deformed aluminium bicrystal. *Philosophical Magazine A*, 80(1):9–25, 2000.

[162] T. Svedberg and K. Runesson. A thermodynamically consistent theory of gradient-regularized plasticity coupled to damage. *International Journal of Plasticity*, 13(6-7):669–696, 1997.

[163] E.B. Tadmor, R. Miller, R. Phillips, and M. Ortiz. Nanoindentation and incipient plasticity. *Journal of Materials Research*, 14:2233–2250, 5 1999.

[164] Lu Tao, Shi Yaowu, and Jiang Lipei. Residual stress distributions and plastic zones in heterogeneous welded plates with a transverse crack. *International Journal of Pressure Vessels and Piping*, 77(9):549 – 553, 2000.

[165] D. Taylor. *The theory of critical distances: a new perspective in fracture mechanics*. Oxford, UK, 2007.

[166] G.I. Taylor. The mechanism of plastic deformation of crystals. part- i: Theoretical. *Proceedings of the Royal Society of London*, 145:362–387, 1934.

[167] G.I. Taylor. Plastic strain in metals. *Journal of the Institute of Metals*, 62:307–324, 1938.

[168] V. Tvergaard. Material failure by void growth to coalescence. *Adv. Appl. Mech.*, 27:83–147, 1990.

[169] R. Venkatraman and J.C. Bravman. Separation of film thickness and grain boundary strengthening effects in al thin films on si. *Journal of Materials Resistance*, 7:2040–2048, 1992.

[170] K.Y. Volokh and J.W. Hutchinson. On lower order strain gradient plasticity theories. *Journal of Applied Mechanics Transactions of the Asme*, 69:862–864, 2002.

[171] G.Z. Voyiadjis and R.K. Abu Al-Rub. Nonlocal gradient-dependent thermodynamics for modeling scale-dependent plasticity. *Int. J. Multiscale Comput. Eng.*, 5:295–323, 2007.

[172] G.Z. Voyiadjis and B. Deliktas. Formulation of strain gradient plasticity with interface energy in a consistent thermodynamic framework. *International Journal of Plasticity*, 25(10):1997–2024, 2009.

[173] G.Z. Voyiadjis and B. Deliktas. Mechanics of strain gradient plasticity with particular reference to decomposition of the state variables into energetic and dissipative components. *International Journal of Engineering Science*, 47(11-12):1405–1423, 2009. <ce:title>Mechanics, Mathematics and Materials a Special Issue in memory of A.J.M. Spencer FRS</ce:title> <ce:subtitle>In Memory of Professor A.J.M. Spencer FRS</ce:subtitle>.

[174] G.Z. Voyiadjis and D. Faghihi. Thermo-mechanical strain gradient plasticity with energetic and dissipative length scales. *International Journal of Plasticity*, 2011.

[175] G.Z. Voyiadjis and W. Huang. A modelling of single crystal plasticity with backstress evolution. *Eur. J. Mech. A Solids*, 15:553–573, 1996.

[176] G.Z. Voyiadjis, G. Pekmezi, and B. Deliktas. Nonlocal gradient-dependent modeling of plasticity with anisotropic hardening. *International Journal of Plasticity*, 26(9):1335 – 1356, 2010.

[177] W. Wang, Y. Huang, K.J. Hsia, K.X. Hu, and A. Chandra. A study of microbend test by strain gradient plasticity. *International Journal of Plasticity*, 19(3):365 – 382, 2003.

[178] D.H. Warner, F. Sansoz, and J.F. Molinari. Atomistic based continuum investigation of plastic deformation in nanocrystalline copper. *International Journal of Plasticity*, 22(4):754–774, 2006.

[179] B. Weber. *Fatigue multiaxiale des structures industrielles sous chargement quelconque*. PhD thesis, INSA de Lyon, 1999.

[180] Y. Wei and J.W. Hutchinson. Hardness trends in micron scale indentation. *Journal of the Mechanics and Physics of Solids*, 51(11 - 12):2037–2056, 2003.

[181] Y. Xiang, T.Y. Tsui, and J.J. Vlassak. The mechanical properties of freestanding electroplated cu thin films. *J. Mater. Res.*, 21:1607–1618, 2006.

[182] Z. Xue, Y. Huang, K. C. Hwang, and M. Li. The influence of indenter tip radius on the micro-indentation hardness. *J. Eng. Mater. Technol.*, 124(3):371–379, 2002.

[183] F. Zhang, R. Saha, Y. Huang, W.D. Nix, K.C. Hwang, S. Qu, and M. Lid. Indentation of hard film on a doft substrate: Strain gradient hardening effects. *International Journal of Plasticity*, 23:25–432, 2007.

List of Figures

List of Tables